OHMIC CONTACTS TO P-TYPE GALLIUM NITRIDE

By

BO LIU

A DISSERTATION PRESENTED TO THE GRADUATE SCHOOL
OF THE UNIVERSITY OF FLORIDA IN PARTIAL FULFILLMENT
OF THE REQUIREMENTS FOR THE DEGREE OF
DOCTOR OF PHILOSOPHY

UNIVERSITY OF FLORIDA

2001

ACKNOWLEDGMENTS

I would like to thank my supervisor, Dr. Paul H. Holloway, for the opportunity and financial aid to study GaN, a promising semiconductor material. I am also grateful for his philosophy on the relation between research and knowledge, for his desire to understand students, and his devotion to improving my communication skills. I treasure the memory of his guidance and help with my research and personal affairs.

I thank my committee members: Drs. Rolf E. Hummel, Kelvin S. Jones, Fan Ren and Wolfgang Sigmund for their valuable contributions. The assistance from the staff of MAIC, Drs. Ren's group, Dr. Jones's group, Dr. Hummel's group and collaborators in the clean room in the Department of Electrical Engineering is highly appreciated.

I thank all of the members in Dr. Holloway's group, both past and present. I appreciate their friendship and patience over the past few years. I enjoyed working with each of them.

I also thank all of the friends I made during my time in Gainesville, including those who favor me as their barber. I thank each of them for making my life in Gainesville so beautiful.

I especially thank my family for their patience, support and encouragement through all my professional endeavors.

TABLE OF CONTENTS

LIST OF TABLES

LIST OF FIGURES

ix

Abstract of Dissertation Presented to the Graduate School
of the University of Florida in Partial Fulfillment of the
Requirements for the Degree of Doctor of Philosophy

OHMIC CONTACTS TO P-TYPE GALLIUM NITRIDE
By

Bo Liu

May 2001

Chairman: Dr. Paul H. Holloway
Major Department: Materials Science and The effects of H_2O_2 treatment, multi-layer

metallization, and Ni cap-layer on Ni/Au have been studied for ohmic contacts to p-GaN.

First, surface H_2O_2 treatments are found to increase the hole concentration by up to 100% in

p-GaN grown by molecular beam epitaxy (MBE), while causing no change in n-GaN or p-

GaN grown by metalorganic chemical vapor deposition (MOCVD). Treatment of 20 min

increased, while treatment >60 min decreased the hole concentration in MBE p-GaN. With

this treatment, the current in Ni/Au contacts increased. The increased hole concentration was

attributed to reduction of nitrogen vacancies or H-Mg complexes in GaN. The decrease of

carrier concentration was attributed to recompensation of shallow acceptors by oxygen

serving as hole traps.

Second, general principles were defined for selecting metals for ohmic contacts to

GaN, a scheme called "NOG" for Nitride-forming metal Over Gallide-forming metal. In

"NOG" a gallide-forming metal dissociates GaN and a nitride-forming metal increases the

nitrogen thermodynamic activity at the interface. Literature data were compared to these

ideas, and experimental data on Ni/Ti/Au, Ni/Al/Au, Pt/Si/Pt/Au, Pt/Mg/Pt/Au were

collected and compared with data from Ni/Au and Pt/Au contacts. Higher currents were

found for schemes based on the "NOG" principles. However, the contact resistivity was still high and thermal stability became a limiting factor.

Last, ohmic contacts to p-GaN were obtained after oxidizing Ni/Au and Ni/Au/Ni contacts. Both Ni/Au/Ni and Ni/Au were shown to have resistivities of $\sim 10^{-4}$ Ω-cm^2. Transparent NiO was obtained and thin Au film formed pores which led to optical transparencies at $\lambda = 450$nm of $>85\%$. The porosity in Au was demonstrated to result from interface and grain boundary energies. Addition of the Ni cap-layer was shown to increase the thermal stability of thin Ni/Au ohmic contacts and increase the light transmittance to 93%, while keeping contact resistivities of low 10^{-4} Ω-cm^2.

CHAPTER 1
INTRODUCTION

As members of the III-V nitrides family, InN, GaN, AlN and their alloys are all wide band gap materials, and can crystallize in both hcp wurtzite (α) and cubic zincblende (β) crystal structures. As shown in Figure 1.1, the wurtzite InN, GaN and AlN have direct bandgaps of 1.9 eV, 3.4 eV and 6.2 eV, respectively, at room temperature [Mor97]. In the cubic form, GaN and InN have direct bandgaps, and AlN has an indirect bandgap. The GaN alloyed with InN and AlN can form a continuous (AlGaIn)N alloy system spanning a continuous range of direct bandgap energies throughout the visible to near UV region of the electromagnetic spectrum. This makes the nitride system very attractive for optoelectronic device applications, such as light emitting diodes (LEDs), laser diodes (LDs) and optical detectors [Mor96]. Various GaN-based electric devices also have been demonstrated for applications in high power/high temperature electronic devices [Table 1.1] because of their intrinsic properties of wide bandgap and high breakdown fields [Cho94, Kha94, She99b Gas98].

In particular, GaN with its band gap of 3.4 eV plays a central role in the alloy system of (AlGaIn)N. Other advantageous properties of GaN include high mechanical and thermal stability, large piezoelectric constant, good thermal properties [Bin97] and the possibility of passivation by forming thin layers of Ga_2O_3 or Al_2O_3 with bandgaps of 4.3eV and 9.2eV respectively.
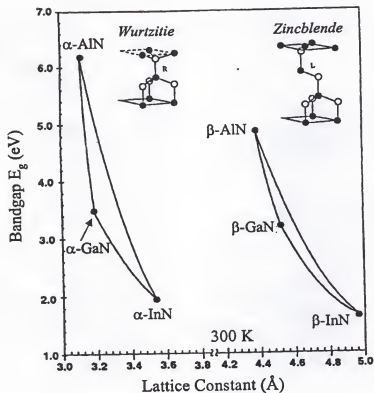
Figure 1.1 Relation of bandgaps and lattice constants of hexagonal (α) and cubic (β) InN, GaN, AlN and their alloys [Mor97]

Because of its wide bandgap and chemical inertness, GaN and related materials are challenging materials researchers. Examples of some challenges include but not limited to growth of heteroepitaxial films [Amb98], the low level of p-type doping because of deep acceptor levels [Mol93] and Mg-H complex [Got95], difficulties in achieving low-resistance ohmic contact to p-GaN [Liu98], slow wet and dry etch rate [Ade93, Pea94], and lack of good passivation films [Uza95], *etc.* This work focuses on formation and improvement of ohmic contacts to p-type GaN.

Table 1.1 GaN-based electric devices [Shu99]

Device	Status	Possible Applications
Schottky barrier diode	Demonstrated for a variety of metals	Switch, FET building block
p-n junction	Demonstrated on both regular and lateral epitaxial overgrowth material	Photodetector, switch, BJT building block
GaN MESFET	Demonstrated	High-temperature digital circuits
GaN MISFET	Demonstrated	High-temperature digital circuits, non-volatile memories
AlGaN/GaN HFET	Demonstrated on sapphire and SiC substrates with record power levels	High-temperature, high power microwave, high temperature digital circuits
AlGaN/GaN and GaN/SiC HBTs	Demonstrated	High-temperature, high power microwave, high power switches
GaN-based piezoelectric and piezoelectric sensors	Demonstrated for GaN and AlGaN/GaN	Pressure sensors, especially for high temperature applications
GaN pyroelectric sensor	Demonstrated for primary and secondary pyroelectric effect	Temperature sensors, especially for high temperature applications

Progress has been made in the past several years in developing reliable ohmic contact to p-GaN [Tre96, Tre97, Hol97, Liu98, Ho99a, Ho99b, Koi99 and Pal00], both for lower specific contact resistance and better thermal stability. Nevertheless, the goals are far from being achieved. It has been proven difficult to obtain sufficiently low contact resistance ($\leq 10^{-6}$ Ω-cm^2) to p-GaN. In GaN based LEDs, Ni/Au are commonly used as ohmic contact on p-type GaN top layer. The low doping levels of the p-GaN usually result in non-ohmic contact, and thereby degrade the device performance. Also, due to the high resistivity of the p-GaN layer, the current from the top electrode can not be spread effectively through the entire device chip, leading to current crowding. Large

Joule heating caused by high operating voltages has been reported to limit the lifetime of continuous wave (CW) laser diodes [Nak97]. For metal semiconductor field effect transistors (MESFETs), an ohmic contact resistivity of mid ~10^{-6} Ω-cm^2 may be acceptable for a channel length of 1 μm [Mur90]. For p-GaN, the best stable ohmic contact resistivity is only 10^{-1} ~ 10^{-3} Ω-cm^2. Ohmic contacts to n-GaN have been developed with resistivities of 10^{-6} Ω-cm^2 [Ren97].

The high specific contact resistances to p-type GaN can be attributed to several factors, including 1) absence of a metal with a sufficiently high work function (The bandgap of GaN is 3.4 eV and the electron affinity is 4.1eV, so a work function of 7.5 eV is needed for a good ohmic contact. Metal work functions are typically ≤ 5.5 eV); 2) difficulty in achieving high hole concentrations in p-GaN because of the deep ionization level of the acceptors (Mg is ~170 meV, others are deeper [Str91]); and 3) the tendency for preferential loss of nitrogen from the GaN surface during processing, which probably result in surface conversion to n-type conductivity. To decrease the contact resistance to p-GaN, high p-type electrical conductivity or lower barrier height at the contacts interface would be helpful.

Specific contact resistivities as low as 10^{-6} Ω-cm^2 have been reported for thin oxidized Ni/Au films [Ho99b]. This contact scheme also showed high (>60%) light transmittance, which is desired in optoelectronics. The reported contact thickness (only 100 Å) was comparable to the GaN surface roughness. Lower contact resistivity and higher light transmittance are obviously desirable.

In this dissertation, H_2O_2 solutions were demonstrated to increase the carrier concentration of MBE grown p-GaN. A "NOG" scheme (Nitride-forming Over Gallide-

forming metals) offers guidance in development of contacts to both n- and p- type GaN epilayers. Low resistance and high transparency contacts to p-type GaN are also studied. It was demonstrated that adding a thin Ni surface cap-layer, to the thin Ni/Au layered contacts improved light transmission and enhanced contact stability.

Thus the scope of this dissertation is as follows.

Chapter 2 presents a review of the physical mechanisms of ohmic contact formation and discusses current literature on ohmic contact to p-GaN.

Chapter 3 summarizes the experimental procedures used in this study, including contact processing parameters and characterization techniques.

Chapter 4 summarizes the use of H_2O_2 solutions to increase the free hole concentration. Possible explanations for increased hole concentration are discussed.

A methodology to choose materials to test for better GaN ohmic contact formation is proposed and discussed in Chapter 5. This procedure ("NOG") is based on the properties of different metal groups. Various contact schemes to p-GaN are tested and discussed.

In Chapter 6, the microstructural evolution of transparent Ni/Au ohmic contacts is reported. The consequence of annealing these layers in N_2 or O_2 ambients are described. Addition of a Ni cap-layer to form GaN/Ni/Au/Ni contacts is shown to increase rather than decrease the optical transparency.

Finally, Chapter 7 is a summary, and chapter 8 discusses future work to improve the understanding of p-GaN ohmic contacts.

CHAPTER 2
REVIEW OF LITERATURE

Many GaN-based electronic and photonic devices have been developed, and all these devices need ohmic contacts to external current and voltage sources. Because of high conductivity, metals are normally used for this purpose. Typically, interfaces between metals and semiconductors have been found to exhibit rectifying properties [Rho88, Bri93]. Although these rectifying properties are useful in some devices, many applications require efficient transport of current across the contact interface. Ohmic contacts are generally required for such applications. Creating low-resistance ohmic contacts to GaN, especially for p-type material, has proved to be one of the major challenges faced in the development of GaN semiconductor technology [Pea97a].

2.1 Growth of GaN and Defects

Because sufficiently large (> 1 cm in diameter) single GaN crystals are generally unavailable for use as substrate for homoepitaxial growth, heteroepitaxial growth of GaN has been used in practice and the choice of substrate is critical to the structural, electrical and morphological properties of the obtained epilayers [Li96, Kob97, Ham98, Kun96, Kur95, Geo96, Sun96, Pop97]. Possible substrate materials typically need to have good matches in thermal expansion coefficients and lattice constants with GaN, and should be resistant to the growth chemistries at high growth temperatures (over 1000°C in certain cases). Sapphire [Kai98, Pop97] and SiC [Pop97, Abe97] are the most popular substrates currently used due to their adequate thermal and chemical stability at high growth

temperatures, excellent structural and surface morphology and availability in large quantities. Other substrates include Si [Vis95], $MgAl_2O_4$ [Kur95], $LiGaO_2$ [Kun96], $NdGaO_3$ [Kur95], quartz glass [Iwa97] and ZnO [Pop97, Dav97].

Metalorganic chemical vapor deposition (MOCVD) [Ama86, Kat94, Kel96, Mor81 and Nak94], molecular beam epitaxy (MBE) [Mou93, Van97] and their derivatives are the techniques most extensively used to grow GaN epilayers. Mg and Si are widely used as p - and n - type dopants. Because of a large activation energy (270 meV) and passivation of acceptors with hydrogen, in which the activation energy is dependent on dielectric constant (GaN, 9.5) and effective mass of the material (GaN, m_e = 0.2 m_0, m_{hh} = 0.75 m_0) [Den97], the ionization of Mg acceptors is less than 1% at room temperature. Typical hole concentrations are ~10^{17} cm^{-3} for p-GaN (although Mg concentration can be as high as 10^{20} cm^{-3}). For GaN grown with the MOCVD method, the as-grown materials typically is unintentionally n-type, which is widely believed to be due to intrinsic nitrogen vacancies. Intentional n-type doping can be easily accomplished using silicon as the donor.

In the MOCVD method, the Ga source materials generally used are $GaCl_3$ (produced by passing HCl vapor over molten gallium), trimethylgallium (TMGa), triethylgallium et al, and the nitrogen source is mostly of ammonia [Dav88, Wal97]. Biscyclopentadienyl (Cp_2Mg) is used as a source of Mg and methyl silane (Si (CH_3SiH_3) as a source of Si [Sun97, Her97]. The MOCVD method has been the leading technique for production of III-nitrides optoelectronic and microelectronic devices. Characteristics of this method include high purity chemical sources, easy composition and uniformity control, high growth rates and abrupt junctions. Since partial pressure of nitrogen in the

CVD reactor is always less than the equilibrium partial pressure of nitrogen over GaN at the high substrate growth temperatures, the samples may contain high concentrations of intrinsic n-type carriers, commonly believed to be nitrogen vacancies [Pan97].

In the MBE process, the fluxes of Ga, Mg and Si are generated by heating high purity elements in the Knudsen or effusion cells [Dav88]. The substrate temperature for MBE growth is typically operated at relatively low temperature at 898K or even lower to 663K [Got81]. Nitrogen is typically supplied as an atomic species using electron cyclotron resonance (ECR) or radio frequency (rf) plasmas [Pop98, Abe97, Mou93].
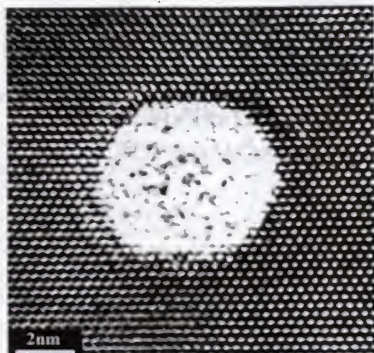
Figure 2.1 A nanopipe in GaN imaged by HRTEM [Kan99]

The GaN-based III-nitride heterostructures are found typically to contain characteristic one-dimensional (edge, mixed and screw dislocations) and two-dimensional (stacking faults and domain boundaries) extended defects [Jai00]. Although the dislocation density is high, the dislocations are usually clustered in local regions of the epilayer, so large volumes of the epilayer are defect free [Pon97]. Nanopipes are also found in GaN with diameters ranged from ~ 5nm to ~ 0.5um and densities as high as 10^8 cm^{-2}, as identified with high-resolution transmission electron microscopy (HRTEM). These nanopipes were reported to be parallel to the c-axis of GaN unit cell [Ven99, Kan99], as shown in Figure 2.1. The main constituents inside these nanopipes were Ga, C and O [Kan99].

A model was constructed to explain the effects of dislocations on minority carriers in GaN epilayers [Jai98], and was found to be consistent with the experimental results. Dislocations and nanopipes are postulated to help explain changes in the carrier densities of MBE grown GaN after room temperature treatment with H_2O_2 solutions in this work.

2.2 Mechanisms of Ohmic Contact

A contact is said to be ohmic when the ratio of the potential drop V across a contact versus the current I flowing through the same contact is linear with a constant, low contact resistance (R_c). Ohmic contacts are characterized by a parameter called specific contact resistance (or resistivity), ρ_c, which is expressed as [She92]

$$\rho_c = (\frac{\partial J}{\partial V})_{V=0}^{-1}.$$ (2.1)
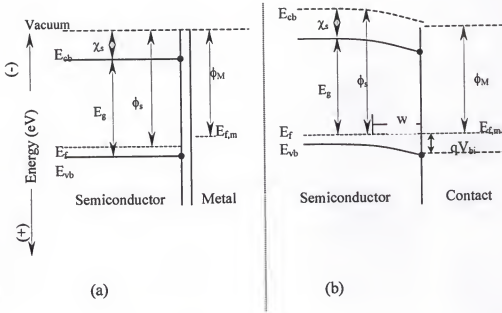
Figure 2.2 Energy diagrams of a metal contact to and semiconductor, explaining formation of ohmic contact to p-GaN (a) Before charge equilibrium; (b) After charge equilibrium.

In general, when a semiconductor of a given electrochemical potential is brought into contact with any phase with a different electrochemical potential, charge will flow automatically across the semiconductor/contact junction (Figure 2.2). For an ideal semiconductor/metal contact (Schottky limit), all the voltage drops across the semiconductor. The contact barrier height for p-type semiconductor, $\phi_{b,p}$, is calculated using the equation [Kum93]:

$$\phi_{b,p} = \frac{E_{f,m} - (\chi + E_g)}{q},$$ (2.2)

where $E_{f,m}$ is the Fermi level of the isolated metal (before contact) and χ is the electron affinity of the isolated semiconductor. In the literature, the work function of a metal, φ (in

electron volts), is often used to estimate the barrier height limiting charge transfer at semiconductor/ metal junctions. The work function is used instead of $E_{f, m}$ because the Fermi level is more difficult to determine experimentally, whereas φ is readily accessible using photoemission or other data. Ideally, a metal with a lower work function than that of an n-type semiconductor or a higher work function than that of a p-type semiconductor can be used to form ohmic contacts to a semiconductor. Unfortunately, it has been shown experimentally that most semiconductor/metal contacts do not obey the predictions of this ideal Schottky limit [Rho88, Kum93]. In a simple model, the Schottky barrier height, ϕ_b, can be expressed as follows [Sze81]:

$$q \cdot \phi_b = q(S \cdot \chi_m + \phi_0) \tag{2.3}$$

where χ_m is the metal electronegativity (Note: not to be confused with χ_s, the electron affinity of the semiconductor), and ϕ_0 represents the contribution of surface states from the semiconductors. The interface index

$$S = \frac{d\phi_b}{d\chi_m} \tag{2.4}$$

is a function of the electronegativity difference $\Delta\chi$ between the cation and anion components of a compound semiconductor, as shown in Figure 2.3* [Ren98]. The reason for the name of "S" factor is just from the shape of the graph. Note the sharp transition around $\Delta\chi = 1$. This S factor should be equal to unity for an ideal semiconductor/metal junction in the Schottky limit. When $S = 1$, the measured barrier height equals the initial contact potential difference obtained from the Schottky limit. The unity of S value means

---

* The electronegativity difference of GaN was labled mistakenly at 1.8 eV in the literature, instead of the true value of 1.23eV as shown in Figure 2.3.
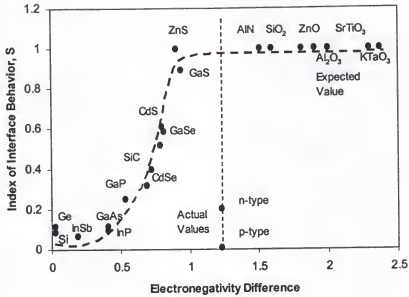
Figure 2.3 Change of the interfacial behavior factor S with different semiconductors [Ren98].

absolutely no pinning of the Fermi level. When $S = 0$, the system is in the regime of strong "Fermi level pinning." This terminology indicates that the Fermi level position at the surface of the semiconductor, measured relative to the vacuum level, does not vary when either the work function or the Fermi level of the contacting phase is changed. For covalent semiconductors with $\Delta\chi < 1$, S is small, and ϕ_b is typically affected by a high density of surface states from dangling bonds, so that it depends weakly on the metal work function. On the other hand, for ionic compound semiconductors, where $\Delta\chi > 1$, the index S approaches unity, and ϕ_b depends strongly on the metal work function. GaN has an electronegativity difference of 1.23 eV(Ga: 1.81eV, N: 3.04eV) [Hsu00], which suggests that the Schottky barrier height should be a function of the metal work function.

The origin of this non-ideal interfacial behavior (Fermi level pinning) is a topic of intense controversy. Bardeen originally proposed [Bar47] that surface states at the

semiconductor/metal interface are the source of this pinning. Chemical reactions, such as stoichiometry changes [Spi86] and alloy formation [Fre81], have also been proposed to explain Fermi level pinning.

For either an ohmic or rectifying contact, current is transported across the interface by mechanisms shown in Figure 2.4. Current transport can be principally ascribed to the following three mechanisms [Sze81]:

1. Thermionic emission (TE) is dominant in low and moderately doped semiconductors with $N_{e(h)} \leq 10^{17}$ cm^{-3}. At low to moderate carrier densities, the wide depletion region prevents tunneling through the barrier. When the barrier height is small, the electrons can be thermally excited over the top of the barrier (thermionic emission, Figure 2.4a). On the other hand, for a high barrier, the vast majority of electrons are unable to overcome this barrier, resulting in non-ohmic (rectifying) contacts.

2. Thermionic-field emission (TFE) is applicable for intermediate doping densities, $\sim 10^{17}$ cm^{-3} < $N_{e(h)}$ < $\sim 10^{18}$ cm^{-3}. Both thermionic and tunnel emission are important (Figure 2.4b).

3. Field emission (FE) is effective in heavily doped semiconductors, $N_{e(h)} > \sim 10^{18}$ cm^{-3}. In this case the depletion region is narrow, and electron or hole tunnel easily from metal to semiconductor or vice versa (Figure 2.4c).

A very useful parameter, KT/E_{00}, can be used [Yan71] to calculate ρ_c for each of these three mechanisms, where E_{00} is the tunneling parameter equal to:

$$E_{00} = \frac{q \cdot h}{4 \cdot \pi} \cdot \sqrt{\frac{N_{e(h)}}{\varepsilon \cdot m^*}} \qquad (2.5)$$
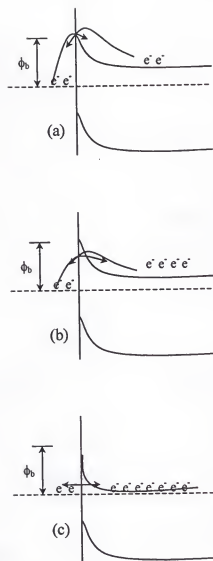
Figure 2.4 Mechanisms of ohmic contact formation. (a) thermionic
emission; (b) thermionic field emission; (c) field emission.

where q is electronic charge, h is the Planck's constant, $N_{e(h)}$ is electron (hole)

concentration, ε is dielectric constant of the semiconductor, and m^* is electron (hole)

effective mass.

For $kT/E_{00} \ll 1$ (heavy doping concentrations), the specific contact resistance is

given by

$$\rho_c \propto \exp(\frac{q \cdot \phi_b}{E_{00}}). \tag{2.6}$$

In this case, the field emission mechanism (FE) dominates current transport. The ρ_c

depends strongly on doping concentration. At high doping concentration, the depletion

width of the Schottky junction is decreased, resulting in high tunneling transmission

coefficients. Hence, even a metal with a low metal work function can still form an ohmic

contact. With this method, as in GaAs, ohmic contacts can be formed on a semiconductor

with a pinned Fermi level [Hol97].

For $kT/E_{00} \sim 1$ (intermediate doping concentrations), a mixture of both thermionic

and tunneling (TFE) transport is observed, and the specific contact resistance becomes

$$\rho_c \propto \exp\left[\frac{q \cdot \phi_b}{E_{00} \cdot \coth(\frac{E_{00}}{K \cdot T})}\right] \tag{2.7}$$

The specific contact resistance in this case depends on both temperature and transmission

coefficient for tunneling.

For $kT/E_{00} \gg 1$ (moderate doping concentrations), the TE mechanism dominates

the current conduction and the specific contact resistance is

$$\rho_c \propto \exp(\frac{q \cdot \phi_b}{K \cdot T}) \tag{2.8}$$

The specific contact resistance is clearly dependent on temperature. At higher temperatures, the thermionic emission current increases and results in a smaller ρ_c.

The term ohmic contact in practice does not necessarily require a linear current voltage characteristic [Rid75]. A metal-semiconductor contact is associated with a space-charge region in which the current-voltage behavior eventually becomes nonlinear, as bias increases. Ideally the contact resistance of the space-charge layer would be negligible relative to the bulk or spreading resistance of the semiconductor contacted by the metal, but this is rarely achieved in practice. A contact is usually acceptable when the voltage drop is very small compared to the drop across the active region of the device, even though the current-voltage behavior of the contact is not strictly linear. This is certainly true for current contacts to p-GaN devices, due to the unavailability of low resistance ohmic contact to p-GaN (see later in Table 2.2).

In theory, the contact resistance can be defined completely if physical and operating parameters are known [Rid75]. The physical parameters are mainly of contact area and thickness, while operating parameters are predominantly temperature and bias. In practice, the contact resistance can be affected seriously by a number of other factors, such as interfacial layers (oxide formation or contamination), surface damage, minority carrier injection, and energetically deep impurity levels or traps.

The most widely used method for determining the specific contact resistance is transfer length method, also often called the transmission line model (TLM) [Ber72,

(a)
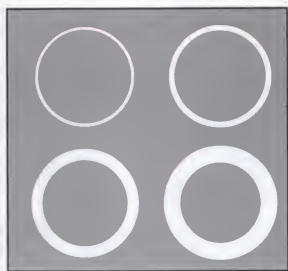
(b)

Figure 2.5 Possible patterns used to measure contact resistance: (a)
linear array; (b) circular contacts [Wil84]. The grey region is
contact metal and the white region presents areas where the
metal has been etched or lifted off leaving bare semiconductor
or an etched mesa.

Wil84]. An array of metal contacts (Figure 2.5) is fabricated with different spacings

between the metal areas. The resistance is measured as a function of the gap spacing.

Extrapolation of the resistance to zero gap spacing gives a value equal to twice the

contact resistance R_c (Figure 2.6). The x-intercept is equal to twice the transfer length, L_t,
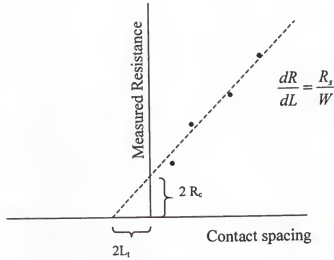
Figure 2.6 Plot of measured resistance vs. contact separation [Wil84]

where $L_t = (\rho_c/R_s)^{1/2}$, ρ_c is the specific contact resistance and R_s is sheet resistance of the semiconductor epilayer. The transfer length is defined as the distance from the edge to where the current in the semiconductor falls to $1/e$ (e being the base of natural logarithm) of its original value. ρ_c can be calculated using the equation:

$$\rho_c = \frac{R_c^2 \cdot w^2}{R_s} = R_s \cdot L_t^2 \tag{2.9}$$

where L_t should be much smaller than the gap spacing between contacts. However, as the spacing become very small, irregular edges may cause a problem. The test pattern should be isolated so that current flow occurs only in the space between pads (no leakage current path), therefore a mesa structure may be needed [Wil84].
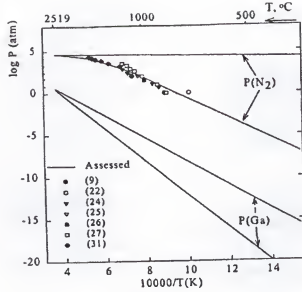
Figure 2.7 Pressure-temperature projection of the three phase equilibra: GaN + liquid + gas. The area inside each envelope represents the two-phase equilibrium of GaN + gas and corresponds to GaN stability [Dav99].

For the pattern in Figure 2.5-(b) with a circular TLM (CTLM), device isolation can be omitted because there is no leakage path for the current flow. The total resistance, R_t, calculation is complex, but when $r/L_t >> 1$, it can be calculated using [Ho99b]:

$$R_t = \frac{R_s}{2 \cdot \pi} \cdot \left[\ln(\frac{R}{r}) + L_t \cdot (\frac{1}{R} + \frac{1}{r}) \right] \tag{2.10}$$

where R_s represents the sheet resistance of p-GaN, R and r denote the radii of the outer and inner circular contacts, respectively, and L_t is the transfer length. The total resistance is measured for different spacings and plotted as a function of $ln(R/r)$. The least square curve-fitting method can be used to obtain a straight linear plot of R_t vs $ln(R/r)$. The slope gives R_s, and the intercept at $ln(R/r) = 0$ is $R_s \cdot L_t / r \cdot \pi$, leading to L_t, so the specific contact resistance, ρ_c, can be expressed as

$$L_t = \left(\frac{\rho_c}{R_s}\right)^{1/2} \tag{2.11}$$

In practice, linear I-V curves cannot always be obtained. To quantify the degree of linearity conveniently, an arbitrary figure of merit [Piq98] is defined as follows:

$$LM = \frac{\frac{dV}{dI}\Big|_{v=5}}{\frac{dV}{dI}\Big|_{v=0}} \tag{2.12}$$

where the derivatives are the resistance at 5V and 0V, respectively, and LM ranges from zero to unity, approaching unity for samples with nearly linear I-V curves.

A good ohmic contact should have a low specific contact resistance, high stability, smooth surface morphology and good edge definition. Because contact resistance usually constitutes a small portion of the total measured resistance, caution must be taken to avoid errors.

Metallic contact layers usually are prepared by vacuum deposition (electron beam or thermal evaporation) followed by heat treatment. The most commonly used method of heat treatment for the metal-semiconductor system is furnace annealing in H_2, N_2, or $N_2 + H_2$ forming gas to protect the contact metals from oxidation. For p-GaN, the annealing environment should not contain H_2, due to the compensation of Mg acceptors with H element [Sug98].

2.3 Ohmic Contact to p-GaN: Present Research Status

Initially, as grown GaN films were unintentionally n-type with a high carrier concentration. This is widely believed to be due to nitrogen vacancies being intrinsic donors [Neu94]. Vacancies result from the large vapor difference between the Ga and N components as shown in Figure 2.7 [Dav99] The nitrogen vacancy lies just below the
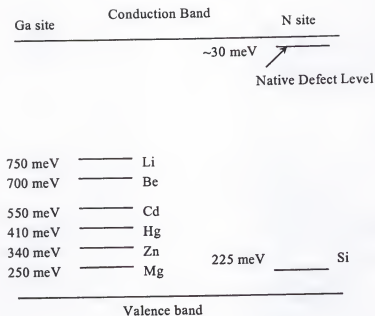
Figure 2.8 Dopant locations in bandgap of GaN [Den97]

conduction band (~ 30 meV), which makes it an efficient donor (Figure 2.8) [Str91, Ben97].

In contrast to n-type, a critical breakthrough was achieved when p-type GaN was reported using Mg dopants followed by low electron beam irradiation (LEEBI) [Aka89]. It has been shown that interstitial hydrogen is incorporated into GaN to form an H-Mg acceptor complex, thus passivating the Mg acceptors. The H-Mg bonds can be broken with LEEBI or high temperature annealing in an inert ambient [Pea96]. Acceptor doping using Be has also been predicted [Ber97]. To understand ohmic contact formation, the subjects of pinned Fermi level, surface cleaning, interfacial metallurgical reactions and data on multilayer metallization schemes are discussed in this section.

2.3.1 Fermi Level Pinning

Semiconductors can be classified into two groups based on the dependence of Schottky barrier height on metal work function. The ionic materials have a direct dependence of barrier height on metal work function whereas covalent materials have a weak dependence, as discussed in section 2.2 and shown in Figure 2.3.

From the ionic nature of GaN (an electron negativity difference of 1.23eV between Ga and N atoms), the Schottky barrier height of GaN is expected to depend directly on the metal work function. The Schottky barrier heights change with the metal work function, but the changes are much less than expected for both doping types of GaN. Mori *et al* [Mor96a] found that the change in Schottky heights is smaller than the difference between the metal work function and the work function of p-GaN for Pt, Ni, Au and Ti metals. The Schottky barrier heights on n-type GaN are also found to depend weakly on the metal work function [Guo95]. In both cases, deposition was made by electron beam evaporation and the contacts were not subjected to heat treatment after deposition. The metal work function was not the dominant factor affecting the Schottky characteristics of Pt and Pd on n-GaN. Rennie et al studied the electrical properties of various metal (Ti, Al, Sn, Cu, Zn, Mo, Ni and Pd) contacts to n-type and p-type GaN in the hope of determining the relationship between metal work functions and barrier heights [Ren98]. Contrary to the expected trend, the Fermi level was calculated to be strongly pinned, with the effect being greater in the p-type material (Figure 2.9). The S factor is shown to be only 0.01 for p-type and 0.21 for n-type GaN (in Figure 2.3), in contrast to the expected $S = 1$ for a completely unpinned Fermi level (Schottky limit).
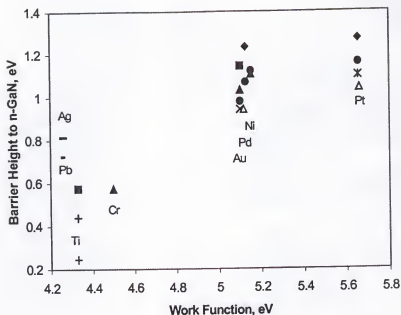
Figure 2.9 Barrier height vs. metal work functions on n-type GaN from various researchers [Cao00]

Another basic consideration is the sum of the p- and n-type Schottky barrier heights for the same metal, which is found to be significantly less than the bandgap of GaN. The measured values of Schottky barrier heights on p-GaN are likely to be affected by the presence of interface states, damage and contamination. More research is necessary to understand the interfacial conditions and properties of metal/GaN contacts.

2.3.2 Surface Preparation of GaN

The preparation of the GaN surface before metallization influences the electrical characteristics of metal/GaN contacts [Kin96]. Cleaning the surface in solvents and common acids or bases is effective in removing a significant fraction of the surface oxides and other contaminants, but these procedures can not produce atomically clean

surfaces. Surface roughness, which can vary depending on the techniques and conditions used to grow GaN epilayers, can influence the uniformity of contacts. One important issue in the processing of ohmic contact to GaN is to understand the semiconductor surface and to find appropriate chemical treatments to clean it before contact metal deposition. Ideally, the metal/semiconductor contact should be oxide- and defect-free, atomically smooth, uniform, and thermally stable.

The most common impurities on the surface after preparation of ohmic contact to GaN include C, H and O from the ambient air, alcohol, methanol, acetone, water, photoresist residues and sample handling, *etc.* [Abe96]. Their effects are discussed below.

2.3.2.1 Hydrogen

A small amount of H_2 in the carrier gas can passivate the electrical activities of Mg and C acceptors in p-GaN during cooling-down from MOCVD growth [Sug98]. This reduces the p-type doping levels unless an annealing step is performed. Annealing at 450 ~ 500°C can restore the free hole concentration but hydrogen atoms do not physically leave the films until a higher (≥800°C) temperature is reached [Pea96]. Low resistivity p-type GaN could be obtained by H_2-free MBE growth without any post-treatment [Sug98].

Hydrogen is predicted to act as a donor (H^+) in p-type GaN, and as an acceptor (H^-) in n-type material [Neu96]. Implantation of $^2H^+$ creates high resistivity materials from both n- and p- GaN [Pea98].

For ohmic contacts to p-GaN, the Mg-H complex may be dissociated at any period during processing. In principle, dissociation of the Mg-H complexes before or

after metallization should have no impact on final resistance. But for Pt/Au, Pt, Pd/Pt/Au and Ni/Au contacts to p-GaN [Kin97], lower ρ_c values were obtained in the absence of premetallization annealing. The post-metallization anneal simultaneously activates the p-dopant and anneals the contact and/or contact interface. Annealing in N_2/O_2 mixture environment decreased the contact specific resistance for ohmic contact to p-GaN by a factor of three [Suz99]. This is attributed to O_2 reacting with H in GaN to form H_2O and uncompensated Mg acceptors. Some researchers disagree with this postulated mechanism.

2.3.2.2 Carbon

Although carbon has been shown to produce p-type GaN, the hole concentration obtained has been limited to 10^{17} cm^{-3} even though the carbon concentration was 10^{20} cm^{-3} or higher [Pan76]. It has been found in other III-V materials that the maximum hole concentration from carbon doping is related to the difference in bond strength between the group III- and group V-carbon sites. In the case of InP, the carbon actually sits on the group III site and acts as a donor resulting in an n-type material. This is also expected to occur in InN and high In concentration alloys of $In_xGa_{1-x}N$ and $In_xAl_{1-x}N$ grown by MOMBE. Carbon has been shown to be a strongly n-type doping element for $x \geq 0.15$ in $In_xGa_{1-x}N$ and $x \geq 0.3$ in $In_xAl_{1-x}N$. As the In concentration is reduced, the tendency increases for carbon to act as an acceptor rather than a donor. It has also been proposed [Abe96] that C displays amphoteric doping behaviors in the nitride with acceptor formation under some conditions (MOMBE grown GaN) and donor formation in other cases (implantation in GaN and growth of In containing alloys).

2.3.2.3 Oxygen

From photoluminescence data [Sei83], it was concluded that oxygen is neither a shallow nor a very deep donor. It has a moderately deep level (about 78 meV below the conduction band edge at 4.2 K) which could form an impurity band near the conduction band edge.

When O is implanted into GaN and annealed at 1100°C [Abe96], it creates n-type doping with an ionization level of ~29 meV. Seifert et al. [Sei83] proposed that substitutional incorporation of oxygen onto nitrogen sites could be the origin of intrinsic free carriers in the growth of highly conductive n-type GaN. Because of the similarity of their atomic radii, both substitutional oxygen and nitrogen vacancies could cause donor defects.

Using an (Al, Ga, In) bubbler to purify the NH_3 during the growth of GaN, a dramatic reduction of carrier concentration in n-GaN is found due to the removal of H_2O/O_2 from the NH_3 [Chu92]. Seifert et al. [Sei83] used Mg_3N_2 to purify the NH_3, and also observed the reduction of as-grown carrier concentrations. Further verification of the contribution of H_2O/O_2 to the increase of the carrier concentration comes from experiments where water is introduced intentionally during growth. The carrier concentrations of the water-injected samples are always above $10^{20} cm^{-3}$.

Chemisorption of oxygen on atomically clean and ordered GaN(0001) surfaces showed that saturation occurs at coverage of 0.4 monolayers [Ber96]. Low energy electron diffraction (LEED) indicates an ordered adsorbate layer, and x-ray photoelectron spectroscopy (XPS) peak of O 1s suggests a single chemically distinct adsorption site.

The oxygen also is reported to react with GaN to form monoclinic β-Ga_2O_3 [Wol97] at 900°C when GaN (both film and powder) is exposed to dry air. An interfacial reaction mechanism is identified as the rate limiting step for oxidation, with an apparent activation energy of ~72 kcal/mole. The oxidation resulted in roughening of the oxide/GaN interface and oxide surface.

2.3.2.4 Cleaning of Surface

As stated earlier, the metal/semiconductor interface should be inert, oxide- and defect- free, atomically smooth and covered by epitaxial metal. For GaAs and other III-V semiconductors, a thin oxide layer (~3 to 20 Å) grows rapidly on the surface when exposed to air, necessitating in-situ cleaning of the GaAs surface under ultra-high vacuum (UHV) for the epitaxial growth of metal films.

For GaN, in-situ deposition of Ga metal followed by thermal desorption under ultra-high vacuum is found to yield atomically clean surfaces using Auger electron spectroscopy (AES) [Kha93]. This has been used in the study of Ni [Ber93] and Al [Ber96b] films on GaN. In-situ nitrogen ion sputtering and annealing can also produce atomically clean GaN surfaces [Ber96a, Hun93].

Ex-situ cleaning is usually used in practical metal deposition. Although solvent cleaning and wet etching with common acids or bases cannot produce atomically clean surfaces, they are effective in removing a significant fraction of the surface oxides and other contamination. This results in relatively intimate metal/GaN interfaces. The effects of aqua regia (HNO_3: HCl = 1:3), HCl: H_2O, HF: H_2O and NH_4OH and NaOH for cleaning the surface of GaN are also investigated [Kin96]. A HCl based solution is found

to be more effective in removing oxides and leaving less oxygen residue, but HF is more effective in removing carbon and/or hydrocarbon contamination. The HCl and HF based solution should be equally effective in removing the total contamination.

The importance of surface preparation is exemplified by cleaning in boiling aqua regia [Kim98] for 10 min and then depositing a layered structure of 200 Å Pd/5000 Å Au in a vacuum of 10^{-7} Torr on p-GaN ($N_h = 2.98 \times 10^{17}$ cm^{-3}). A good contact resistance, ρ_c = 4.3×10^{-4} Ω-cm^2, was obtained on as-deposited samples. With no surface treatment, samples deposited with the same metallization exhibited a high resistance of 2.1×10^{-2} Ω-cm^2. The lower contact resistivity is attributed to removal of the surface oxide from the p-GaN surface. Similarly, with a short time interval between the GaN film growth and metal film deposition, a good ohmic contact is also possible as obtained in Ref. [Jan99] even if the samples are only ultrasonically degreased with trichloroethylene, acetone and methanol for 5 min each step. A contact resistivity of $\sim 3 \times 10^{-3}$ Ω-cm^2 is found for as deposited p-GaN/Pt/Ni/Au samples, and a value of 5.1×10^{-4} Ω-cm^2 is reported after annealing at 350°C for 1 min in an inert ambient.

2.4 Interfacial Metallurgical Reactions

Interfacial reactions are critical to the formation of ohmic contacts to semiconductors, whether they have a large or a small bandgap. Interfacial reactions can lead to disruption of interfacial contamination layers consisting of native oxides, hydroxides, and hydrocarbon/organic residue layers due to reaction or adsorption [Hol97]. Although some work has been reported on contact schemes to p-GaN, little information is available about the metallurgical reactions on the metal/p-GaN system.

Calculations about the transition metal-Ga-N systems have been performed on the metallurgical reactions of metals with GaN in the absence of experimental studies [Moh96]. According to the enthalpy of reactions to form gallides and nitrides, all transition metals can be classified into three groups, the late, early and middle transition metals. They correspond to the gallide-forming, nitride-forming and neutral metals discussed for the "NOG" contact scheme in Chapter 4:

2.4.1 Gallide-forming Metals

These are mainly group VIII metals. The group VIII metals are characterized by the absence of intermediate phases in the metal-N binary systems with either positive or small negative enthalpies of formation (Table 2.1). For Ru, Rh, Pd, Ir and Pt, no metal nitrides have been reported, although these systems have not been investigated thoroughly. The nickel nitrides are believed to be metastable under 1 atmosphere or lower N_2 pressures at and above room temperature, and osmium nitrides are not considered because no thermodynamic data are available. In contrast to nitrides, group VIII metals form many metal gallides, like NiGa, Ni_2Ga_3, etc.

Two types of tie line configurations are predicted for metal-Ga-N phase diagrams for these gallide-forming (late transition) metals. Figure 2.10 shows the Ni-Ga-N tie-line configurations with different N_2 pressures as an example. Changing the pressure of N_2 represented at the top corner of the isothermal phase diagram can alter the tie-line configuration. In an annealing environment, N_2 is also predicted to have effects on how far the metal/GaN reaction can be driven in these systems.
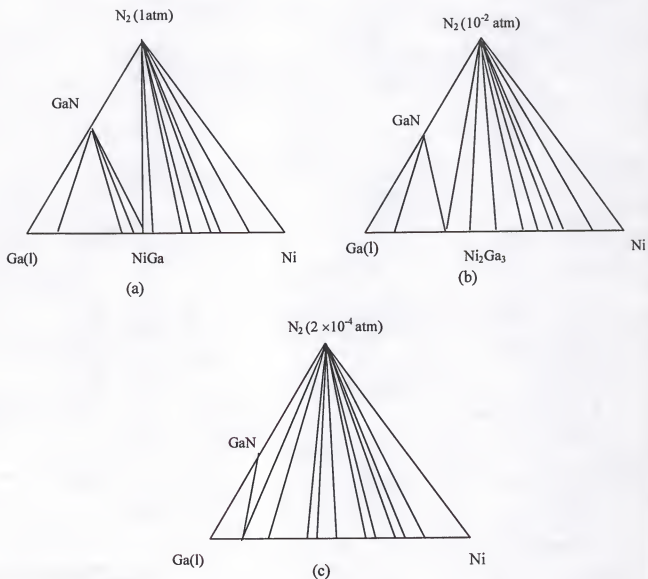
Figure 2.10 Calculated Ni-Ga-N diagram at 600°C. The nitrogen corner of the diagram represents (a) N₂ at 1 atm; (b) N₂ at 10^{-2} atm and (c) N₂ at 2×10^{-4} atm [Moh96]

Higher reaction temperatures increase driving forces for reactions between these metals and GaN. At 600°C, a tie-triangle between NiGa, GaN and N_2 gas at 1 atmosphere is observed (Figure 2.10-a). Assuming that a Ni contact is much thinner than the underlying GaN layer, Ni/GaN is favored to react under 1 atmosphere of N_2 at thermodynamic equilibrium. The entire contact should be converted to NiGa/GaN, and nitrogen gas is released during the reaction. In the calculation, it was also shown that a tie line exists between Ni_2Ga_3 and GaN in the phase diagram. However, the equilibrium partial pressure of N_2 over a Ni_2Ga_3-GaN contact would be less than 1 atmosphere. Thus, there would be a driving force for a Ni_2Ga_3 contact to react with N_2 at 1 atmosphere to form NiGa and GaN. Of course, the reaction would be too slow to be observed, just as in the case of GaN, which does not grow appreciably on liquid Ga at 600°C under 1 atmosphere of N_2, even though the reaction is very thermodynamically favorable.

The prediction of reactions between Ni and GaN is supported by experimental data. The growth of thin Ni films on GaN [Ber93] is examined and a pronounced reaction occurrs upon annealing above 600°C in vacuum. Ga_4Ni_3 is identified by x-ray diffraction (XRD) along with Ni in the as-deposited film [Guo96]. Although no reaction is found for Ni on GaN in as-deposited state, after annealing at various temperatures between 400 and 900°C, a trend of increasing Ga in the reacted films is observed with increasing temperature [Ven97]. New phases consistent with Ni_3Ga and NiGa are found.

The tie-line configuration predicted for these metal-Ga-N diagrams is strongly affected by the stability of the metal gallides, the temperature of the isothermal section and the N_2 pressure of interest. Thermodynamic data shows that Pd and Pt gallides are

Table 2.1 Comparison of experimental and calculated values for the heat of formation ΔH^{for} of related gallides and nitrides. Published experimental values for the entropy of formation, ΔS^{for}, have been added when available. The units for ΔH^{for} and ΔS^{for} are kJ/mol and J/(K·mol) respectively [Boe88]

System	Compound	ΔH^{for}_{exp}	ΔH^{for}_{calc}	ΔS^{for}
Sc – Ga	ScGa	—	– 68	—
Sc – N	ScN	– 157 (T unknown)	– 184	—
Ti – Ga	TiGa	—	– 51	—
Ti – N	TiN	– 169 (298 K)	– 146	– 48
		– 173 (298 K)	—	—
V – Ga	V_2Ga_5	– 11 (763 – 953 K)	– 18	– 3.8 (763 – 953 K)
	V_6Ga_5	– 16 (763 – 953 K)	– 28	– 5.1 (763 – 953 K)
	V_3Ga	– 19 (763 – 953 K)	– 20	– 13.8 (763 – 953 K)
V – N	VN	– 109 (298 K)	– 76	– 45 (298 K)
	V_2N	– 90 (298 K)	– 74	– 33
Cr – Ga	$CrGa_4$	– 7.6 (850 K)	– 8	+ 2.9 (850 K)
	Cr_5Ga_6	– 4.7 (850 K)	– 15	+ 4.8 (850 K)
	Cr_3Ga	– 3.3 (850 K)	– 12	+ 2.7 (850 K)
Cr – N	CrN	– 53 (298 – 1800 K)	– 22	– 35 (298 – 1800 K)
	Cr_2N	– 31 (298 – 1800 K)	– 35	– 17 (298 – 1800 K)
Mn – Ga	MnGa	—	– 34	—
	Mn_3Ga_2	—	– 34	—
Mn – N	Mn_5N_2	– 34 (298 K)	– 44	—
	Mn_4N	– 26 (298 K)	– 31	—
Fe – Ga	$FeGa_3$	– 20 (298 K)	– 10	—
	Fe_6Ga_{11}	– 33 (298 K)	– 16	—
	Fe_7Ga_6	– 35 (298 K)	– 18	—
Fe – N	Fe_2N	– 1.3 (298 K)	– 11	—
	Fe_4N	– 16 (298 K)	– 7	—
		– 2.2 (298 K)	—	—
		– 2.4 (298 – 860 K)	—	—
Co – Ga	$CoGa_3$	– 45 (298 K)	– 18	—
		– 29 (1100 K)	—	—
	CoGa	– 41 (298 K)	– 31	—

Table 2.1 – Continued

		– 32 (298 K)	—	—
		– 36 (1173 K)	—	– 5.4 (1173 K)
		– 38 (1173 K)	—	—
Co – N	Co$_3$N	+ 2 (298 K)	+ 1	—
Ni – Ga	Ni$_3$Ga$_7$	– 34 (300 K)	– 37	—
	Ni$_2$Ga$_3$	– 45 (300 K)	– 33	—
	NiGa	– 38 (300 K)	– 37	—
		– 47 (298 K)	—	—
		– 43 (1023 K)	—	—
		– 43 (1223 K)	—	– 2.9 (1223 K)
	Ni$_3$Ga$_2$	– 36 (300 K)	– 37	—
		– 45 (298 K)	—	—
Ni – N	Ni$_3$N	+ 0.2 (292 K)	+ 6	—
Ru – Ga	RuGa	—	– 34	—
Ru – N	RuN	—	+ 49	—
Rh – Ga	RhGa	—	– 53	—
Rh – N	RhN	—	+ 46	—
	Rh$_5$N	—	+ 11	—
Pd – Ga	Pd$_3$Ga	– 59 (1000 K)	– 51	—
	Pd$_{88}$Ga$_{12}$	– 27 (1000 K)	– 24	—
Pd – N	PdN	—	+ 48	—
	Pd$_5$N	—	+ 12	—
Os – Ga	OsGa	– 28 (298 K)	—	—
Os – N	Os$_5$N	—	+ 12	—
Pt – Ga	Pt$_3$Ga	– 44 (1000K)	– 46	—
	Pt$_{94}$Ga$_6$	– 6.7 (1000K)	– 11	—
Pt – N	PtN	—	+ 62	—
	Pt$_5$N	—	– 18	—

particularly stable among the group VIII metal gallides. The reaction of these metals with GaN is thermodynamically favorable. They form metal gallides and release N_2 gas, even under 1 atmosphere of N_2 at room temperature, although these reactions may be extremely slow at this temperature.

2.4.2 Nitride-forming Metals

Be, Mg, Ca, Sr, Ba, Al and transition metals like Sc, Ti, V, Y, Zr, Nb, La, Hf and Ta are nitride-forming metals. Si can also be classified into this group because of the large enthalpy of the Si-N reaction. The majority of the non-transitional metal-nitrides have low electrical conductivity, hence only the transition metals are considered [Table 2.1]. In contrast to the late transition metals, these early transition metals form metal nitrides of considerable thermodynamic stability. These metal-N binary systems all contain a refractory metal mono-nitride (MN phase). Some of them actually exist over a wide range of compositions and some systems contain nitride phases besides mono-nitride.

In all of the systems for which no ternary phases have been reported (Sc, Y, Zr, La and Hf metals), the common feature in the calculated phase diagrams is a tie line between the MN phase and GaN. Such a tie line would also be expected for the (Nb, Ta, V, and Ti)-Ga-N systems, as long as tie lines to any ternary phases do not alter this situation. At room temperature, the predicted MN-GaN tie lines are stable against competing tie lines by at least 40kJ/g-atom, due to the enhanced thermodynamic stability of the MN phases. Even at 600°C, these tie lines still represent a negative enthalpy of reaction of more than 15kJ/g-atom. Figures 2.11-a and b. show the calculated Zr-Ga-N
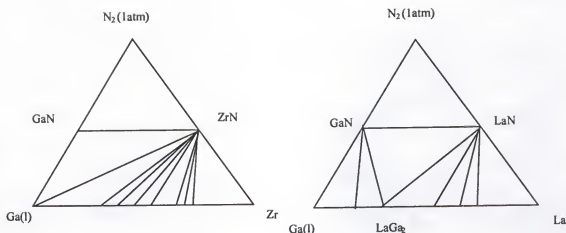
Figure 2.11 Calculated (a)Zr-Ga-N and (b) La-Ga-N isothermal diagram at 298K [Moh96]

and La-Ga-N diagrams. To simplify the diagrams, the ranges of homogeneity of the binary phases are neglected. Taking ZrN as an example, there is not enough data to predict the exact compositional range in equilibrium with GaN. In contrast to the results of gallide-forming metals, the temperature and N_2 pressure represented in the nitrogen corner of the diagram have less dramatic effects on the calculated phase diagrams, at least over the range of temperature and pressure normally encountered in contact processing.

The phase diagram for the Ti-Ga-N system at 800°C is shown in Figure 2.12 [Moh97]. According to this diagram, if a N_2 pressure of 1 atm is maintained continuously over the contact, the Ti/GaN contact would be thermodynamically favorable to extract nitrogen from the annealing environment, ultimately resulting in a TiN/GaN contact. This result is expected because only TiN and GaN are simultaneously in equilibrium with N_2 gas at 1 atm. The contact would therefore come to equilibrium with GaN without any net consumption of GaN through an interfacial reaction. However, there may be competition
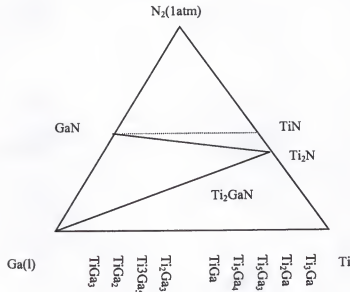
Figure 2.12 Calculated phase diagram for Ti-Ga-N at 800°C [Moh97]

between nitrogen incorporation into the film and metallurgical reaction at the non-equilibrium Ti/GaN interface. Because the Ti contact surface is usually covered by a protective metal layer (like Au), the reaction of metals with the annealing environment is usually hampered. A Ti contact would react with GaN to ultimately form TiN_x and leave liquid Ga remaining on the GaN. This situation is more favored when contacts are annealed under a lower N_2 partial pressure.

Reactions of metals with GaN to form nitrides plus Ga is expected to decrease the hole concentration at the metal/p-GaN interfacial region due to a subsequent increase of N vacancies in the interfacial region. However, before the formation of stable nitride, these metals could allow more nitrogen atoms to diffuse into the semiconductor/metal interface. This can decrease the nitrogen vacancy concentration and is expected to

increase the hole concentration. So, the contact could be expected to exhibit low resistance at short time, but degrade to higher resistance at long time after the formation of stable nitrides. Literature data are discussed relative to this concept in Chapter 5. Specifically, Ta/Ti metallization forms low resistance contact to p-GaN, but degrades after a few days [Suz99]. This is also believed to be the reason that Ti, Al and Ti/Al forms good ohmic contact to n-GaN [Les96, Cor98, Ruv96]. Interfacial reactions should also contribute to ohmic contact of W and WSi$_x$ to n-InGaN and n-InN [Var97a, Var96a, Var97b].

2.4.3 Neutral Metals

Neutral metals include Cr, Mn, Mo, Tc, W and Re. Cr and Mn can form compounds to both Ga and N (see appendix A). The Mo-Ga, W-Ga and Re-Ga binary phase diagrams are characterized by an absence of intermediate phases under atmospheric pressure and negligible miscibility between liquid Ga and the metals. Figure 2.13 shows the W-Ga-N and Re-Ga-N diagrams at 600°C. Both W and Re are expected to be in thermodynamic equilibrium with GaN at room temperature and 600°C. Although W$_2$N, WN and ReN$_{0.43}$ are reported to form, none of these nitrides are expected to be stable at 600°C under 1 atmosphere or lower N$_2$ pressures. Mo is predicted to be more like a gallide-forming metal because a tie-triangle is predicted at 600°C between a metal gallide, GaN and N$_2$ gas at 1 atmosphere in the Mo-Ga-N diagram.

The Cr is found to form a contact with linear I-V curves to p-GaN after annealing at 900°C for 15 sec [Tre97]. This is speculated to result from the reaction of Cr with both Ga and N. This dual reaction may improve the carrier concentration in the metal/p-GaN
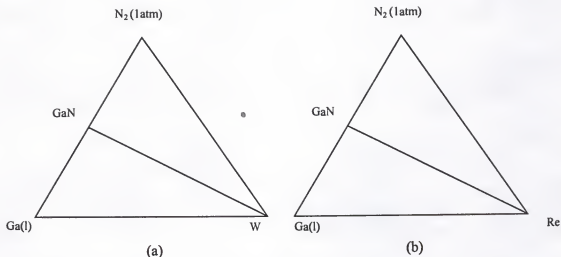
Figure 2.13 Calculated (a) W-Ga-N and (b) Re-Ga-N diagram at 600°C [Moh96]

contact region under some condition, but this improvement may vary in performance with the change of temperature and time.

2.4.4 Thermal Stability

An increase of operating or processing temperature would allow Mg-H complexes to dissociate (to reactivate the p-type dopants), thus the carrier transport via thermionic emission could increase as temperature increased. The kinetics of interfacial reaction may be also increased. All these effects would improve the ohmic contact quality.

The temperature is shown experimentally to have a strong influence on the contact properties. Detailed studies of the electrical properties of the Pt/Au contacts to p-GaN revealed that the I-V linearity improves significantly with measurement at higher temperatures [Kin97]. At room temperature, a slightly rectifying I-V curve is observed, while at 200°C and above the I-V curve is linear. When temperature is increased from 25°C to 350°C, the specific contact resistance is found to decrease by nearly one order of

magnitude. A minimum ρ_c of $4.2 \times 10^{-4} \ \Omega \cdot cm^2$ is obtained for a Pt/Au contact at 350°C. The behavior of Pt, Pd, Ni is also studied on n-GaN as a function of annealing temperature [Dux97]. The Pt film began to form submicron spheres and islands after annealing above 600°C, and the Pd and Ni films changed their morphology to islands for Pd/GaN and Ni/GaN interfaces, respectively. Delamination occurred at Pd/GaN interfaces upon annealing above 700°C, but no delamination occurred at Ni/GaN interfaces because of a SiO_2 cap layer on the Ni film. No structural changes are observed below these temperatures using XRD and RBS analysis.

The delamilation of metal contacts on GaN was explained with the concept of thermal stress generated by differences in thermal expansion coefficients between metals and GaN. The surface energy and linear coefficient of expansion ($6 \times 10^{-6} \ K^{-1}$) of GaN are lower than most metals. Since the thermal expansion coefficient of Pd ($11.7 \times 10^{-6} \ k^{-1}$) is almost twice that of GaN, the change between room temperature and the annealing temperature generates an extension stress causing delamination. It may be necessary to use metals with low surface energies and low thermal expansion coefficients to avoid this delamination problem. Stable, non-reactive contacts that can withstand high temperatures are desired.

It is believed that the current is governed by thermionic emission in current p-GaN samples with carrier concentration level of $10^{17} \ cm^{-3}$. The improvement in I-V linearity at high temperature is attributed to the increase in thermal energy of carriers which enables them to activate over the barrier. On the other hand, because the large ionization energy for Mg, ~250 meV as shown in Figure 2.8, the percentage of activated Mg acceptors is low. The increase of operating energy would increase the activation

percentage of Mg acceptors, and improve the hole concentration. Increased carrier density could lead to field emission or thermionic field emission as the dominant mechanism of charge transport. As temperature increases, the I-V linearity improves and the contact resistance decreases significantly. At temperature above 200°C, the I-V curve exhibits ideal ohmic behavior and the resistance is constant with current.

2.5 Metallization Schemes and Analysis

Of significant interest in the improvement of GaN devices is a p-type ohmic contact of low resistance. Common reported values are around 10^{-2} ohm-cm^2 but a lower limit has been reported of 3×10^{-5} Ω-cm^2 for a doping level of 7×10^{17}cm^{-3} [Suz99]. Recently, contact schemes with better performance have been demonstrated. These include oxidized thin Ni/Au [Ho99b, Koi99] and polarization-charge-based contacts [Li00]. In this section, the current published contact schemes are compared and the mechanisms analyzed. Based on these contact mechanisms, the contact schemes are classified into conventional or non-conventional methods. Conventional methods mean formation of contacts via interfacial reactions to improve doping levels in the contact region in the GaN epilayer. Non-conventional methods used innovative designs to increase the carrier concentrations other than by interfacial metallurgical reactions.

2.5.1 Conventional Contact Schemes

These contacts fall into the scheme of the "NOG" concept developed below in Chapter 5. They will be analyzed in the discussion section in that chapter. In Table 2.2, the contact schemes, processing condition and contact resistivities are summarized.

Table 2.2 Current metallization schemes of ohmic contact to p-GaN

Metalization (*)	ρ_c, Ω-cm^2	N_d(cm^{-3})	Comment	Refer
Au250	53	1×10^{18}	800°C,10 min in N$_2$	[Sim96]
Au100	0.026	Mg 1×10^{20}	AD, 1mA bias	[Mor96]
Au32/Mg32/Au170	214	1×10^{18}	Linear AD, more resistive w/ 750°C,15 sec in N$_2$	[Smi96b]
Co80/Au100	8.1×10^{-3}	1.6×10^{17}	AD	[Fun99]
Cr20/Au300	1.2×10^{-4}	1.4×10^{20}	500°C, 1 min in N$_2$	[Yoo96]
Cr20/Au300	2×10^{-1}	2.7×10^{18}	700°C, 1min in N$_2$	[Yoo96]
Cr20/Au300	1×10^{-3}	1.4×10^{20}	AD	[Yoo96]
Cr50/Au100	$<4.3\times10^{-1}$	9.8×10^{16}	900°C, 15 sec in N$_2$	[Yoo96]
In200/Au100	1.5×10^{-1}	1.6×10^{17}	500°C, 1.5 min	[Fun99]
In15/Zn20/In55/Au100	1.7×10^{-1}	3.1×10^{17}	RT~500°C, 1.5 min	[Fun99]
Mg120/Au100	Bad	1.6×10^{17}	Up to 850°C	[Fun99]
Mn50/Au100	Bad	1.6×10^{17}	Up to 850°C	[Fun99]
Ni100	0.015	Mg 1×10^{20}	AD, 1mA bias	[Mor96]
Ni80/Au100	1.8×10^{-1}	1.6×10^{17}	500°C, 1.5 min	[Fun99]
Ni80/Au100	3.1×10^{-2}	3.1×10^{17}	500°C, 1.5 min	[Fun99]
Ni20/Au500	3.4×10^{-1}	$0.1\sim1\times10^{17}$	500°C, 30 sec	[Kim97a]
Ni10/Au40	$\sim10^{-2}$	8.4×10^{17}	500°C,10 min in vac	[Ish97]
Ni10/Au5	$<10^{-4}$	$2*10^{17}$	400~500°C, 10min in O$_2$	[Ho99a]
Ni5/Au5	4×10^{-6}	$2*10^{17}$	500°C, 10min in air	[Ho99b]
Ni80/Au100	3.8×10^{-1}	2.2×10^{17}	500°C, 1.5 min	[Fun99]
Ni?/Au?	1.2×10^{-2}	5.5×10^{16}	1mA bias,700°C, 10 min	[Kin97]
Ni15/Cr15/Au500	$\sim8.3\times10^{-1}$	$0.1\sim1\times10^{17}$	500°C, 30 sec in N$_2$	[Kim97a]
Ni15/Cr15/Au500	8.3×10^{-2}	$0.1\sim1\times10^{17}$	AD	[Kim97a]
Ni25/Mg5/Ni25/Si240	9.6×10^{-4}	3×10^{17}	400°C, 10min PR/30 min RTA in N$_2$	[Kam98]
Ni25/Mg11/Ni25/Si240	6.6×10^{-3}	3×10^{17}	400°C, 10min PR/30 min RTA in N$_2$	[Kam98]
Ni25/Mg8/Ni25/Si240	2.2×10^{-3}	3×10^{17}	400°C, 10min PR/30 min RTA in N$_2$	[Kam98]

42

Table 2.2- continued

Metallization	ρ_c	N_D	Conditions	Ref.
Ni25/Mg8/Ni25/Si240	2.5×10^{-3}	3×10^{17}	450°C, 30 min in N$_2$	[Kam98]
Ni25/Mg8/Ni25/Si240	4.5×10^{-3}	3×10^{17}	500°C, 30 min in N$_2$	[Kam98]
Ni8/Zn132/Au100	2.5×10^{-1}	3.1×10^{17}	400°C, 1.5 min	[Fun99]
Ni45/Zn-Au46	3.6×10^{-3}	4.4×10^{17}	600°C, 2 min in N$_2$	[You98]
Ni2.5/Zn10/In10 /Ni47.5/Au100	2.3×10^{-1}	2.2×10^{17}	600°C, 1.5 min	[Fun99]
Pd20/Au500	9.1×10^{-3}	9×10^{16}	500°C, 30 sec in N$_2$	[Kim97b]
Pd20/Au500	9.1×10^{-3}	9×10^{16}	500°C, 30 sec in N$_2$	[Kim97b]
Pd20/Au500	2.9×10^{-2}	2.98×10^{17}	AD, no clean, 3×10^{-7} Torr	[Kim98]
Pd20/Au500	4.3×10^{-4}	2.98×10^{17}	AD,	[Kim98]
Pd20/Au20/Pd20/Au500	$\sim9\times10^{-3}$	9×10^{16}	AD	[Kim97b]
Pd20/Au20/Pd20/Au500	$\sim9\times10^{-3}$	9×10^{16}	500°C, 30 sec in N$_2$	[Kim97b]
Pd20/Au20/Pt20/Au500	$\sim9\times10^{-3}$	9×10^{16}	AD	[Kim97b]
Pd20/Au20/Pt20/Au500	Mid 10^{-2}	9×10^{16}	500°C, 30 sec in N$_2$	[Kim97b]
Pd?/Pt?/Au?	1.0×10^{-2}	$5\sim6\times10^{16}$	1mA bias, 700°C, 10 min	[Kin97]
Pd?/Pt?/Au?	1.7×10^{-2}	$5\sim6\times10^{16}$	1mA bias, AD	[Kin97]
Pt?	3.4×10^{-2}	5.5×10^{16}	1mA bias, AD	[Kin97]
Pt100	1.3×10^{-2}	Mg 1×10^{20}	AD, 1mA bias	[Mor96]
Pt?/Au?	5.7×10^{-3}	5.5×10^{16}	750°C, 10min, cap/GaN	[Kin97]
Pt20/Au300	$\sim1.8\times10^{-3}$	1.4×10^{20}	AD	[Yoo96]
Pt20/Au300	2×10^{-1}	2.7×10^{18}	700°C, 1min in N$_2$	[Yoo96]
Pt/Au	4.2×10^{-4}	$5\sim6\times10^{16}$	Measured at 350°C	[Kin97]
Pt20/Ni30/Au80	$\sim3\times10^{-3}$	3×10^{17}	AD	[Jan99]
Pt20/Ni30/Au80	5.1×10^{-4}	3×10^{17}	350°C, 1min in N$_2$	[Jan99]
Ta50	$>10^{-3}$	7×10^{17}	800°C, 20min/Vac	[Suz99]
Ta60/Ti40	3×10^{-5}	7×10^{17}	800°C, 20min/Vac	[Suz99]
Ti50	$>10^{-3}$	7×10^{17}	800°C, 20min/Vac	[Suz99]
Ti100	3.5×10^{-2}	Mg 1×10^{20}	AD, 1mA bias	[Mor96]
Ti20/Pt80/Au300	4×10^{-4}	1.4×10^{20}	AD	[Yoo96]
Ti20/Pt80/Au300	2.5×10^{-3}	2.7×10^{18}	700°C, 1min in N$_2$	[Yoo96]
Zn50/Au100	4.9×10^{-2}	1.6×10^{17}	750°C, 1.5 min	[Fun99]

Metallization thickness unit: nm

?: Not reported;

AD: As Deposited.

2.5.2 Non-conventional Contact Schemes

Recently the use of thin Ni/Au to p-GaN for both low resistance and high-transparency ohmic contact has been extensively studied [She99b, Koi99, Ho99a, Ho99b, Che99, Mae99]. Transparent NiO is a p-type semiconductor with a wide bandgap, which varies from 3.6 to 4.0eV [Sat93]. Lower specific contact resistance values (<1.0×10^{-4} Ω cm^2 for 100Å Ni/50ÅAu and later of 4×10^{-6} Ω-cm^2 for 50Å Ni/50Å Au) are obtained [Ho99a, Ho99b]. Some Au-based contacts (Ni/Au, Co/Au, Cu/Au, Pd/Au and Pt/Au) annealed in an O_2 partial pressure are also found to reduce the contact resistance, ρ_c, and the sheet resistivity of p-GaN epilayers (ρ_s) [Koi99].

While significant progress has been made on ohmic contacts to p-GaN by oxidizing the thin Ni/Au, different mechanisms have been suggested to explain the results. Murakami's group [Koi99] ascribed the low contact resistance to formation of an intermediate semiconductor layer (ISL) with high hole concentration caused by removal of hydrogen atoms which were bonded with either Mg or N atoms in the p-GaN epilayer. Ho et al [Ho99a, Ho99b, and Che99] explained the results as being due to the formation of a p-NiO layer directly on the p-GaN layer surface. This NiO layer is believed to act as a low barrier ISL and small islands of Au bridged the current path via electron tunneling. This microstructure resulted in the reduction of the Schottky barrier height (ϕ_b) at the p-GaN/metal interface. However, Murakami's group [Mae00] further studied a variety of Ni/Au based contacts, such as 500Å NiO/500Å Au, 500Å NiO (Li)/500Å Au, 50Å Ni/500Å NiO (Li)/50Å Au, 50Å Ni/200Å Li_2O/500Å NiO/500Å Au and 50Å Ni/200Å Li_2O/50Å Ni/500Å NiO/500Å Au (much thicker than the 50Å Ni/50Å Au in Ho's work),

using a method of sputter deposition and annealing in an O_2 ambient for 5min in the temperature range of 300 to 500°C. They found that all contact schemes with NiO midlayer did not reduce the ρ_c to values lower than the conventional Ni/Au contact annealed in N_2 ambient. From these results, they concluded the p-NiO did not act as the ISL to reduce the Schottky barrier height at the p-GaN/Au interface.

Although, the resistivity of NiO can be decreased by an increase in Ni^{3+} ions, or addition of monovalent atoms, such as lithium, or increased nickel vacancies and/or interstitial oxygen concentration [Ant92], NiO usually remain very resistive [Sat93]. Stoichiometric NiO is an insulator with a resistivity of the order of 10^{13} Ω-cm at room temperature [Adl70]. Because of the insulation of NiO, the poor contact performance in the work of [Mae00] might be due to the large thickness of NiO film and non-epitaxial sputtered NiO in the contacts, resulting in larger resistance in the contact. The data from those contacts with thick NiO layers may be insufficient to evaluate the role of p-NiO, as proposed by Ho [Ho99b].

An interesting scheme was proposed to form ohmic contacts to p-GaN using internal electric field caused by polarization effects [Li00]. Due to spontaneous and piezoelectric polarization effects, sheet charges can be induced in the $Al_xGa_{1-x}N/GaN$ materials system, and low specific contact resistance can be attained in contacts based on polarization fields at lower doping levels. In this way, a polarization-charge-based contact becomes a viable alternative to the formation of ohmic contacts to p-GaN. Experimental work showed that a spontaneous polarization vector could be formed and pointed to the substrate in the $Al_{0.2}Ga_{0.8}N/GaN$ superlattice structure. Ni contacts to this

structure resulted in a specific resistivity of 9.3×10^{-4} Ω-cm^2 after annealing at 400°C for 300sec.

CHAPTER 3
EXPERIMENTAL PROCEDURES

3.1 Introduction

This chapter describes the experimental procedures that were followed for sample cleaning and preparation of electrical contact to p-GaN. The procedures consisted of an initial cleaning of the samples followed by metal contact deposition. These contacts were then heat treated and characterized in terms of their electrical properties, surface composition, surface morphology and interfacial reaction products.

3.2 Contact Preparation

The p-GaN films used in these experiments were either purchased from SVT Associates grown with a Molecular Beam Epitaxy technique (referred to as MBE-GaN, 1μm-thick) or grown by low pressure Metalorganic Chemical Vapor Deposition (referred to as MOCVD-GaN, 2.5μm-thick). Mg and Si were used as doping elements in p- and n-type GaN, respectively. The SVT 1μm-thick p-GaN epitaxy film was grown on the c-plane of sapphire substrates with an rf N_2 plasma and a solid Ga source. The substrate temperature was of 700^oC and the growth rate was of 0.5μm/hr. A 350Å-thick AlN was used as a buffer layer before the deposition of a 1μm thick p-type GaN film using elemental Mg as the p-type dopant. The GaN film was as-grown p-type with no post-growth activation. SIMS data showed about 10^{20} cm^{-3} for the actual level of Mg in the film. A hole concentration (p-type) of $1.1 \sim 3.5 \times 10^{17}$ cm^{-3}, and an electron

concentration of $7 \sim 9 \times 10^{18}$ cm^{-3} (n-type) were measured by Hall measurement at room temperature for the MBE- and MOCVD- GaN.

For the H_2O_2 treatment experiments, samples (5 mm × 5 mm) were cleaned with ultrasonically agitated acetone (5 min), methanol (5 min) and boiling aqua regia (10 min) sequentially before being flushed with DI water. All samples were blown dry with N_2 gas between each step. These samples were then quickly placed into an electron beam evaporator system for contact deposition (using the "NOG" metallization principles as developed in Chapter 5), through a van der Pauw shadow mask [10] at a base pressure of $<10^{-6}$ Torr. One sample was not treated further, i.e. kept in the as-cleaned state with contacts deposited. Other samples (with contacts on the surface) were immersed in H_2O_2/H_2O solutions (1:1 and 1:5) for 30 sec or 300 sec followed by DI water rinse, N_2 blow dry, and a short time (<60sec) dry at 80°C in air.

The contact metals used in the "NOG" scheme consisted of Ni/Au, Ni/Ti/Au, Ag/Ti/Au, Ni/Al/Au, Pt/Au, Pt/Si/Pt/Au and Pt/Mg/Pt/Au with the first listed metal being deposited first and adjacent to the GaN. The Ni/Au and Pt/Au were mainly used for comparison, and the first layer of either gallide-forming metal (Ni, Pt), or neutral metal (Ag) was used to study the effects of different gallide-forming metals on the contact resistance. Ti, Al, Mg, Si were used as the second layer because they are nitride-forming metals. It is difficult for Al to absorb H from the GaN lattice, therefore metallization with Al were evaluated to test whether the contact resistance was decreased when using an Al layer. If it is, this would argue against H extraction postulated by Suzuki *et al* [Suz99]. Al reacts readily with O to form an insulator, Al_2O_3, which is expected to increase the specific contact resistance. Mg was used because it is the p-type doping element in p-

GaN. It was postulated that Mg in the metallization would increase the hole concentration in the contact interface region. Si was tested because of its strong tendency to form nitrides (Deh93).

All samples were degreased prior to deposition using ultrasonicated acetone followed by methanol, each for 5min., and blown dry by N_2. Any native oxide was then removed using boiling aqua regia for 10min followed by a 5min DI rinse and N_2 blow dry. Either regular (square) TLM patterns or circular TLM (CTLM) patterns, discussed in Chapter 2, was used for contact resistivity measurements. For square TLM patterns, the leakage path was isolated with a technique of inductively coupled plasma (ICP) dry etching using $Ar + Cl_2 + N_2$ plasma under a pressure of 5 mTorr. For the CTLM patterns, the outer ring contact of the mask has a diameter ($2R$) of $350\mu m$ and the inner dot contact's diameters vary ($2r$) between 340 to 310 μm to result in contact distances of 5, 10, 15 and $20\mu m$. Ohmic contacts are characterized by plotting the total resistance versus the contact spacings. The specific contact resistance and sheet resistance were derived from this plot as discussed in Chapter 2. The CTLM pattern was transferred to the multilayer metal contacts by a photolithographic lift-off process. Positive photoresist (AZ1529) were used in these experiments. Prior to metal deposition the samples were etched with 10% diluted HF for 30sec to remove native oxides. The samples were then immediately introduced into the vacuum chamber for contact deposition.

For contacts used in Hall measurements, the Van der Pauw configuration [Van58] was employed to determine both the Hall coefficient and the resistivity of the GaN films, as shown in Figure 3.1. Dot contacts of multiple metal layers of 25Å Ni/500Å Ti/500Å Au and 100Å Ni/500Å Ti/500Å Au were used to form the ohmic contacts to p-GaN.
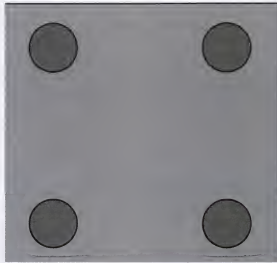
Figure 3.1 Configuration of contacts used in Hall measurement.

These contacts were deposited through a shadow mask with the dot size of $\Phi 0.4$mm, and the distance between two contacts of 4mm.

All contacts were deposited in an electron beam evaporation system with a glass bell jar. The system was pumped with a Varian oil diffusion pump backed by a two-stage mechanical rotary vane pump, providing a base pressure of $10^{-6} \sim$ low 10^{-5} Torr. The metal charge in the electron beam well consisted of metal pellets with the following purities: Ni (Target Materials Inc., 99.98%); Ti (Cerac, 99.95%); Au (Materials Research Corporation, 99.95%); Pt(99.95%, Johnson Matthey, Inc.), Al (Cerac, 99.99%), Mg (Cerac, 99.99%), Si (semiconductor grade) and Ag (Cerac, 99.99%). The metal layer thickness was monitored using a quartz crystal oscillator. The contact thickness varied with different experiments and will be noted in the results sections.

For RTA (Rapid Thermal Annealing) experiments, all metallization schemes were heat treated in a custom 50cm quartz tube with a 25cm hot zone and flowing N_2 or O_2

(high purity, 99.995%) as the ambient. The gas flow rate was monitored with a

MANOSTAT® flow meter with a typical setting of 110 standard cubic centimeter per

minute (sccm).

3.3 Characterization

Contacts on GaN were characterized in the as-deposited state and following each

of the above described heat treatments. Their electrical properties (I-V) and surface

composition, surface morphology and interfacial reaction products were also

characterized. A group of characterization techniques of I-V, light transmittance

measurement, Hall measurement, Auger electron spectroscopy (AES) [Bru92], X-ray

photoelectron spectroscopy (XPS) [Sib96], scanning electron microscopy (SEM) [Lee93]

and transmission electron microscopy (TEM) were used in this study.

The electrical properties of all contacts were investigated using room temperature

current-voltage (I-V) measurements between two front surface dot contacts or the

concentric dot/ring pattern described above. The I-V data were obtained by measuring the

current flow between two adjacent top contacts under an applied bias. The ohmic or

rectifying nature of the contacts could be determined by the linearity of the I-V curves

and total resistance. The reverse-bias breakdown voltage of rectifying contacts could also

be determined from their I-V characteristics.

To evaluate the possibility of increased electrical conductivity from surface

leakage current after the H_2O_2 treatment in Chapter 4, all of these samples were measured

after contact deposition, and then cleaned with acid ($1HCl + 2H_2O$) followed by base

($1KOH + 2H_2O$) solutions for 10 min in each step, and rinsed with DI water after each

cleaning step. The I-V data were collected again without additional treatment. As shown

below, the I-V data were unchanged by this treatment.

The light-transmission characteristics of the Ni/Au and Ni/Au/Ni contacts (in

Chapter 5) were measured with a commercial Zeiss UV grating monochrometer over the

wavelength range of 300 to 700nm. The light transmission through the GaN film with

and without the metal contact were measured on each sample at either a fixed or variable

wavelength (Figure 3.2). The ratio of these two transmission values (I_1/I_2) at $\lambda = 450$nm

was reported as the light transmittance through the Ni/Au "transparent" ohmic contacts.

The repeatability of the data were checked with three sets of data obained from each

sample. The data reported are generally the average of these three measurements.

For Hall measurements, a computer controlled MMR$^{®}$ commercial measurement

system was used. The Van der Pauw method [Van58] was employed to determine both

the Hall coefficient and the resistivity of the films. Dot contacts of 100Å Ni/500Å Ti/

500Å Au were used for p-GaN. All were deposited with an electron beam evaporator
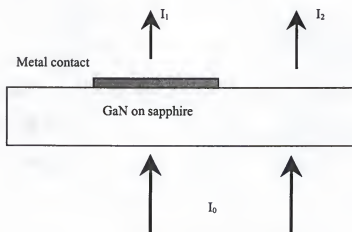
Figure 3.2 Schematic of light transmittance measurement

through a shadow mask. The dot diameter was of 0.4 mm, and the distance between two contacts was 4 mm. A magnetic field of 3 kilo-Gauss was chosen automatically by the computer program to improve the accuracy of the Hall coefficient and resistivity values.

Scanning electron microscopy (SEM, JEM 6400) was used in the secondary eletron or back scattering eletron mode to characterize the surface morphology of the grown films as well as the deposited layers in an attempt to determine the microstructure evolution and possible flaws that could cause high contact resistance.

Transmission electron microscopy (TEM, JEOL 200CX) was performed with 200 keV acceleration voltage for plane view analysis after H_2O_2 solution treatment to detect any defects in MBE-GaN

The surface of the GaN film was characterized by atomic force microscopy using a Nanoscope III system from the Digital Instruments, Inc. The AFM was operated in the tapping mode, and the height data was used in this work.

Auger electron spectroscopy (AES) [Bru92] was used to measure the elemental composition of the atoms in the surface region using a Perkin-Elmer PHI Model 660 scanning Auger microprobe (SAM). AES surface N(E) survey spectra from these GaN samples were recorded over the energy range of 50 to 2050 eV using a 5 keV, 30 nA electron beam with a diameter of ~1 μm. Depth profiles were also collected. With this technique, all elements of the layers can be determined except for H and He and generally down to a value of 0.1~ 1at%. The interfaces of the layers can be analyzed with a resolution approaching 100Å to determine possible compound formation.

X-ray photoelectron spectroscopy (XPS) [Sib96] or electron spectroscopy for chemical analysis (ESCA) is an analytical technique similar to AES except the incident

energetical beam is x-rays. This technique is usually used for chemical state identification of surface species. XPS was used in this study to provide information on chemical bonding and compound formation that were not apparent from AES profiles. These measurements were performed with a Perkin-Elmer PHI Model 5100 ESCA system. Two large samples were used (10×10 mm) in this analysis. The ESCA data were collected using an Al X-ray source (K_α, hv = 1486.6 eV) and a hemispherical analyzer set at a pass energy of 35.75 eV. For these studies the ESCA source area was 4 mm × 6 mm.

Secondary ion mass spectrometry (SIMS) was used to determine impurity levels at the surface or in the films through depth profiling and was used to measure trace dopant profiles through the structure. SIMS is capable of quantifying the impurity levels for many elements depending on their detection sensitivity. However, SIMS has a limited possibility of providing useful information following heat treatments when diffusion distance are large. In this work, SIMS was used to detect the oxygen and hydrogen impurity levels in the H_2O_2 treated samples. This analysis were performed using a Cs^+ primary ion beam and negative secondary ion detection. The raster size was 250×250 μm^2, and the counts were taken only from the central 75×75 μm^2.

CHAPTER 4
EFFECTS OF H_2O_2 SOLUTION TREATMENT ON p-GaN

4.1 Introduction

As described in Chapter 2, the high vapor pressure difference between gallium and nitrogen in GaN could lead to preferential loss of nitrogen and a gallium-rich surface. In this Chapter, stabilization of the surface of MBE grown GaN with H_2O_2 solutions is demonstrated. It is found that the H_2O_2 treatments are able to increase the carrier concentration by a factor of two. and lead to higher current levels through contacts for MBE p-GaN.

As discussed in Chapter 2, oxygen is reported to react with GaN to form monoclinic beta-Ga_2O_3, with many polytypes being observed [Wol97, Roy52]. Annealing GaN in a O_2 ambient is reported to dissociate the Mg-H complex and reactivate the Mg acceptors [Suz99]. Also, cleaning in common acids or bases or solvent is effective in reducing the amount of surface oxides and other contamination. The effects of aqua regia ($1HNO_3 + 3HCl$) [Kim98], HCl [Kin96], HF [Kin96], KOH [Lee99], and $(NH_4)_2S$ [Cao00] on removing of native oxides on GaN have been reported.

This chapter describes how H_2O_2 solution was used to clean/passivate the p-GaN film after contact deposition. Hydrogen peroxide was shown to increase the epilayer conductivity. Hydrogen peroxide is an active oxidant, and may be expected to react with GaN to form gallium oxide and/or gallium hydroxide to break up the Mg-H complexes and reactivate the Mg acceptors. These effects will be discussed.

54

For I-V and Hall measurements, two types of metallization were used. For the treatments using $1H_2O_2:5H_2O$ (volume ratios hereafter referred as 1:5), and 1:1 solutions, a contact scheme of 25Å Ni/500Å Ti/500Å Au was used, where the first metal layer is deposited onto the GaN epilayer. For treatments with 5:1 and "pure" (37%) H_2O_2, the contacts are 100Å Ni/500Å Ti/500Å Au, because this contact scheme led to higher current and more linear I-V curves, as discussed in Chapter 5.

4.2 Modification of Electrical Conductivity

4.2.1 Effects of H_2O_2 Concentration

Remember, for these experiments, dot contacts were deposited onto GaN epilayer as described in Chapter 3 using a shadow mask., then the entire sample, including the contacts were treated with H_2O_2 solution. The I-V results after immersing the sample in 1:5 or 1:1 solutions are shown in Figure 5.1. The current transported in the samples was found to increase as the soaking time and H_2O_2 concentration increased from 30 to 300 sec and from 1:5 to 1:1, respectively. Compared to the as-cleaned state, an increase of ~100% in the magnitude of current was found after immersion in the $1H_2O_2:1H_2O$ solution for 300sec as shown in Figure 4.1a.

The I-V curves after immersion in the 5:1 and "pure" H_2O_2 treatment are shown in Figure 4.2. Straight, linear I-V curves were found for as-deposited contacts of 100Å Ni/500Å Ti/500Å Au treated with concentrated H_2O_2 solution (Figure 4.2), as compared to those with the 25Å Ni/500Å Ti/500Å Au contacts and treated with a solution with lower H_2O_2 concentration (Figure 4.1). The highest currents were achieved in the 5:1 treated samples. In the as-deposited state, after a "pure" H_2O_2 treatment, the highest
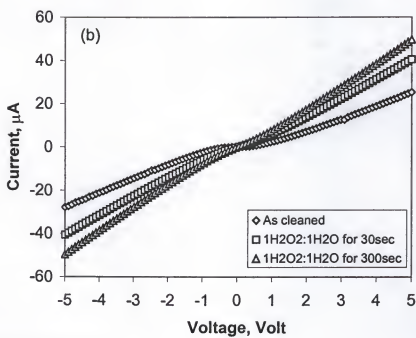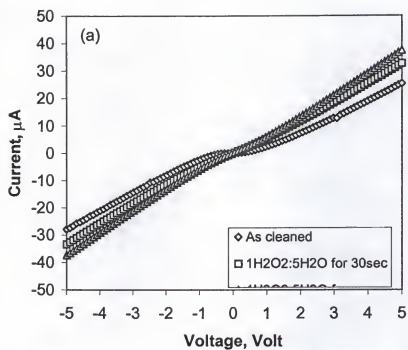
Figure 4.1 Effects of H_2O_2 solution treatment on the I-V curves of 25Å Ni/500Å Ti/500Å Au to MBE p-GaN. (a) 1:5 solution; (b) 1:1 solution
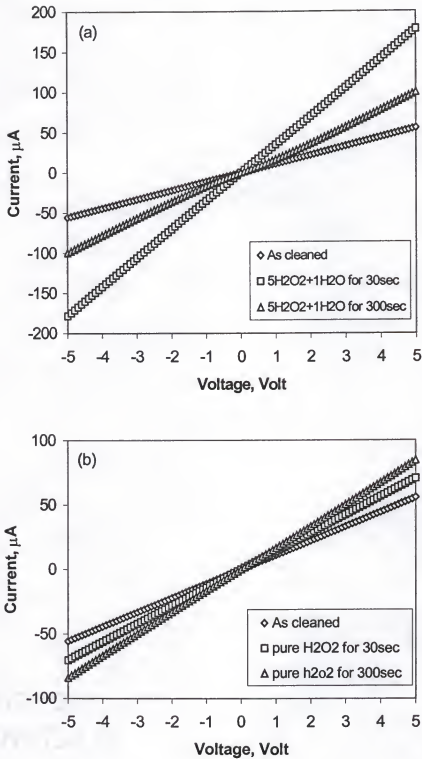
Figure 4.2 Effects of H_2O_2 solution treatment on the I-V curves of 100Å Ni/500Å Ti/500Å Au to MBE p-GaN. (a) 5:1 solution; (b) "pure" (37%) H_2O_2
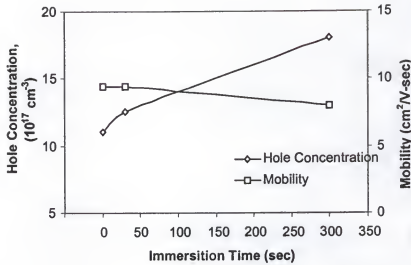
Figure 4.3 Hall measurement results of MBE p-GaN after immersion in 1:1 solution.

current increase after 300sec was ~50%, while the increase after a 5:1 solution treatment was ~200%. For samples treated in 1:5 and 1:1 solutions, the increases in current at 5V are 41% and 89% respectively with a treatment of 300sec.

The Hall data for the samples treated with 1:1 solutions are shown in Figure 4.3, An increase of about 70% was found for the carrier concentration after immersion for 300sec, consistent with the increased current found for the treatment. The decrease in hole mobility is within experimental errors.

4.2.2 Effects of Extended Immersion Time

Using the 5:1 solution, the effects of 20 to 60 min extended treatment times were studied. The I-V data are shown in Figure 4.4 and the Hall data are shown in Figure
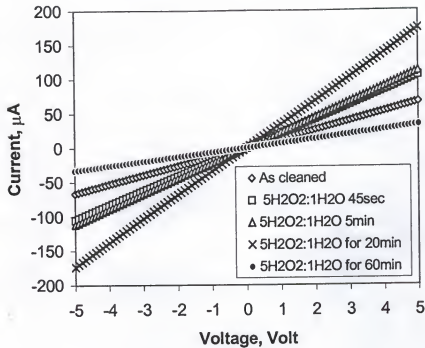
Figure 4.4 Effects of H_2O_2 solution treatment with extended time on the I-V curves of 100Å Ni/500Å Ti/500Å Au to MBE p-GaN.

4.5. Compared to as cleaned (no H_2O_2 treatment), an immersion time of 20min resulted in a 200% increase in the current level. As the immersion time was further increased to 60min, the current level dropped to ~50% of the as cleaned state. These Hall data show that the hole concentration and mobility first increase and then decrease as the immersion time increase, consistent with the I-V data.

For MBE-GaN, n-type GaN was also treated with H_2O_2 for times of 10, 30, 300, 1200 and 3600sec using the 5:1 solution. The Hall data are shown in Figure 4.6. Short treatment times did not change the electron concentration or mobility within experimental error. At 30 and 300sec, the electron concentration increased (~12%), but these changes and the mobility changes are still in experimental errors (~15%).
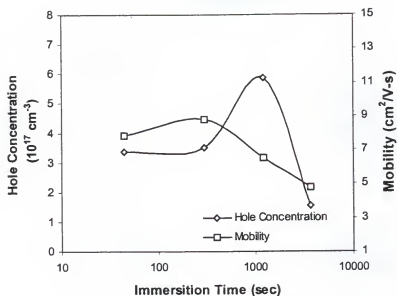
Figure 4.5 Effects of 5H$_2$O$_2$: 1H$_2$O solution treatment with extended time on Hall measurement results of 100Å Ni/500Å Ti/500Å Au to MBE p-GaN.

All these results were obtained on epilayers of p- or n-GaN grown on sapphire by MBE, as described in Chapter 3. For comparison, epilayers grown by MOCVD were also treated with the same solutions and methods. The I-V and Hall data as shown in Figure 4.7, and no changes above the experimental noise levels were detected, even after treatment time up to 60min. Thus the effects of peroxide treatment depend upon the growth history of the p-GaN

4.2.3 Stability of the Increased Electrical Conductivity

The stability with time of these modified electrical properties was monitored with I-V and Hall measurements every two days for two weeks. The improved electrical
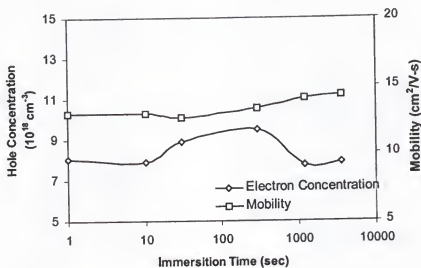
Figure 4.6 Hall measurement results of $5H_2O_2$: $1H_2O$ solution treated MBE n-GaN
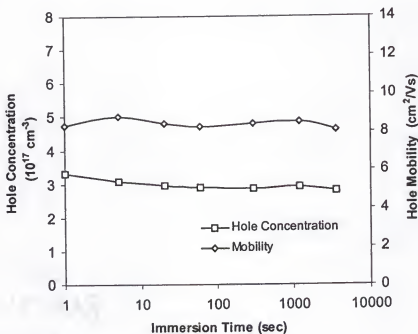
Figure 4.7 Effects of H_2O_2 treatment on MOCVD p-GaN.
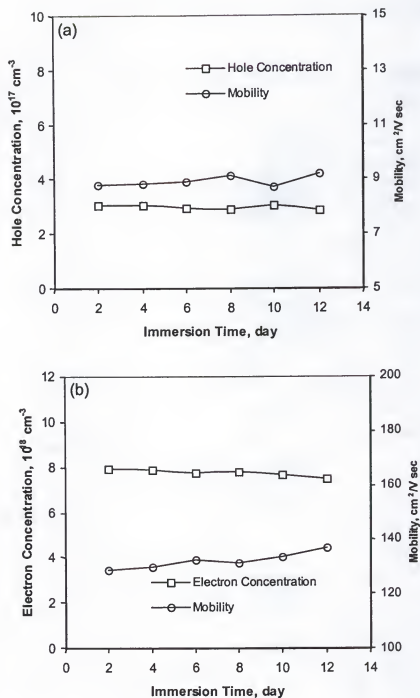
Figure 4.8 Hall measurement on stability of H_2O_2 treated samples. (a) n-GaN; (b) p-GaN. Both were treated with 5:1 solution for 20min.

Table 4.1 Atomic concentration of elements from AES surface survey analysis in MBE p-GaN after a $xH_2O_2:yH_2O$ treatment for either 30 or 300sec

	As cleaned	1:5 for 30sec	1:5 for 300sec	1:1 for 30sec	1:1 for 300sec
C	4.9	6.3	5.2	5.9	3.5
Cl	1.9	1.0	1.1	0.8	1.0
Ga	52.0	48.5	47.6	47.2	49.0
N	33.7	36.4	39.1	37.5	39.4
O	7.6	7.8	7.0	6.7	7.1

conductivity was found to be very stable. Figure 4.8 shows the Hall data for (a) p-type, and (b) n-type GaN treated with 5:1 solution for 5min and 20min respectively.

4.3 Structural Characterization

4.3.1 AES

Auger peaks from Ga, N and O plus C and Cl were detected from samples after aqua regia cleaning and minimum exposure to air. The surface composition changed after the H_2O_2 solution treatment, as shown in table 4.1. Compared to the as-cleaned state, a slight increase of N ($3 \sim 6\%$) and a slight decrease of Ga ($3 \sim 5\%$) were found. Small increases of C (except for the 1:1 for 300sec treatment) and decreased Cl also resulted from the H_2O_2 soaking. The atomic concentrations of oxygen remained fairly constant instead of increasing with the H_2O_2 immersion. This result was surprising because oxide or hydroxide formation was expected from this treatment of the GaN surface due to the reaction with H_2O_2.

4.3.2 ESCA

The ESCA spectra for the Ga 2p, Ga 3d and O1s photoelectron peaks are shown in Figure 4.9 for the as-cleaned (boiling aqua regia, no H_2O_2 treatment) and soaked ($1 H_2O_2$:1 H_2O solution for 300sec) surfaces. The $Ga2p^{1/2}$ and $Ga2p^{3/2}$ peaks are at binding energies of 1118.5 and 1145.4 eV, similar to standard data [Mou95]. Comparing the peaks of samples before and after H_2O_2 immersion, no binding energy shift in the $Ga2p^{1/2}$ and Ga $2p^{3/2}$ spectra (Figure 4.9-a) were found. However, energy shifts of 0.85 and 1.1 eV to higher binding energies were measured for the Ga 3d (Figure 4.9-b) and O 1s (figure Figure 4.9-c), respectively, as shown in Table 4.2.

4.3.3 SIMS

Secondary ion mass spectrometry (SIMS) depth profiling was performed to determine any changes in the Ga, N, O and H levels. Two different sites were analyzed in each sample. While no significant variation in Ga and N levels were found, large differences in the levels of H and O were found between the two sites on each samples. The results are shown in Figure 4.10 for each sample. These results suggested that the H and O levels were not uniform and had large variations even over the same sample. Because the impurities were not uniform, systematic comparison of O and H levels with the change of immersion time was impossible by SIMS.

4.3.4 AFM

The AFM technique was used to characterize the surface morphology of both MBE- and MOCVD-GaN epilayers with and without H_2O_2 treatments.
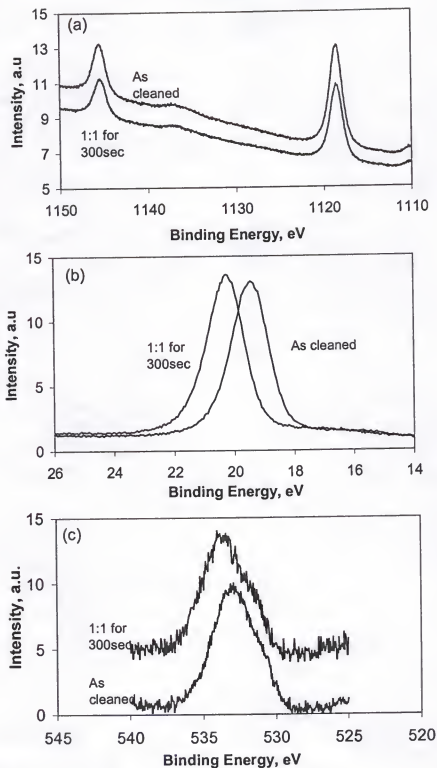
Figure 4.9 Comparison of XPS peaks from as-cleaned and 1:1, 300sec H_2O_2 treated GaN. (a)Ga 2p; (b) Ga 3d; (c)O 1s.

Table 4.2 XPS results from a 1:1, 300sec H_2O_2 cleaned p-GaN sample

Surface Treatment	Ga2p3/2	Ga2p1/2	Ga3d	O1s
As-cleaned	1118.5	1145.3	19.4	532.9
$1H_2O_2$:$1H_2O$ for 300sec	1118.5	1145.3	20.25	534.0
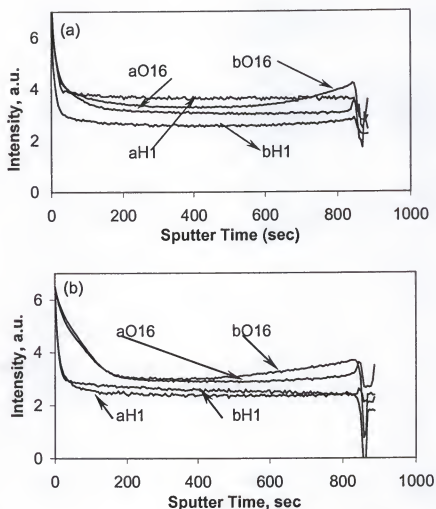
Figure 4.10 Negative SIMS depth profile for 5:1 H_2O_2 solution treated p-GaN
film (a) as-cleaned state; (b) immersed for 45sec; (c) immersed for 5min;
(d) immersed for 20min and (e) immersed for 60min. Data from 2
different points (a, b) on each sample are shown
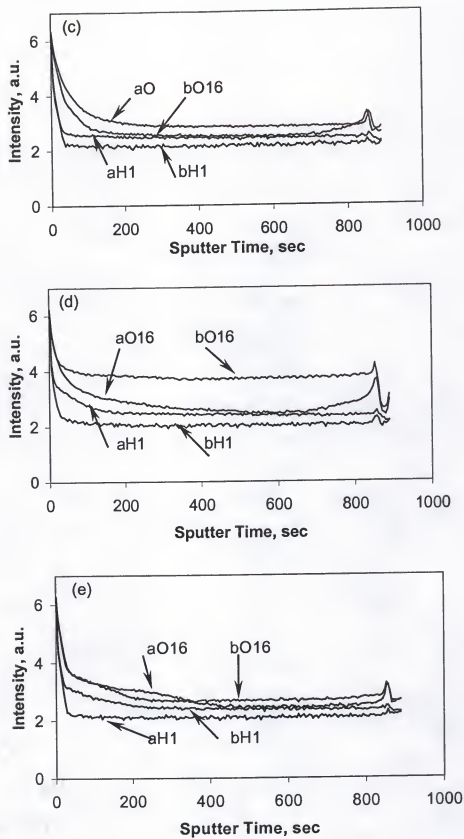
Figure 4.10-Continued
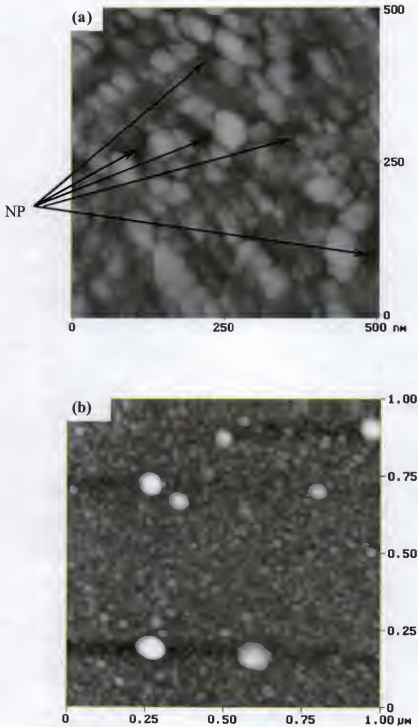
Figure 4.11 AFM images of GaN. (a) MBE-GaN, RMS roughness is of 2.6nm; (b) MOCVD-GaN, RMS roughness is 0.7nm.The points on the MBE-GaN surface labeled NP are potentially nanopipes as discussed in the text.
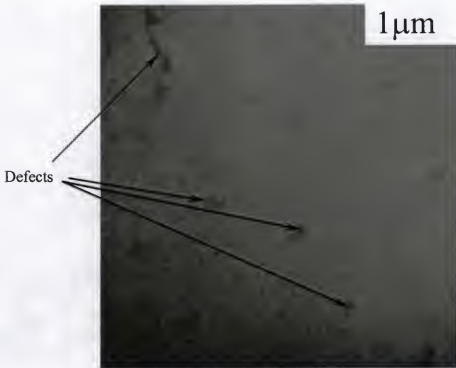
Figure 4.12 Microsturcture of MBE-GaN (TEM, plane-view)

The AFM images for both types of samples are shown in Figure 4.11. The as-cleaned MBE-GaN and MOCVD-GaN had RMS surface roughness of 2.6 nm and 0.7 nm, respectively. Not only is the MBE epilayer rougher, but they also exhibited numerous areas labeled "NP" on Figure 4.11a. As discussed below, these are possibly nanopipes which allow quick transport of atoms throughout the epilayers. The density of the "NP" points was $\sim 10^{10}$ cm^{-2}. Microstructure obtained with TEM plane view observation of the MBE GaN showed the presence of defects, as in Figure 4.12. While the character of the defects were not studied in detail, the larger dark defects are
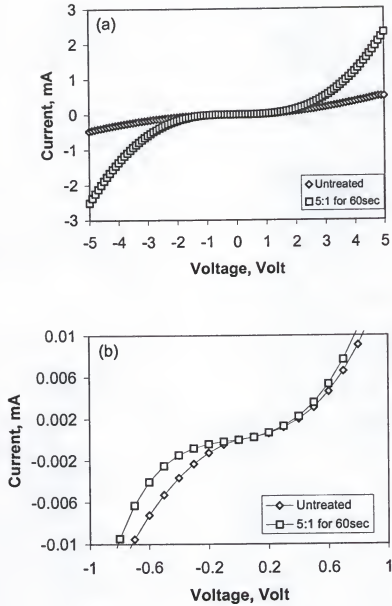
Figure 4.13 Effects of 5:1, 60sec H_2O_2 treatment on the I-V of 500Å Ni/500Å Au to MBE p-GaN. (b) is the same to (a) but in a smaller scale.

consistent with nanopipes. Their density, while still large, is only 10^8 cm^{-2} compared to the density of 10^{10} cm^{-2} reported from Figure 4.11-(a).

4.4. Application in Formation of Ohmic Contact to p-GaN

As shown above, the peroxide treatment of MBE p-type GaN can increase the

hole concentration although the immersion time and solution concentration must be

controlled.Increased hole concentration would allow formation of a lower resistance

ohmic contact, so this technique was combined with the Ni/Au contact scheme for both

MBE and MOCVD p-GaN. Figure 4.13-(a) shows the I-V data for Ni/Au contacts on

MBE p-GaN. Increased currents at the same voltage was found for voltages > 2V after

treatment with a 5:1 solution for 60sec. However, at voltages < 1 V, the current was

lower than for an untreated surface, as shown in Figure 4.13-(b). Lower currents are

attributed to incomplete removal of oxide from the contact interface. The results from the

MOCVD p-GaN show similar results. As a consquence, the increased conductivity of

MBE-GaN did not result in reduced contact resistance as expected, presumably due to the

dominance of interfacial reaction layers on current transport.

4.5 Discussion

Considering both hole and electron carriers, the electrical conductivity of a

semiconductor material is usually described by [May90]:

$$\sigma = q \cdot (n \cdot \mu_n + p \cdot \mu_p) \tag{4.1}$$

where σ is electrical conductivity, q is the electron charge, n and p and μ_n and μ_p are

electron and hole concentrations and mobilities, respectively. In a p-type semiconductor,

the majority carriers are holes, so the effects of electrons could be omitted because their

concentration is so small. The electrical conductivity is only related to the hole

concentration and mobility. The opposite is true for the case of n-GaN. From Figure 4.3,

the hole mobility is shown to be constant within experimental error, but the carrier concentration increased after immersion in the $1H_2O_2:1H_2O$ solution.

As the Hall contacts were deposited before the treatment in H_2O_2 solutions, the effects of H_2O_2 on the metal/GaN interface can be omitted. Possible reasons to account for the increased electrical conductivity after the $H_2O_2:H_2O$ immersions then might include: (a) a surface layer (e.g. gallium oxide) could form which if more conductive than GaN could lead to surface leakage currents, (b) etching of GaN by the H_2O_2 solution to reduce the epilayer thickness, (c) reduced hydrogen passivation of Mg, or (d) formation of Ga-O compounds to stabilize the excess Ga atoms and decrease the concentration of N vacancy donors.

A reaction of the type

$$yH_2O_2 + xGa = Ga_xO_y + yH_2O \qquad (4.2)$$
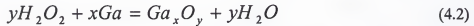
was possible in this experiment, resulting in a Ga_xO_y oxide. As no data is available to calculate the gallium oxide thickness in this reaction, the thickness was assumed to be very thin. If this oxide layer (or other possible reaction products) was more conductive than the GaN, then the increased conductivity after H_2O_2 immersion could be explained by a surface leakage current between the contact structures. However, literature data show that Ga_2O_3 is normally an insulating dielectric layer on the GaN [Ren99]. Various acid and base solutions [Sam73] were reported to be effective for removal of the Ga_2O_3 layer.

If the peroxide treatment created a conductive surface layer, then the conductivity should decrease after re-cleaning the surface with an acid or base solution. In contrast, the
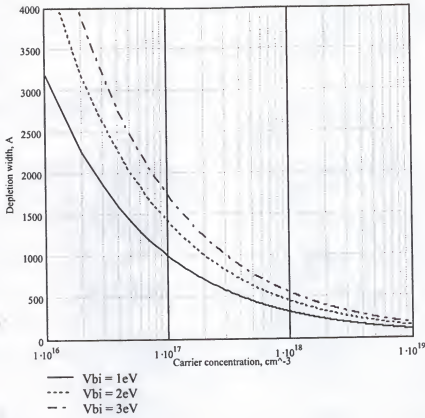
Figure 4.14 Relation among width of depletion region, carrier concentration and built-in potential in GaN

I-V data after the acid and base solution cleaning showed a slightly increased (rather than a decreased) conductivity, so surface leakage current is discounted.

If this Ga_2O_3 layer can create a depletion region in p-GaN due to the band bending effects, the carrier concentration might be changed. To consider this effect, the depletion width in p-GaN was calculated. The equation used in this calculation is [Sze81]:

$$W = \sqrt{\frac{2\varepsilon V_{bi}}{qN_A}} \tag{4.3}$$

where W is the depletion width, $\varepsilon = \varepsilon_s \, \varepsilon_0$ is semiconductor permitivity, ε_s is

semiconductor dielectric constant, ε_0 is vacuum permitivity, V_{bi} is built in potential, N_A is

acceptor concentration, and q is the magnitude of electronic charge. Using the value of ε_s

= 10.4 for GaN [Ho99b] and $q = 1.6 \times 10^{-19}$ C, the width of the depletion region in GaN

related with carrier concentration was calculated for different built-in potentials as shown

in Figure 4.14. At the hole concentration of $2\sim 3 \times 10^{17}$ cm^{-3}, the depletion region is

~ 1000 Å. Compared to the thickness of 1 μm, this depletion region is narrow, and is not

expected to cause carrier change of 50% or higher.

Oxygen impurities incorporated into p-GaN from the H_2O_2:H_2O solution could

cause a surface conversion to n-GaN and result in increased I-V conductivity. When O

was implanted into GaN and annealed at 1100°C [Abe96], it created n-type doping with

an ionization level of ~29 meV. Seifert et al [Sei83] proposed that oxygen

substitutionally incorporated into nitrogen sites could be the origin of the free electron

carriers in highly conductive n-type GaN. In the present case, oxygen incorporation

should increase the electron concentrations in n-GaN, but decrease the hole concentration

in p-GaN because of compensation. This might be used to explain any increased

electrical conductivity in n-GaN, but not in p-GaN. Thus, an increased oxygen level from

H_2O_2 treatment is also discounted.

The etching of GaN can also lead to the change of carrier concentration in the

measured results. Pearton et al [Pea93] have reported on the chemical etching of GaN

films in aqueous 30-50% NaOH solutions at an etch rate of ~2nm/min, although other

authors [You97, Min96, Var96b] did not observe any open-circuit etching in the dark in

alkaline solutions. Weyher et al [Wey97] found the etch rate of [0001] oriented bulk GaN

crystals and epitaxial GaN layers in aqueous KOH to depend upon the face exposed to the etching solution. The N-terminated face is etched in alkaline solutions but the Ga-terminated face remains unaffected. Similar crystallographic dependency of wet etching was also reported by Stocker et al [Sto98]. In addition to open-circuit etching in the dark, studies were also performed on open circuit photoetching of GaN. Minsky et al [Min96] noted photoetching of GaN in aqueous KOH and HCl solutions. The etch rate seemed to be an order of magnitude higher in alkaline solutions. Extended study of the photoetching behavior of GaN in KOH solutions [You97] found that the etch rate was dependent on the incident light intensity, the doping of the material, and the KOH concentration (pH values of the solutions). Peng et al [Pen98a, Pen98b] also demonstrated the open-circuit photoetching in aqueous KOH and H_3PO_4 solutions to be pH dependent. When illuminated from a 253.7-nm mercury line source, etching of GaN was observed in solutions with pH values ranging from 11 to 15. The GaN etch rate was 90nm/min at pH = 14.25, but drops rapidly for pH values above or below 14.25.

The relation of pH value with the H_2O_2 concentration in the H_2O_2/H_2O solutions is shown in Figure 4.15. For the solution used in this work, the pH value of the 5:1 solution is around 5.5, of the 1:5 solution is about 4.7 and of the "pure" H_2O_2 solution is around 4.6 ~ 4.7 (Note the concentration of H_2O_2 in "pure" H_2O_2 is about 37%.), which are significantly smaller than the reported peak values of 12 or over.

If the GaN has been etched by the H_2O_2 solution, the GaN film thickness would decrease and the apparent carrier concentration would decrease the original values of film thickness was used. If only the etching effect was involved, the measured carrier concentration would decrease monotonically. This prediction is inconsistent with the
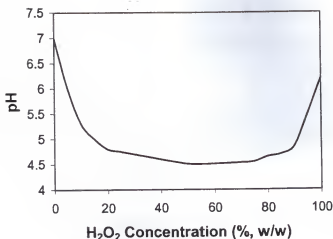
Figure 4.15 Relation between pH values and H_2O_2 concentration
in H_2O_2/H_2O solutions [Per00]

results obtained in this study where the carrier concentration increased with short time

treatment and decreased with longer time of treatment. Besides, the measurement of GaN

epilayer thickness with profilometer and depth profiles showed no significant difference

in the film thickness.

Another possible explanation of increased electrical conductivity may be related

to the reaction of

$$OH^- + H^+ = H_2O \tag{4.4}$$

i.e. the removal of H from the GaN film. It is well known that H compensates Mg

acceptors in p-GaN [Sug98, Ama89]. In fact, a similar mechanism of H removal from

GaN was used to explain the low resistance of Ta/Ti contacts to p-GaN [Suz99]. It was

speculated that Ta/Ti can withdraw (absorb) H from Mg-H complexes, thus reactivating

the Mg acceptor near the contact interface. If this argument was correct, the I-V data

would be expected to continually increase with extended treatment time because more

hydrogen could be removed and more Mg acceptors reactivated. The I-V data in this work showed the conductivity decreased as the immersion time was extended. So the H removal cannot explain all of the results obtained. Additional physical or chemical processes must be involved during the immersion of GaN epilayers in H_2O_2 solutions, as discussed below for surface injection of isoelectronic oxygen donors.

Finally, formation of gallium oxides can reduce the excess Ga atoms, resulting in a decreased nitrogen vacancy concentration, and the hole concentration should increase due to less compensation by nitrogen vacancies, as discussed in Chapter 2. In addition to the formation of Ga oxides, dissociation of H_2O_2 to H_2O to yield O could result in the formation of chemisorption bonds with GaN. This would explain the increase in binding energies for the Ga3d due to an increased net charge on the oxygen versus nitrogen atoms resulting from the larger electronegativity of oxygen [Deh93]. The oxygen electronegativity (3.44 on the Pauling scale) is larger than that of nitrogen (3.04), so higher gallium bonding energies were expected for the Ga-O versus Ga-N bonds. Oxygen bonds decrease the electron concentration in the Ga valence orbitals which results in a weaker screening effect of the nuclear charges by the inner electrons, so the binding energy of Ga3d should increase as observed [Cza75]. If only Ga_xO_y formed, these arguments predict a lower binding energy for the O1s, whereas an increased binding energy was measured. This suggests that $Ga(OH)_3$ formed rather than Ga_xO_y. The argument of $Ga(OH)_3$ formation is consistent with increased binding energies of both the Ga3d and O1s in the results shown above. It also could be consistent with removal of H from the Mg acceptors to form hydroxyl bonds. The typical depths of hydrogen incorporation and maximum concentration measured in various processing steps were

Table 4.3 Relation of hydrogen incorporation and processing steps [Pea97b]

Process	Temp, °C	Maximum [H] (cm^{-3})	Incorporation Depth (μm)
H_2O boil	100	10^{20}	1.0
PECVD SiN$_x$	125	3×10^{19}	0.6
Dry Etch	170	$10^{19} \sim 10^{20}$	>0.2
Implant isolation	25	Dose dependent	2.0
Wet etch	85	2×10^{17}	0.6

compiled in Table 4.3 [Pea97b]. Based on these data, it is clear that even at room temperature, such large incorporation distances have not been demonstrated for nitrogen vacancies or changes in excess Ga profiles.

A model of the amphoteric roles of O is presented here. One effect of O could be the combination of excess Ga and O (or OH$^-$) to form stable compounds with reduction of donor N vacancies, but a second effect could be the incorporation of donor O impurities into the GaN lattice which should compensate Mg acceptors.

Formation of $Ga(OH)_3$ could also modify the concentration of excess Ga and effectively reduce the N vacancies in the GaN film. The high vapor pressure of nitrogen above GaN could lead to desorption of N, excess Ga and high concentration of compensating donors in the surface region. Immersion of GaN samples in H_2O_2 solutions could potentially reduce the concentration of excess Ga atoms by formation of oxides or hydroxides. In the literature, oxidation of Ga with O leads to several polytypes for oxidation products [Wol97].

Theoretical [Neu995] and experimental [Wet97] studies have also shown that oxygen is a relatively shallow donor which can be present at high concentrations ($10^{16} \sim 10^{19}$ cm^{-3}) in undoped GaN films. High concentration of oxygen resulted in high background free electron concentrations commonly observed in as-grown films. The

formation energy for substitution of O onto the N sites is much lower than onto the Ga sites, and the covalent radius and ionicity of O and N are similar. The group VI element O would contribute one extra electron to the conduction band and increase the free electron concentration after incorporation into the GaN lattice. The electrical conductivity should decrease for the p-GaN, as observed. In this experiment, the decrease of electrical conductivity after a long time (60min) immersion is believed to result from this mechanism.

As the immersion time increased, two processes could compete to influence the change of carrier concentration. Reduction of compensation by removal of H, excess Ga or N vacancies should increase the hole concentration and conductivity. As more oxygen atoms were incorporated substitutionally into the GaN films decreased hole concentration and mobility would be expected at long times.

While the competing effects at short versus long time on excess Ga and V_N qualitatively explain the experimental results, the question remains as to whether there is sufficient atomic mobility at room temperature to make this a viable mechanism.

The diffusion of oxygen in GaN has been studied using the ^{17}O in SiO_2/GaN interface [Pea99] and the diffusion depth was found to be ~400 ~ 500Å for as-deposited films. It was also found dislocation pipe diffusion led to larger regions of diffusion around threading dislocations. The overall transport of the oxygen is dominated by the pipe diffusion which is along the dislocation axis only. The square of the diffusion distance in the dislocation is given by

$$X^2 = 2 \cdot D_d \cdot t \tag{4.5}$$

where D_d is the diffusivity in the dislocation, and t is the diffusion time. The least square fit to the data led to the equation [Pea99]:

$$D = (4.5 \pm 2.2) \cdot 10^{-12} \cdot \exp(-\frac{0.23 \pm 0.12 eV}{k \cdot T}) \qquad (4.6)$$

where k is the Boltzmann's constant. The activation is approximately half of the expected value of diffusion in bulk material.

Using these two equations (4.5 and 4.6), the diffusivity was calculated to be between 2.38×10^{-18} and 8.8×10^{-14} cm^2/sec (using the upper and lower limit of the data in equation 4.6) and the diffusion distance at which the oxygen concentration equals to the background concentration of 10^{17}cm^{-3} was between 18.5 Å and 0.355μm for a time period of 60 min. With the experimental times used in this study, it is difficult to believe that the oxygen could diffuse deep enough into the GaN film at room temperature to react with excess Ga over a 1μm epilayer by a uniform transport mechanism. It is much more reasonable to expect rapid diffusion down to a defect perpendicular to the surface, such as a dislocation core or nanopipe, with diffusion out of the core or pipe, parallel to the surface, over much shorter distances.

Defects like nanopipes, screw dislocations and others have been reported in GaN and are known to be paths of enhanced mobility for oxygen and hydrogen. Nanopipes with diameters ranging from 5nm to 0.5μm were reported at a densities of ~10^8 cm^{-2}. They were reported to be parallel to the c-axis of GaN unit cell [Ven99, Kan99] as shown in Figure 2.1. The main composition of nanopipes was Ga, C and O [Kan99], as discussed in Chapter 2. Considering the high chemical activity of O in the H$_2$O$_2$ solution, diffusion of O or H along these nanopipes and out of the GaN or nanopipes into the

surface or GaN lattice would be logical and would explain the results from H_2O_2 treatments. With the help of these nanopipes, the point defects are expected to be extracted or to reach the deep site of the epilayer easily.

Based on this model of enhanced atomic diffusion along nanopipes, the expected increase of carrier concentration from passivation of these defects (using the nanopipe as an example) was predicted as following.

For the perfect crystals with no nanopipe, the total concentration of holes would be

$$N = N_h \cdot S \cdot t \tag{4.7}$$

where N_h is the average hole concentration in this perfect crystal, S is the sample surface area, and t is the sample thickness. With the incorporation of nanopipes, the amount of
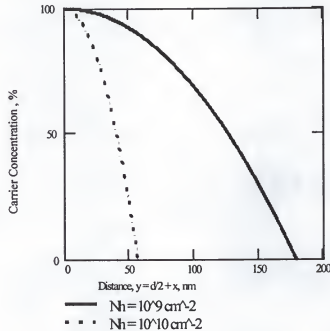
Figure 4.16 Relation of carrier concentration decrease and nanopipe density in GaN

carriers will be changed. If the dislocation/nanopipes are perpendicular to the sample surface, extending through the thickness of epilayer film, and the hole carriers are completely removed in the dislocation/nanopipes and over the depletion distance around the dislocation/nanopipes without effecting the carrer density in the "perfect" region beyond the depletion distance, the reduced carriers concentration N_h' would be:

$$N_h' \cdot S \cdot t = N_h \cdot [1 - \pi \cdot (\tfrac{d}{2} + x)^2 \cdot N_p] \cdot S \cdot t \qquad (4.8)$$

where x is the average depletion distance around the nanopipes, d is the average nanopipe diameter, and N_p is the nanopipe density with a unit of cm^{-2}.

The reduced carrier concentration compared to the perfect crystal will be:

$$\Delta N_h = \frac{N_h'}{N_h} = 1 - \pi \cdot (\tfrac{d}{2} + x)^2 \cdot N_p = 1 - \pi \cdot y^2 \cdot N_p \qquad (4.9)$$

where since x is of the same order of magnitude as d and exerts the same influence on the change of hole concentration, the values are added together as defined as y. Figure 4.16 shows the relationship between carrier concentration decrease and the influence of dislocation/nanopipe size and density. At a density N_p of 10^9 cm^{-2}, the carrier concentration would be reduced by 50% with a y distance of 126nm. At a nanopipe density of 10^{10} cm^{-3}, the y distance of only 40nm would result in the same reduction.

In the AFM image shown in Figure 4.11-a, the "cavities" labeled "NP" are suspected to be nanopipe or dislocation sites and their density is calculated to be 4×10^{10} cm^{-2} with a size of 10 ~50nm. The y distance for p-GaN with our measured carrier concentration increase of ~100% is calculated to be 40nm. These values are in good agreement with the calculated depletion of holes assuming the nanopipe surface cause depletion of carriers. The variation in O and H from SIMS data (Figure 4.10) would be

consistent with the literature data [Kan99] showing that nanopipes were rich in Ga, O and C. The result that O and H at one point was continually higher than another one was consistent with the published results, and is also consistent with the assumption that the direction of these nanopipes were parallel to the c-axis of GaN unit cell. It should be noted that analysis size of SIMS is $75 \times 75 \ \mu m^2$, which means each analysis covered an area containing many nanopipes. The results from the SIMS analysis in this work suggest the nanopipe/dislocation sizes and/or density are not uniform.

4.6 Summary

The effects of H_2O_2 treatment on GaN had been studied using the I-V, Hall, AES, ESCA, SIMS, AFM and TEM. It was found that the electrical conductivity increases after short (< 20 min.) H_2O_2 solution treatments with contact already deposited. The magnitude of the current change was related to the H_2O_2 concentration, with $5H_2O_2$: $1H_2O$ solutions giving best results. The Hall data showed that while the carrier mobility exhibited changes <10%, the average hole concentrations could be changed by up to 100%. According to AES data, the Ga atomic concentration was decreased, N increased and O not changed after the H_2O_2 treatment. Using the ESCA analysis, formation of $Ga(OH)_3$ was shown to result from H_2O_2 treatments. With SIMS depth profiling, big variations of H and O were found across the samples, consistent with published work and AFM data from this study. Based on the possible reactions between GaN and H_2O_2, reasons for the increased conductivity of MBE grown p-GaN were discussed, and a model of reaction with oxygen to deplete nitrogen vacancies or compensating H at short time, and injection of O donors at long times, was proposed.

CHAPTER 5
"NOG" SCHEME FOR OHMIC CONTACT TO p-GaN

5.1 Introduction

When Maruska and Tietjen [Mar69] used a chemical vapor deposition technique to make GaN layer in the late 1960's, the GaN was highly conductive n-type even when not deliberately doped. Two dominant mechanisms were speculated to explain intrinsic n-type as-grown materials. One was nitrogen vacancies and another was of unintentional oxygen doping. The N vacancy was considered to be a donor because a N vacancy would form a void surrounded by four Ga atoms contributing three electrons. Two of these three electrons could reconstruct and leave a single electron that could be donated to the conduction band. This model was later questioned, and instead unintentional oxygen was proposed to be the donor in as-grown GaN [Pan73]. Oxygen with its six valence electrons on a N site (N has five valence electrons) would be a single donor.

The proposed "Nitride-forming metal Over Gallide-forming metal" ("NOG") scheme in this chapter is based on interfacial reactions to control the Ga and N to decrease N vacancies. Based on the review above and in Chapter 2, N vacancies would be at least one of the reasons for a high concentration of donors in GaN

Metallurgical reactions of transition metals with GaN have been reviewed in Chapter 2. Only the principles of the "NOG" scheme and its applications are presented in this chapter. Applications of "NOG" include interpreting published literature results and designing/testing new contact schemes in this study.

84

5.2 Principles of "NOG" Scheme

Since there is a large difference in the vapor pressures of Ga and N, there may be a high concentration of N vacancies, V_N, in as-grown epilayers. A high V_N condition is equivalent to a Ga-rich condition. An opposite situation could be postulated: if a N-rich condition could be created in as-grown GaN films, which is equivalent to creating Ga vacancies, the as-grown GaN should be intrinsic p-type. This condition has not been achieved in bulk GaN films, probably because of the high vapor pressure of N in equilibrium with GaN. Instead, this postulated condition leading to p-GaN might be achieved by interfacial reactions in the contact region. If extra N atoms could be kept between the contact metal layer and the bulk p-GaN film, a N-rich condition could be formed at the metal/GaN interface. The extra N atoms could fill the V_N positions and create Ga vacancies acceptors. If such Ga vacancy acceptors were shallow and reached a sufficient concentration ($>10^{18}$ cm^{-3}), the interfacial region could become p$^+$-GaN and current transport could be dominated by field emission. A low resistance ohmic contact could be obtained as a result. Even a decrease in the V_N concentration should increase the free hole concentration in the contact region. These are the postulates upon which the "NOG" scheme is based. While these reasons seem sound, the "NOG" scheme has not led to new and improved contacts. It is worth a while however to review the progress made using these ideas.
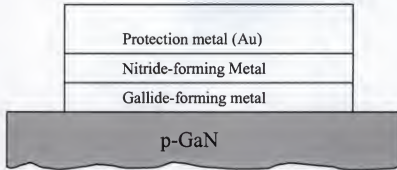
Figure 5.1 Principle of "NOG" scheme.

According to the enthalpy of the metallurgical reactions, all transition metals were classified into three groups in Chapter 2: gallide-forming, nitride-forming and neutral metals with respect to reactions with GaN. Metals for forming "NOG" contacts were selected based upon this classification.

The structure of a "NOG" contact is illustrated in Figure 5.1. A gallide-forming metal adjacent to GaN is followed by a nitride-forming metal, which is covered with a layer of protective metal (such as Au). Under suitable annealing conditions, the gallide-forming metal reacts with GaN to form stable gallides and release N atoms. This first metal layer must both dissociate the GaN lattice and prevent or slow down the nitrogen out-diffusion. The nitride-forming metal layer would help to keep the released N atoms in the contact interfacial region and create a high N chemical potential.

5.3 Comparison with Published Contact Results

The achievement of low resistance ohmic contact to p-GaN is of great importance to GaN device performance. Many studies have been reported along with postulated

mechanisms to explain reduced contact resistance, such as interfacial reactions eliminating barriers [Hol97] and doping the surface region [Tre96, Tre97], GaN regrowth [You98, Tre96], H extraction [Suz99] and Ni oxidation [Ho99a, Ho99b]. A few representative contact schemes are discussed here based on the principle of "NOG" to show the possible applications of this contact scheme. The discussion remains strictly speculative.

The contact scheme of Ni/Au [Fun99, Kim97a, Ish97, Kin97, Tre97] has been widely used for GaN device fabrication. Based on the "NOG" principles, this lower resistance for these contacts results from the reaction between Ni and GaN[Ber93, Guo96, Ven97]. The Ga would react with Ni to form stable gallides and reduce excess Ga atoms. Reduced excess Ga is expected to result in reduced concentrations of V_N and less compensation of acceptors. This would result in higher free hole concentrations in the interfacial region. The success of some other contact schemes, like Pd/Au[Kim98, Kim97b], Pt/Au [Kin97, Mor96, Yoo96], Pd/Au/Pt/Au [Kim97b], Pd/Pt/Au [Kin97] and Pt/Ni/Au [Jan99], could be explained by the same mechanism. As discussed in Chapter 2, Pd and Pt formed more stable gallides than Ni, so it is not surprising that contacts with lower specific resistance were obtained with Pd/Au and Pt/Au contacts

A relatively low specific contact resistance (3.6×10^{-3} Ω-cm^2) was obtained with Ni/Zn-Au [You98] on p-GaN with a carrier concentration of $N_h = 4.4 \times 10^{17}$cm^{-3}. The authors reduced the time between p-GaN film growth and contact metal evaporation in a high vacuum system. They postulated that Zn was an acceptor and that the Zn-Au alloy layer increased the interface carrier concentration. Zn is an acceptor in GaN, but the energy level is deep (E_A = 570 meV)[Pan97] and therefore should not be ionized at room

temperature. Based on the "NOG" scheme, the mechanism should be the same as the Ni/Au scheme discussed above, although the Zn might help increase the carrier concentration in the contact region at high temperatures. The main reason for improved contact performance with Ni/Zn-Au probably came from the limited time for native oxide to grow on the GaN and the use of high vacuum for metallization. Optimum contact resistance would not be predicted for this Ni/Zn-Au metallization because no reaction was found between Zn and GaN and no nitride forming component exist in the contact.

A low resistivity (3.2×10^{-5} Ω-cm^2) ohmic contact to p-GaN was produced with Ta/Ti metallization after a high temperature anneal (800°C for 20 min) [Suz99]. The authors postulated that Ta and Ti were able to remove hydrogen from Mg-H complexes and therefore reduced compensation of the acceptors. It was also found that a dual layer structure of both Ta and Ti formed better contacts than a single layer of either Ta or Ti, although both Ti and Ta were reported to have stronger binding energies with hydrogen than Mg. Although more hydrides are possible, it was reported in the literature that the common hydrides to Mg, Ti and Ta were MgH, TiH$_2$ and TaH$_{0.5}$, and the enthalpy for MgH (-0.77 eV/atom) was more negative than for TiH$_2$ (-0.68 eV/atom) or TaH$_{0.5}$ (-0.417 eV/atom) as shown in Table 5.1 [Fuk93]. This means that MgH is more energetically favored than the TiH$_2$ or TaH$_{0.5}$. For these reaction products, Ta and Ti might not be able to reduce the amount of H in MgH. After a few days, the resistance of the Ta/Ti ohmic contacts increased to a much higher value. This was attributed by Suzuki *et al* to a reverse transport of compensating hydrogen from the Ti/Ta layers back to the interface region and recompensation of Mg acceptors. Contrary to the H mechanism, the "NOG" scheme would be consistent with a postulate that Ta and Ti would dissociate the GaN

Table 5.1 Enthalpy and entropy of hydride formation [Fuk93]

System	$\Delta H^{\alpha \to \beta}$ (eV/atom)	$\Delta S^{\alpha \to \beta}$ (eV/atom)	T (^oC)
Li –LiH	− 0.82	− 8.1	600 – 900
Na – NaH	− 0.59	− 9.8	500 – 900
K – KH	− 0.61	− 10.1	288 – 415
Rb – RbH	− 0.56	− 10.2	246 – 350
Cs – CsH	− 0.59	− 10.2	245 – 378
Mg – MgH	− 0.77	− 8.1	440 – 560
Ca – CaH	− 0.95	− 8.4	600 – 800
Sr – SrH_2	− 1.03	− 9.4	<1000
Ba – BaH_2	− 0.91	− 8.6	470 – 550
Sc – ScH_2	− 1.04	− 8.7	>600
Y – YH_2	− 1.18	− 8.7	600 – 950
YH_2 – YH_3	− 0.93	− 8.3	250 – 350
La – LaH_2	− 1.08	− 9.1	600 – 800
LaH_2-LaH_3	− 0.87	—	—
Ce-CeH_2	− 1.07	− 8.9	600 – 800
CeH_2-CeH_3	− 1.24	—	—
Pr-PrH_2	− 1.08	− 8.8	600 – 800
Nd-NdH_2	− 1.10	− 8.8	650 – 840
Sm-SmH_2	− 1.16	− 9.8	—
Gd-GdH_2	− 1.02	− 7.9	600 – 800
Er-ErH_2	− 1.18	− 9.4	—
Ti (hcp) – TiH_2	− 0.68	− 6	<300
Zr (hcp) – ZrH_2	− 0.98	− 9	400 – 500
Hf-HfH_2	− 0.68	− 6	600 – 900
V-$VH_{0.5}$	− 0.37	− 6.5	0 – 100
V-VH_2	− 0.21	− 9	50 – 120
Nb-$NbH_{0.65}$	− 0.48	− 8	0 – 80
Nb-NbH_2	− 0.21	− 8	25
Ta-$TaH_{0.5}$	− 0.41	− 6	<50
Mn(α)-MnH	− 0.11	− 7 (assumed)	450 – 730
Ni-NiH	− 0.30	− 7 (assumed)	20
Pd-$PdH_{0.5}$	− 0.40	− 5	-78 – 175

and release N atoms. The released N atoms would increase the nitrogen chemical potential and result in reduced V_N concentrations, before formation of TaN_x and TiN_x compounds.

If the argument of hydrogen removal is correct, the sheet resistance of the p-GaN epilayer should decrease first and increase later during the contact degradation. Before contact degradtation, removal of hydrogen would reactivate the Mg acceptors, the carrier concentration in p-GaN would thus increased, and the sheet resistance should decrease. During the contact degradation, hydrogen move back into the p-GaN layer, compensating Mg acceptors and increasing the sheet resistance of the p-GaN. On the other hand, based on the "NOG" argument of nitrogen release and nitride formation, the sheet resistance would be predicted to decrease continuously because the released nitrogen would move to the contact interface and decrease the V_N concentration on the GaN surface. In practice, the sheet resistance was found to decrease continuously even after the degradation of the contacts [Mur99].

The differences in the thermodynamic and kinetic properties of Ta and Ti (Ta is stable and Ti is active) might explain why Ta/Ti form better contacts than Ta or Ti individually. From the concept of "NOG", both metals might form good ohmic contacts in certain situations. In fact, Bour et al use Ti/Au as ohmic contacts to p-GaN in the as-deposited state for polycrystalline GaN LEDs [Bou00]. However, degradation of the contacts might proceed quickly. Low contact resistance are only observed if the measurement is done immediately after processing with the correct rapid thermal annealing (RTA) conditions. Observation of an increased resistance with time at room temperature can also be explained using the "NOG" postulate since formation of stable

nitrides would consume nitrogen atoms and create V_N, and thus increase the compensation of holes in the contact region. Some nitrides like Ta_3N_5 are insulators, whose formation at the interface would increase contact resistance. The electrical conductivity of selected nitrides are listed in Table 5.2.

For Ni/Mg/Ni/Si [You98] contacts, specific contact resistivities of $\approx 10^{-3}$ Ω-cm^2 were measured with a free hole concentration of 3×10^{17} cm^{-3}. These ohmic contacts also degraded after annealing at 500°C for 20min. The authors postulated a mechanism for contact formation which is known to occur for AuGeNi/GaAs contacts [Hol97] in which Ni first reacts to form a ternary compound with GaAs, and this ternary phase is subsequently dissociated by formation of binary NiGe, Ni_xAs_y and Au-Ga solutions. The release of Ga and As from the ternary phase allows solid phase epitaxial regrowth of GaAs in the presence of Ge dopant, leading to a n^+-GaAs regrowth layer and an ohmic contact [Hol97]. The authors in the study of Ni/Mg/Ni/Si postulated that regrowth of GaN and NiSi led to ohmic contacts. Using the principles of the "NOG" scheme, formation of an ohmic contact would result from dissociation of the GaN with Ni and formation of $NiGa_x$ compounds and N atoms. This would increase the activity of N in the interfacial region, which might create a N-rich condition and a more highly doped p-type interfacial region. The formation of MgN_x and SiN_x would consume the extra N atoms and lead to the degradation of these contacts.

The idea of interfacial reactions and control of vacancies, which is the basic tenet of the "NOG" scheme, can and does apply to ohmic contact to n-GaN as well as p-GaN. Lester, *et al.* [Les96] reported that aluminum produced an ohmic contact of 10^{-3} Ω-cm^2 to n-GaN. This is reasonable because of the matched work function of Al and GaN, plus Al

Table 5.2 Electrical conductivity of selected nitrides [Sam75]

Phase	Resistivity, $\mu\Omega\cdot$cm	T, $^{\circ}$C	Specific electrical conductivity, $\Omega^{-1}\cdot$cm^{-1}	Comment
Ca_2N	5×10^6	―	0.2	
Sr_2N	2×10^5	―	5	
ScN	25.4	25	39, 400	
YN	93	25	10, 750	
LaN	100	25	10, 000	
CeN	17	25	58, 800	
PrN	110	25	9, 100	
NdN	75	25	13, 330	
SmN	~120	25	~8, 330	
EuN	~120	25	~8, 330	
GdN	~200	25	~5, 000	
TbN	~200	25	~5, 000	
DyN	100	25	10, 000	
HoN	110	25	9, 100	
ErN	79	25	12, 650	
TmN	180	25	5, 550	
YbN	9×10^3	25	111	
LuN	360	25	2, 780	
ThN	―	―	―	Metal type Conductivity
UN	183	22	5, 460	
NpN	85	4 K	11, 750	
	~430	82 K	~2,380	Curie Point
	380	647	2, 630	
$TiN_{0.79}$	85	27	11, 750	
$TiN_{0.83}$	78	27	12, 800	
$TiN_{0.87}$	70	27	14, 300	
$TiN_{0.97}$	40	27	25, 000	
$ZrN_{0.82}$	30	27	33, 330	
$ZrN_{0.85}$	28	27	35, 700	
$ZrN_{0.92}$	20	27	50, 000	

Table 5.2 - Continued

$ZrN_{0.97}$	18	27	55, 500
HfN	32	27	31, 300
V_3N	123.0±10	20	8, 140
$VN_{0.71}$	127	27	7, 880
$VN_{0.80}$	96	27	10, 400
$VN_{0.85}$	81	27	12, 350
$VN_{0.87}$	77	27	13, 000
$VN_{0.93}$	66	27	15, 150
$VN_{0.96}$	60	27	16, 660
Nb_2N	142	20	7 042
$NbN_{0.75}$	109	27	9, 180
$NbN_{0.80}$	92	27	10, 900
$NbN_{0.89}$	72	27	13, 900
$NbN_{0.95}$	65	27	15, 400
NbN	54	27	18, 500
Ta_2N	263	20	3, 800
TaN	198	20	5, 050
Ta_3N_5	$\sim10^{10}$	20	$\sim10^{-4}$
Cr_2N	84±5	20	11, 900
CrN	640 ± 10	20	1, 562
Mo_2N	19.8	20	50, 500
Ni_3N	2.8×10^3	25	357.1

is also a nitride-forming metal which could create more nitrogen vacancies in the contact region. The contact resistance of Al/n-GaN increased by 50% upon annealing at 575°C. The postulated reason [Les96] was formation of a wide bandgap AlN layer at the interface. The specific contact resistance was improved to 8×10^{-6} Ω-cm^2 by the use of a Ti/Al bilayer metals annealed at 900°C, presumably due to the formation of TiN at the interface of Ti/Al (and Ti/Al/Ni/Au) contacts [Ruv96b, Fan96, Lin94]. Depletion of N in the GaN surface region with nitride-forming metals (e.g. Ti) would create more V_N, and

result in an n^+-GaN layer with improved electron tunneling probability and lower contact resistance.

Experimental data were collected in this study from Ni/Au, Ni/Ti/Au, Ag/Ti/Au, Ni/Al/Au, Pt/Au, Pt/Si/Pt/Au, Pt/Mg/Pt/Au contacts to p-GaN. Ni and Pt are used because they are gallide-forming metals, while Ag is a neutral metal with no reaction with GaN or the second Ti layer. Ti and Al are used because they are nitride-forming metals and also because the Al forms no hydride (so the possibility of hydrides might be excluded). Current-voltage (I-V) data showed that more current is obtained in the ternary or quaternary layer contacts designs using the "NOG" scheme, which is consistent with predictions. Although complete ohmic contacts were not formed with this metallization, the increased current shows the behavior expected from the "NOG" scheme.

The p-GaN used in the Ni-based contacts were MBE epitaxy films, while those with Pt-based contacts were MOCVD GaN epilayers as described in Chapter 3. For Ni-based contacts, a Ni layer was deposited first in all contacts, and Ti and Al were used as nitride-forming metal. The thickness of Ni was varied from 20Å, 100Å to 200Å to study the effects of Ni thickness on the contact property and to find the best Ni thickness for later studies. The thickness of Ti or Al and of the protection Au is selected to be 500 Å. The effects of annealing on the current through Ni/Au and Ni/Ti/Au contacts was studied at temperatures of 300 °C, 500 °C or 800°C for times of 30 sec or 5 min in flowing ultra high purity N_2 gas.

The effects of Mg and Si layers on the contact performance were also studied with Pt as a gallide-forming metal because Si and Mg both are strong nitride-forming

elements. Mg is the p-type doping element in the p-GaN epilayer. Effects of annealing at temperatures of 600°C or 800°C were also studied for these Mg and Si contacts using flowing N_2 as the protection gas. The p-GaN epilayers were grown with MOCVD method.

5.4.1 Effects of Ti and Al as Nitride-Forming Metals

Figure 5.2 shows the I-V data for as deposited Ni/Au, Ni/Ti/Au and Ni/Al/Au contacts. The film thickness are shown in the legend with the unit of Å. Addition of Ti or Al to the Ni and Au contacts resulted in higher current levels by up to a factor of >4 at 5V. Ti increased the current more than Al, although all contacts were still rectifying.

Figure 5.3 showed the effects of Ni thickness on the contact I-V data in as-deposited state. The current through 20Å Ni/500Å Ti/500Å Au was lower than that of 500Å Ni/500Å Au contacts, while the current through the 100Å Ni/500Å Ti/500Å Au contacts was higher than that of the 500Å Ni/500Å Au contacts. The current for 200Å Ni/500Å Ti/500Å Au contacts was similar to that from the 500Å Ni/500Å Au contacts.

The effects of annealing on 500Å Ni/500Å Au and 200Å Ni/500Å Ti/500Å Au contacts are shown in Figure 5.4. The as-deposited samples of both 500Å Ni/500Å Au and 200Å Ni/500Å Ti/500Å Au had similar current levels. The current in 500Å Ni/500Å Au contacts increased continually upon annealing at 300 and 500°C, while annealing at 800°C decreased the current slightly. For 200Å Ni/500Å Ti/500Å Au contacts, a 300°C, 30 sec anneal resulted in slightly higher current, and a 5 min anneal at 300°C resulted in a four-fold increase in current at 5V. The contacts annealed at 300°C for 5min or 500°C for 30sec exhibited similar currents, and current from both were comparable to or higher than that from a 500Å Ni/500Å Au contacts annealed at 500°C for 5min. After a 500°C, 5min
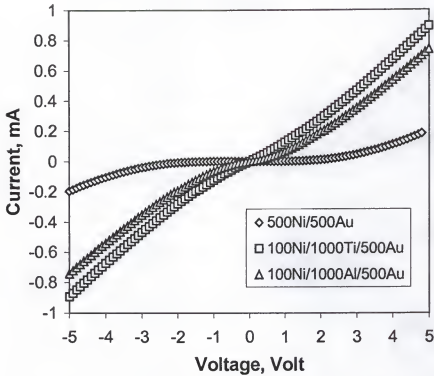
Figure 5.2 I-V of Ni/Au, Ni/Ti/Au and Ni/Al/Au on p-GaN, as deposited state.

annealing, the current through the 200Å Ni/500Å Ti/500Å Au contacts decreased to a level which was close to that of as-deposited contacts. Annealing at 800°C for 5min resulted in a very low current (not shown). Similar degradation of contact versus annealing time and temperature was reported by Suzuki, *et al* [Suz99] and Ho, *et al* [Ho99a].

The higher current through as-deposited contacts, but serious degradation of the Ni/Ti/Au contact showed that while the nitride-forming metal (Ti) was helpful in reducing the contact resistance at the as-deposited states, it also led to the contact thermal instability. This would be consistent with a reaction between Ti and N and formation of TiN_x which resulted in the generation of V_N's at the contact interfacial region.
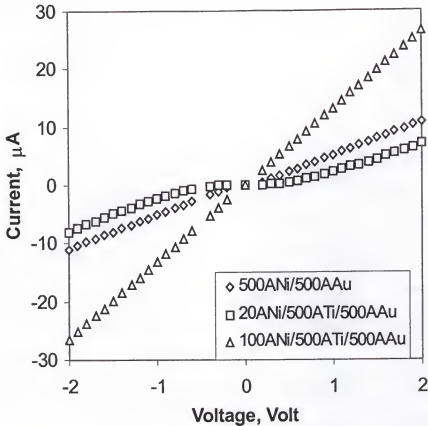
Figure 5.3 Effects of Ni thickness on the I-V of Ni/Ti/Au contact to p-GaN

5.4.2 Effects of Si and Mg as Nitride-Forming Metals

The contact thickness used in this part of study were 500Å Pt/500Å Au, 100Å Pt/50Å Si/ 500Å Pt/500Å Au and 100Å Pt/50Å Mg/500Å Pt/500Å Au. An additional Pt layer was added to these contacts in hopes of achieving better protection of Si or Mg against the oxidation.

The I-V data from as deposited 500Å Pt/500Å Au, 100Å Pt/50Å Si/ 500Å Pt/ 500Å Au and 100Å Pt/50Å Mg/500Å Pt/500Å Au are shown in Figure 5.5. The 100Å Pt/50Å Si/ 500Å Pt/500Å Au showed higher currents than Pt/Au contacts, while currents

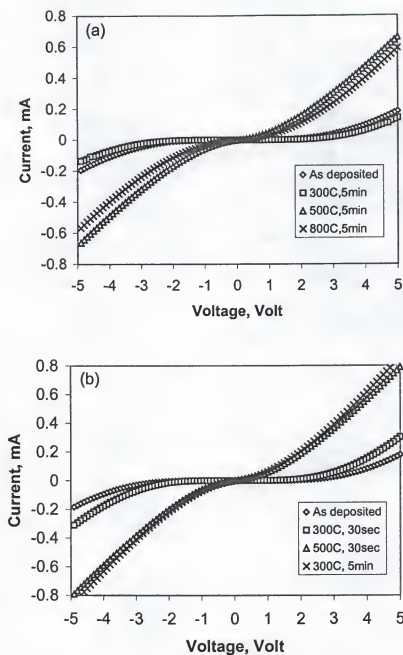Figure 5.4 Effects of thermal annealing on I-V data. (a) 500Å Ni/500Å Au and (b) 200Å Ni/500Å Ti/500Å Au contact.
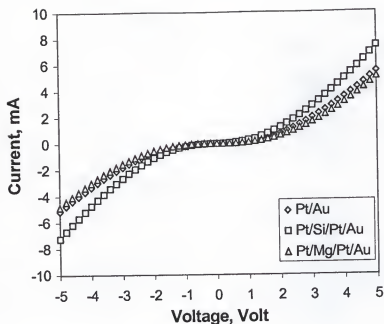
Figure 5.5 I-V curves of 500Å Pt/500Å Au, 100Å Pt/50Å Si/500Å Pt/500Å Au and100Å Pt/50Å Mg/500Å Pt/500Å Au contact on p-GaN, as-deposited
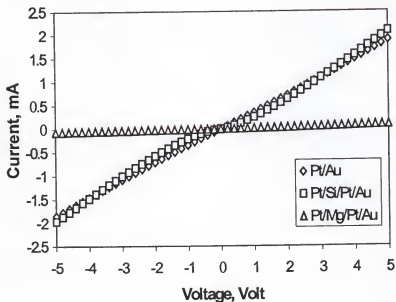

Figure 5.6 I-V curves of 500Å Pt/500Å Au, 100Å Pt/50Å Si/500Å Pt/500Å Au and 100Å Pt/50Å Mg/500Å Pt/500Å Au contact on p-GaN, 600°C for 1min annealing
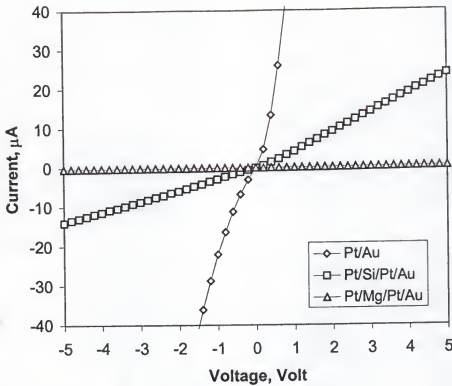
Figure 5.7 I-V curves of 500Å Pt/500Å Au, 100Å Pt/50Å Si/500Å Pt/500Å Au and 100Å Pt/50Å Mg/500Å Pt/500Å Au contact on p-GaN, 800°C for 1min annealing

from 100Å Pt/50Å Mg/500Å Pt/500Å Au contacts were lower than those in 500Å Pt/500Å Au contacts. All contacts were rectifying.

The change in current levels versus voltage data after high temperature annealing at 600°C or 800°C for 1 min. are shown in Figures 5.6 and 5.7, respectively. The I-V data for the 500Å Pt/500Å Au and 100Å Pt/50Å Si/500Å Pt/500Å Au became more linear while the current for 100Å Pt/50Å Mg/500Å Pt/500Å Au became very low. Annealing at 800°C decreased the current level in the 100Å Pt/50Å Si/500Å Pt/500Å Au and 100Å Pt/50Å Mg/500Å Pt/500Å Au contacts, while that from 100Å Pt/500Å Au contact remained relatively, but lower in magnitude than as-deposited contacts (Figure 5.5).

AES depth profiles for 500Å Pt/500Å Au contacts are shown in Figure 5.8. Compared to the as-deposited state (a), diffusion of Pt and Au was found after the annealing. Figure 5.9 showed the depth profiles of 100Å Pt/50Å Si/500Å Pt/500Å Au contacts. Compared to profiles of 100Å Pt/500Å Au contacts, less interfacial diffusion was found after annealing at 600°C (comparing Fig. 5.9b with 5.8b), but the Si peak height decreased compared to as-deposited data. Less diffusion of Pt was expected due to formation of Pt silicides [Oka90]. Annealing further at 800°C promoted more interfacial reactions and diffusion so that Si accumulated at the contact surface. Oxygen also accumulated on the sample surface, along with higher N levels than those for the as-deposited state.

For 100Å Pt/50Å Mg/500Å Pt/500Å Au contacts, as shown in Figure 5.10, the as-deposited state exhibited a Mg peak at the contact/p-GaN interface, along with higher level of oxygen. Annealing at 600°C leveled the Mg peak at the interfacial region, but a huge accumulation of Mg and O was found at the contact surface. The inset in Figure 5.10-b shows the Mg and O peaks. The N level was higher than that of 100Å Pt/50Å Si/500Å Pt/500Å Au contacts, and both were higher than for the 500Å Pt/500Å Au contacts. Annealing at 800°C made the Mg and O accumulation wider at the contact surface, and the interfacial region was wider than for 500Å Pt/500Å Au and 100Å Pt/50Å Si/500Å Pt/500Å Au contacts.

From the above results, Mg is not good as the nitride-forming metal because of thermal instability. The Mg contacts became almost insulating after annealing at 600°C and 800°C for 1min. This is understandable because Mg metal reacts strongly with oxygen.
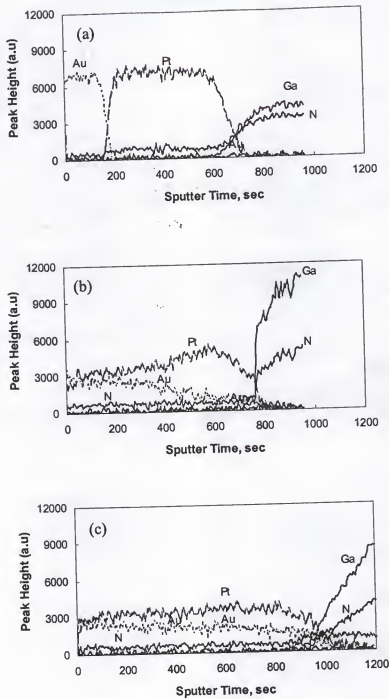
Figure 5.8 AES depth profile of Pt/Au contact on MOCVD p-GaN. (a) As-deposited; (b) 600°C for 1min; (c) 800°C for 1min
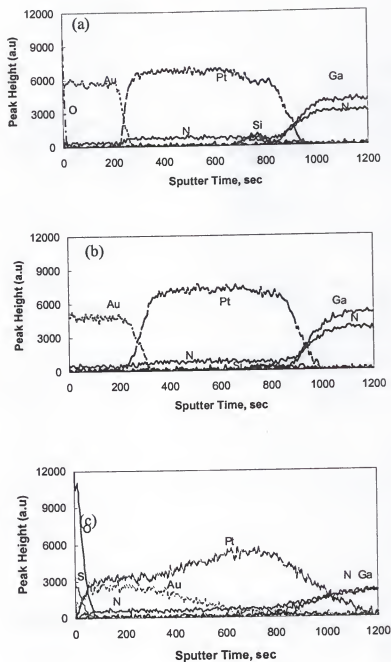
Figure 5.9 AES depth profile of Pt/Si/Pt/Au contact on MOCVD p-GaN. (a) As-deposited; (b) 600°C for 1min; (c) 800°C for 1min
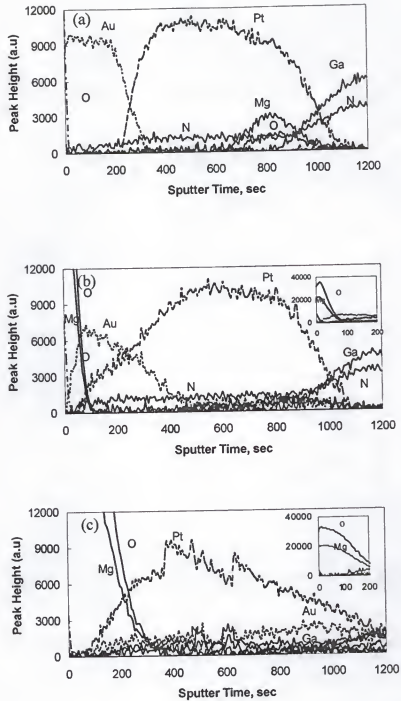
Figure 5.10 AES depth profile of Pt/Mg/Pt/Au contact on MOCVD p-GaN. (a) As-deposited; (b) 600°C for 1min; (c) 800°C for 1min
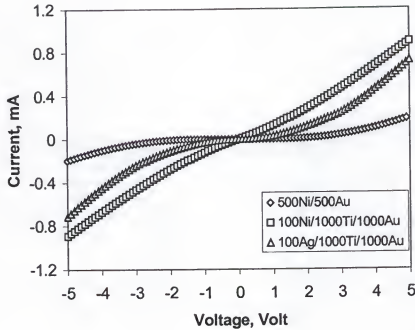
Figure 5.11 I-V of 500Å Ni/500Å Au, 100Å Ni/1000Å Ti/1000Å Au and 100Å
Ag/1000Å Ti/1000Å Au on p-GaN, as deposited state

5.4.3 Neutral Metals

The effects of a neutral metal, Ag, upon I-V data were compared with those from

Ni as the first contact layer. The Ag did not react with either GaN or Ti metal [Oka90], so

its role in the Ag/Ti/Au contact is only to separate the Ti from GaN.

The I-V data (Figure 5.11) showed that the current through 100Å Ag/1000Å Ti/

1000Å Au contacts was below that through 100Å Ni/1000Å Ti/1000Å Au contacts, but

higher than the 500Å Ni/1000Å Au contact. The I-V plots were highly non-linear due,

presumably, to the absence of interfacial reactions between Ag and GaN to stabilize the

Ga atoms and release the N atoms, in contrast to the reaction between Ni and GaN.
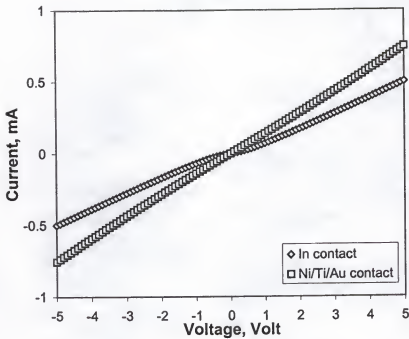
Figure 5.12 Comparison of In metal and 100Å Ni/500Å Ti/500Å Au as ohmic contact for Hall measurement

Another interesting comparison was between 100Å Ni/500Å Ti/500Å Au and the plain In contacts (Figure 5.12). Because good ohmic contacts of high current and linear I-V plots to p-GaN are not routinely available, most researchers use plain In and the Van der Pauw configuration for Hall measurements. The 100Å Ni/500Å Ti/500Å Au contacts were prepared with the shadow mask described in Chapter 3, while the In contacts were soldered to p-GaN surface. The In (with a diameter of ~1 mm) contact had a larger contact area than the 100Å Ni/500Å Ti/500Å Au contacts (with a diameter of 0.4 mm). The 100Å Ni/500Å Ti/500Å Au contacts exhibited higher current and more linear I-V data, even though their area was smaller.

5.5 Discussion

The "NOG" contact scheme proposed in this section was shown to be qualitatively consistent with the behavior of metal contacts on GaN. The reactions between the contact metals schemes and GaN could determine the electrical properties of the contacts. Presumably, the reactions between gallide-forming metals and GaN gettered excess Ga in the interface region, thereby decreasing the nitrogen vacancies and increasing the hole concentrations. Reactions between nitride-forming metals and GaN increased the nitrogen vacancy concentrations and enhanced the electron concentrations in the contact region.

Consistent with the principles of "NOG", the first Ni layer in both Ni/Ti/Au and Ni/Al/Au contacts was a gallide forming metal which could release N atoms upon reaction with GaN. This Ni layer also act as a barrier by slowing down the rate of nitride compound formation, reducing the extent of reactions between N or Al and Ti. This would maintain a higher activity of N at the GaN surface to reduce the V_N concentration, and result in less acceptor compensation. The observed higher current is consistent with this qualitative prediction. A high contact resistance for thin gallide-forming metal (20Å Ni) could result from the extent of interfacial reaction being too limited to affect V_N concentration or the Ni layer is too thin to prevent quick formation of stable nitride (TiN_x) and thus to increased V_N concentrations.

The driving force of metal reactions to Ga and GaN can be calculated using the equation of

$$\Delta G = \Delta H - T \cdot \Delta S \qquad (5.1),$$

Table 5.3 Calculated driving forces of metal reactions to Ga and GaN

Reaction	ΔG_{300} (kJ/mol)	ΔG_{1000} (kJ/mol)	T_c for $\Delta G = 0$ (K)
$Ga + \frac{1}{2} N_2 = GaN$	-77.6	-2.5	752.7
$Co + Ga = CoGa$	-39.4	-35.6	7592.6
$Ni + Ga = NiGa$	-36.1	-34.1	12758.6
$Pt + Ga = PtGa$	-40.1	36.7	666.5
$Co + GaN = CoGa + \frac{1}{2} N_2$	38.2	-32.9	676.5
$Co + GaN = CoGa + N$	510.9	439.9	5331.9
$Ni + GaN = NiGa + 1/2N_2$	41.5	-31.4	698.7
$Ni + GaN = NiGa + N$	514.2	441.4	5242.2
$3 Ni + GaN = Ni_3N + Ga$	104.8	91.6	5831.1
$Pt + GaN = PtGa + 1/2N_2$	5.5	-67.4	352.7
$Pt + GaN = PtGa + N$	477.4	402.5	4763.4
$Cr + GaN = CrN + Ga$	-19.1	-32.3	< 0
$2 Cr + GaN = CrN + CrGa$	-22.3	-5.7	1237.9
$3 Cr + GaN = Cr_2N + CrGa$	87.1	153.5	< 0
$2 Cr + GaN = Cr_2N + Ga$	47.7	-15.3	830.5
$Ta + GaN = TaN + Ga$	-137.3	-124.6	7905.8
$Ti + GaN = TiN + Ga$	-223.3	-215.0	18987.4
$3Mg + 2GaN = Mg_3N_2 + 2Ga$	-211.2	-346.6	<0
$3Si + 4GaN = Si_3N_4 + 4Ga$			

where ΔG is Gibbs free energy change, ΔH and ΔS are enthalpy and entropy change for the reaction, and T is the temperature in Kelvin [Deh88]. Using the data provided in the literature [Boe88, Deh93], the driving forces for reactions between typical metals and GaN are calculated as in Table 5.3. The negative values showed that reactions between gallide-forming metals of Co, Ni and Pt with Ga and GaN are thermodynamical favorable if the produced nitrogen exists in the form of nitrogen gas (N_2), or combines with nitride-

forming metals (Cr, Ta and Ti, etc.) to form nitrides, but is not favorable if the released nitrogen exists in atomic state (N).

The "NOG" contact scheme uses these properties of gallide formation and uses a nitride-forming metal to keep the nitrogen activity high in the contact region. However, thermal stability became a serious problem in the "NOG" contact metals tested in this study. Thermal instability resulted from the large diffusion distances of nitride-forming metals, as illustrated below.

The temperature dependence of the diffusion coefficient in a solid is well described by a semi-empirical formula [Deh96]

$$D = D_0 \cdot \exp(-\frac{Q}{R \cdot T}) \qquad (5.2)$$

where D_0 is a diffusion factor, Q is the activation energy, R is the universal gas constant and T is temperature in Kelvin [Deh93]. The characteristic diffusion distance, λ, is usually written as:

$$\lambda = \sqrt{4 \cdot D \cdot t} \qquad (5.3)$$

where the D is given above in equation (5.2).

The diffusion data of a few metals in nickel are listed in Table 5.4 [Gri97]. The diffusion coefficients at 973 K and the characteristic diffusion distance for $t = 1$ hour were also calculated and are shown in the table. At 973 K (700°C), the characteristic diffusion distance is much larger than the Ni contact thickness used in this work. The diffusion data of N is not available. Using the diffusion data of O (due to similarity in atomic radii and atomic affinity between O and N), the diffusion distance is estimated to be between 18.5 Å and 0.355μm for a time period of 60 min as shown in Chapter 4. The large diffusion distances of contact components are probably a major cause of the thermal stability

Table 5.4 Calculation of diffusion characteristic distance of selected metals in nickle [Gri97]

Metal	Temperature Range, K	D_0, cm²/sec	Q, kJ/mol	D at 973 K	λ, nm
Al	1070-1250	1.1	249	2.6×10^{-14}	193.23
Au	1200-1400	2	272	2.4×10^{-15}	59.06
Cr	940-1170	0.03	171	1.3×10^{-11}	4329
Mg	1070-1250	2.3×10^{-5}	131	1.5×10^{-12}	1497
Si	1079-1250	10.6	271	1.5×10^{-14}	149.42
Ti	1400-1600	11.1	322	2.0×10^{-18}	1.716

problem in the "NOG" scheme. To alleviate the problem, better metal layer should be found to prevent serious diffusion of these nitride-forming metals.

5.6 Summary

New principles to be used to select metal layers used for contacts to p-GaN were proposed and called Nitride-forming metal Over Gallium-forming metals — "NOG". The "NOG" contact scheme is based on reactions between the contact metals and GaN. Gallide-forming metals can bond to Ga and release N atoms, while addition of nitride-forming metals should result in increased N concentrations and activity in the contact interface before the formation of stable nitrides. These N atoms could fill nitrogen vacancies, with a consequent higher hole concentration and better ohmic contact. These results were qualitatively obtained in comparison of as-deposited Ni/Ti/Au, Ni/Al/Au, Pt/Si/Pt/Au and Ag/Ti/Au contacts with Ni/Au and Pt/Au contacts.

Explanations based on "NOG" principles of published data as well as data from the current study were discussed. In the "NOG" scheme, metals were classified as

gallide-forming, nitride-forming or neutral metals. Published results for ohmic contacts to p- or n-GaN were compared to "NOG" principles. Higher currents through contacts with both gallide- and nitride- forming metals were presented (e.g. Ni/Al/Au and Ni/Ti/Au), as compared to Ni/Au contacts with only a gallide-forming and neutral metal. Mg and Si were also studied as nitride-forming elements. The Si contacts showed increased current, but Mg decreased the current levels versus Pt/Au contacts. These results were explained based on metallurgical reactions between the contact elements and GaN.

Even though the use of both gallide and nitride forming metals slightly reduced the contact resistance, poor thermal stability was observed for metallization based upon the "NOG" scheme. The annealing temperatures degraded the "NOG" contacts more quickly than those having no nitride-forming metals. This was explained based on the formation of nitrides which would decrease the activity of N atoms in the contact region. This would create more nitrogen vacancies and further reduce the already low hole concentrations.

EFFECTS OF Ni CAP LAYER ON THIN Ni/Au CONTACTS TO p-GaN

6.1 Introduction

Recently, a new approach to reduce the contact resistivity for p-GaN was reported to result from annealing Ni/Au contacts in an oxygen ambient (pure oxygen or air). Both the sheet resistance and specific contact resistance were found to be reduced [Koi99]. A low ρ_c of 4×10^{-6} $\Omega\cdot$cm^2 was obtained with 50Å Ni/50Å Au contacts after annealing in air [Ho99b]. While this value would be sufficiently low to be used in patterned small area contacts, most contact resistances were much higher ($\approx 10^{-4}$ Ω-cm^2). The mechanisms to explain these low contact resistivities were postulated to be reduction of acceptor-compensating hydrogen [Koi99], or formation of a NiO layer [Ho99b, Che99, Hol00]. NiO is a p-type wide bandgap semiconductor. It can potentially reduce the Schottky barrier height (ϕ_b) at the p-GaN/contact interface if it has the expected large work function (or $E_g + \chi$). In the study by Ho et al [Ho99b], it was found that equal thicknesses of Ni and Au resulted in the best electrical properties. Low values of specific contact resistance of 4×10^{-6} Ω-cm^2 and 8×10^{-6} Ω-cm^2 were obtained from contacts of 50Å Ni/50Å Au and 200Å Ni/200Å Au. The contact resistance increased for thicker contacts.

Because of its wide bandgap (4.0 eV) [Hüf92], NiO also is transparent to visible light allowing it to be used as transparent electrodes for optoelectronic devices and window coatings [Sat93]. Since $\rho_c \approx 10^{-4}$ Ω-cm^2, which is too high to be used for small

area patterned ohmic contacts, a transparent contact is used in LEDs over the entire emitting surface. With such a large area, the contribution of the contact to the total device resistance is very small. The contact contribution to total device resistance increases for thin contacts and decreases for thick contacts. But the light transmittance decreases as the contact thickness increases according to the equation [Hum98]:

$$I = I_0 \cdot e^{-\alpha \cdot d} \tag{6.1}$$

where I_0 is initial light intensity, I is transmitted light intensity, α is the light attentuation constant and d is distance the light travels through a material. Therefore the thickness of the tranparent contact is a compromise between these opposed trends for resistance versus transmittance.

Another consideration for the thickness of the transparent Ni/Au contacts is the surface roughness. The reported root mean square (RMS) surface roughness of GaN epilayers grown under typical MOCVD processing conditions is normally $\approx 10\text{nm}$ [Cao00]. As shown in Figure 4.11-(a), with a RMS roughness of 2.7nm, the peak-to-valley distance is around 18.8nm for MBE-GaN. This is greater than the thickness of 50Å Ni/50Å Au contacts. In a recent report on polycrystalline GaN LEDs, the surface roughness was much larger; and contact coverage was one of the major factors limiting device performance [Bou00]. To make this thin Ni/Au contact scheme more robust, the thickness needs to be increased.

In this work, an outer Ni cap-layer was added to Ni/Au contacts making them Ni/Au/Ni contacts. The effects of the additional Ni layer on contact resistance and light transmittance were studied. Annealing of this contact in O_2 transformed the extra Ni into a transparent NiO layer, with little negative effects on the light transmittance or light

transmittance. Thus the Ni cap-layer can increase the contact thickness, achieve better coverage, and still keep the same light transmittance and contact resistance. Optimization of the Ni/Au ratio was studied by changing the Au layer thickness in the sandwich Ni/Au/Ni structures.

The thickness of the Ni layer was kept constant at 50Å for comparison with published work. Two gold thicknesses of 50Å and 100Å were used, so the contacts studied were 50Å Ni/50Å Au, 50Å Ni/50Å Au/50Å Ni, 50Å Ni/100Å Au/50Å Ni (referred to as 50/50, 50/50/50 and 50/100/50 hereafter). Ho et al [Ho99b] reported that the best Ni/Au contact resistance was obtained by annealing at a temperature of $500^{\circ}C$ for 10min. After an anneal of $600^{\circ}C$, the contact degraded significantly. Due to the increased Ni thickness in this work, the best anneal temperature and time for Ni/Au/Ni were expected to be higher and longer, so anneal temperatures of 500, 550 and $600^{\circ}C$ and times of 1, 5, 10 and 30min were selected. Specific contact resistance and light transmittance were measured, and SEM, AES and XPS were used to study microstructural evolution and interfacial reactions.

6.2 Contact Electrical Properties

The electrical properties of the contacts were characterized by the current levels at a constant voltage, and by specific contact resistance. The specific contact resistance for these contacts was calculated using the circular transfer length method (CTLM) patterns shown and discussed in Chapter 3. Annealing time was first kept constant at 10min to study the effects of annealing temperatures. After selection of the best annealing temperature, the annealing time was optimized.
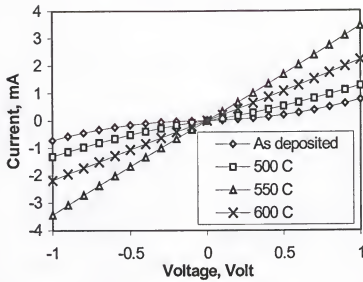
Figure 6.1 Effects of anneal temperature on I-V of 50/50 contact

Formation of NiO was important to the contact properties, and the electrical conductivity of NiO was found to be related to its composition [Sat93]. To determine whether the annealing temperature and time influenced the compositon and/or electrical conductivity of the contact pad, the resistance within a single patterned contact (not between two patterned contacts) was measured with a two point probes approach. The resistance calculated from these data have contributions from ρ_{NiO}, ρ_{Au} and ρ_{GaN}.

6.2.1 Annealing Temperature

Figure 6.1 depicts the effects of annealing temperature on the I-V curves for a constant time of 10min for 50/50 contacts. The as deposited contact was rectifying. After annealing at 500°C for 10min, the I-V curve became more but was not completely linear. After annealing at 550°C, the contact became less resistive with straight, linear I-V with

higher current levels. After 600°C annealing, the I-V data were still linear although the current level decreased.

The I-V data obtained from the 50/50/50 contacts are similar to data from 50/50 contacts, except that the current level is slightly higher for the as deposited state. As compared to the as-deposited sample, both the current and linearity increased as the annealing temperature was increased from 500°C to 550°C to 600°C. Completely linear I-V data were obtained at 600°C. However, a current of only ~1.5mA at 1V was obtained, which is lower than the current in 50/50 contacts. The current at 550°C was between that for samples annealed at 500°C and 600°C. Annealing at 700°C, as compared to 600°C sample, significantly decreased the current levels.

For 50/100/50 contacts, increased annealing temperatures increased the current, with the maximum current obtained after 600°C anneal (0.4mA at 1V). However, completely linear I-V curves were not obtained for this scheme, and the current through as-deposited contacts was lower as compared to that from 50/50 and 50/50/50 contacts.

The values of ρ_c are shown in Figure 6.2 for 50/50, 50/50/50 and 50/100/50 contacts versus anneal temperature. For non-linear I-V curves, the resistance at 0.2 V was used for this calculation. The lowest contact resistivity for the 50/50 contacts was 5.3×10^{-4} Ω-cm^2 at 550°C, and the resistivity was 1.52×10^{-3} at 600°C. For the 50/50/50 scheme, the lowest specific contact resistance was 6.2×10^{-4} Ω-cm^2 at 600°C. Annealing at 700°C increased the specific contact resistance by more than one order of magnitude. The 50/100/50 contacts all had high resistivity ($>10^{-2}$ Ω-cm^2) at all annealing temperatures. From these data, an annealing temperature of 600°C was selected for 50/50/50 and 50/100/10 contacts.
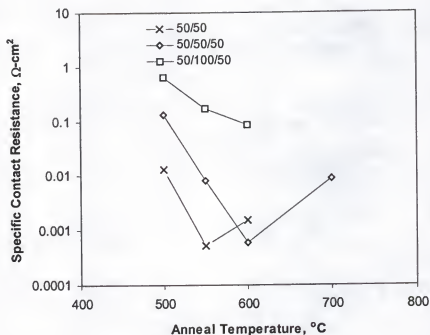
Figure 6.2 Effects of annealing temperature on the specific contact resistance of the 50/50, 50/50/50 and 50/100/50 contacts

6.2.2 Effects of Annealing Time

For the 50/50 contacts, annealing at 600°C for 1 min. increased the current slightly, and completely linear I-V data were obtained with 10min anneals. Increasing annealing time to $\geq$30min resulted in lower, nonlinear current.

I-V data for 50/50/50 contacts showed similar trends as found for 50/50 contacts except for a smaller decrease in current levels for 30min anneals.

The trends were similar for 50/100/50 contacts, except that a decrease in current was not found for annealing at $\geq$30min. The current continued to increase for all times at

T = 600°C for 50/100/50 contacts, although its values were always lower than those for the 50/50 or 50/50/50 contacts.

The specific contact resistance results versus time at 600°C are shown in Figure 6.3. The 50/50 and 50/50/50 contacts show minimum specific resistance of 1.52×10^{-3} Ω-cm^2 and 6.16×10^{-4} Ω-cm^2, respectively, after 10 min. anneals. The specific resistance of 50/100/50 contacts continually decrease with increased annealing time, with a minimum value of 1.6×10^{-2} Ω-cm^2 after annealing for 30min.

The effects of annealing time at 600°C on contact pad resistance is shown in Figure 6.4. The resistance for the 50/50 contact pads increased sharply for 10min anneal, but remained constant between annealing times of 10 and 30min. The 50/50/50 resistance of contact pads increased continuously. The contact pad resistance remained at a low value for the 50/100/50 contact, although it increased slightly with annealing time.

6.2.3 Effects of O_2 Flow Rate

Effects of oxygen flow rates (60 to 130 liter/min) on the 50/50 and 50/50/50 contacts were studied after 10 min anneals at 500°C. A MANOSTAT® gas flow meter was used to set flow rates of 60 liter/min or 130 liter/min. In 50/50 contacts, the lower O_2 flow rate resulted in smaller currents, while the larger O_2 flow rate enhanced the current level between two contact pads. Increased current between pads with larger O_2 flow rates was also found for 50/50/50 contacts.

For the 50/50/50 contact schemes. The contact pad resistance increased at higher O_2 flow rates through the furnace, contrary to the decrease of specific contact resisitvity
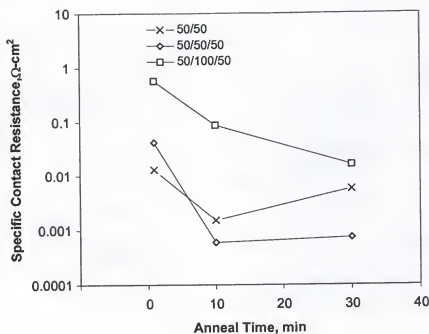
Figure 6.3 Effects of annealing time on the specific contact resistance of 50/50, 50/50/50 and 50/100/50 schemes annealed at 600°C.

observed with an increased O_2 flow rates. The reasons for change in specific contact resistance and contact pad resistance are unknown.

6.3 Light Transmittance

Applications of GaN in optoelectronic devices like light emitting diodes (LEDs) and laser diodes (LDs) are important. Because the specific contact resistance of current ohmic contacts to p-GaN is too high (~10^{-2} to 10^{-3} Ω-cm^2), a large contact area is used to reduce the contribution of the contact to the total resistance. Light emission through the
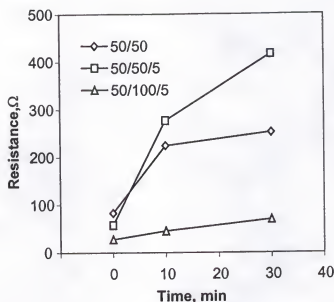
Figure 6.4 Effects of anneal time on resistance of contact pads at 600°C

p-contact is necessary, requiring a transparent contacts. To maximize the emission, the p-type contacts must be as transparent as possible. The results of annealing temperature, time and change of O_2 flow rates on light transmittance is reported below.

6.3.1 Effects of Annealing Temperature

Figure 6.5 shows the change of light transmittance in the 50/50, 50/50/50 and the 50/100/50 contacts with annealing temperatures. In the as deposited state, the 50/50 was the thinnest contact, so the transmittance was higher than that of the 50/50/50 and 50/100/50 contacts. Similarly, the 50/50/50 scheme had a better transparency than the 50/100/50 scheme in the as-deposited state, and this situation remained true after annealing at 500°C for 10min. For all three contacts, an increase of annealing temperature improved the light transmittance, with the maximum values obtained at 600°C.
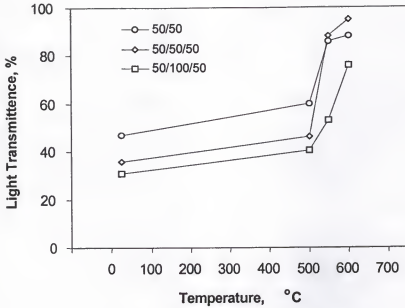
Figure 6.5 Comparison of light transmittance at λ = 450 nm. Increased annealing temperature led to higher light transmittance (anneal time = 10 min).

Surprisingly, 50/50/50 contacts showed the highest light transmittance, which was more than 93%. In contrast, 87% and 75% were measured for 50/50 and 50/100/50 contacts, respectively, after annealing at 600°C for 10min.

6.3.2 Effects of Annealing Time

The relation between light transmittance and annealing time at 600°C is shown in Figure 6.6. The light transmittance reached a maximum at 10min for the 50/50 (88%) and 50/50/50 contacts (94.5%), and decreased slightly as the annealing time increased to 30min. The 50/100/50 contact reached a value of light transmittance of 76% at 10min and continued to increase to 79% for 30min. At 30 min , the 50/50/50 contact (88%) was still more transparent than the 50/50 contact (83%).
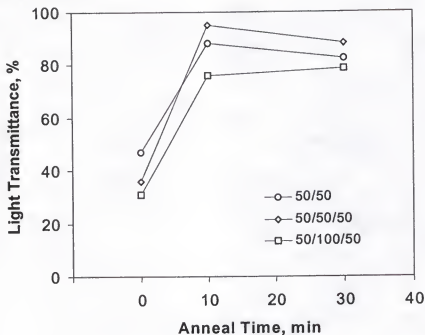
Figure 6.6 Effects of annealing time on light transmittance at $\lambda = 450$ nm

6.3.3 Effects of O_2 Flow Rates

The effects of O_2 flow rates on the light transmittance are shown in Figure 6.7 for anneal temperature of 500°C. The annealed contacts show higher transparency than as-deposited contacts (47% for the 50/50 contacts and 36% for the 50/50/50 contacts). The high O_2 flow rate (130 liter/min) results in higher light transmittance in both contact schemes. The 50/50 (50% at low flow rate and 63% at high flow rate) contacts were more transparent than the 50/50/50 contacts (46% at low flow rate and 55% at high flow rate) at both flow rates, which is contrary to the relative transmittance of 50/50 versus 50/50/50 contacts annealed at 600°C (see Figure 6.6).
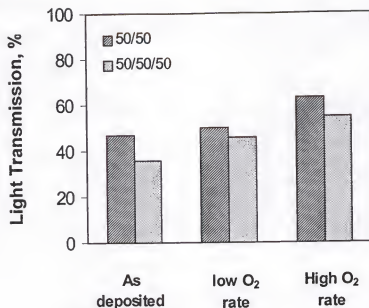
Figure 6.7 Effects of O_2 flow rates on light transmittance for $500^{\circ}C$, 10min anneals (low rate = 60 liter/min, high rate = 130 liter/min).

6.4 Microstructure Characterization

6.4.1 SEM

Figure 6.8 to 6.11 shows the microstructures imaged with backscattering electrons for the 50/50, 50/50/50 and 50/100/50 contacts on p-GaN. All as-deposited and short time annealed ($600^{\circ}C$ for 1 min.) films are featureless to SEM. Annealing times of 5min results in the formation of a light colored network structure, and an increase to 10min enhanced this network structure. Energy dispersive spectroscopy (EDS) point chemical analysis (Figures 6.12 and 6.13) shows the light region is Au rich while the dark region is Ni rich. The feature sizes are ≤ 0.5 μm. Because the excitation volume diameter (~1 μm) is larger than the average feature size, the presence of Au in EDS spectra from the dark regions (Figure 6.13) is not unusual.
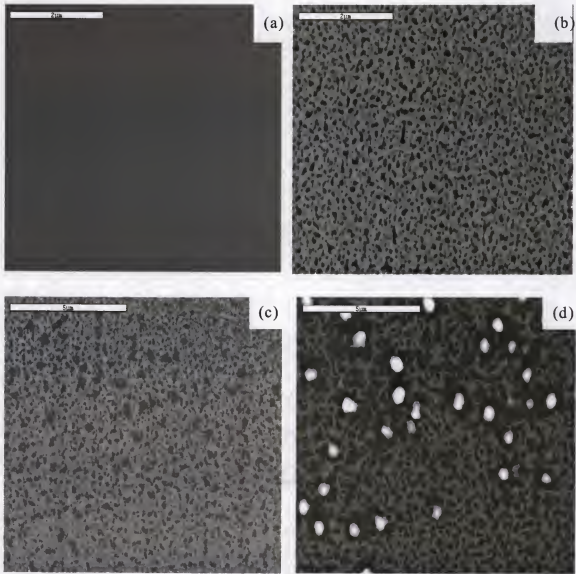
Figure 6.8 Microstructure of the 50/50 contact after annealing. SEM
backscattering electron image after (a) 600°C for 1 min; (b) 600°C
for 5 min; (c) 600°C for 10 min and (d) 600°C for 30 min.
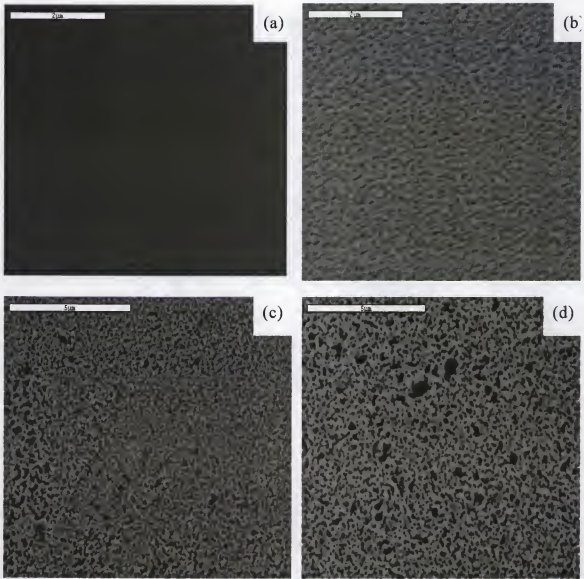
Figure 6.9 Microstructure of the 50/50/50 contact after annealing. SEM backscattering electron images after (a) 600°C for 1 min; (b) 600°C for 5 min; (c) 600°C for 10 min and (d) 600°C for 30 min.
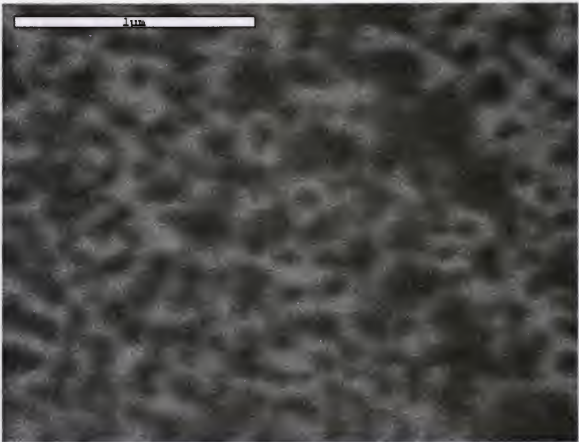
Figure 6.10. SEM backscattering electron image of same sample as in
Figure 6.9-(d) but at a higher magnification showing the Au film
is still continuous.

As the annealing time is increased from 1 min to 5 min, a very uniform microstructure

developed in the 50/50 contact scheme. The 50/50/50 contact exhibited a similar

microstructure except smaller pores were observed in the white Au matrix. In the

50/100/50 contact, the microstructure consists of larger pores and better defined

boundaries between white and dark regions. These microstructures were maintained in all

three contacts during increased anneal time from 5 to 10 min, except in all instances there

Figure 6.11 Microstructure of the 50/100/50 contact (SEM backscattering image) after annealing at (a) 600°C for 1min, (b) 600°C for 5min, (c)600°C for 10min, and (d)600°C for 30min.

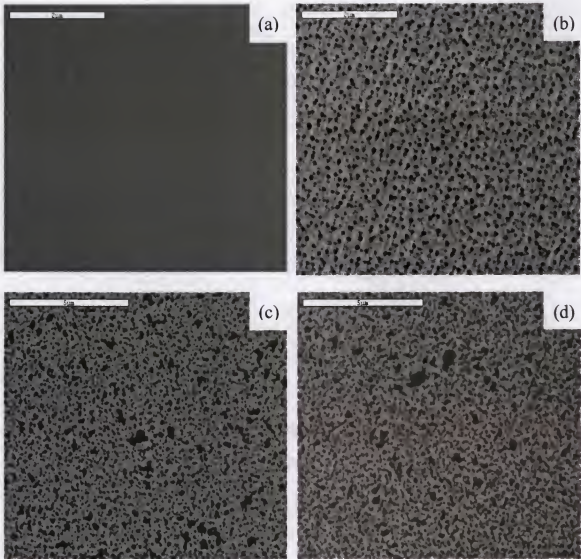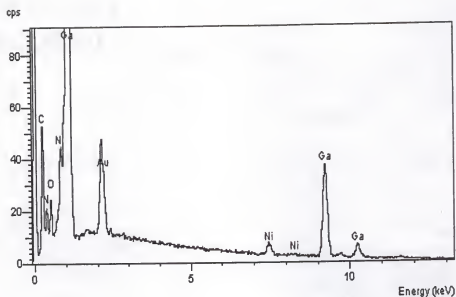Figure 6.12 EDS analysis of the light region in Figure 6.16-c showing a larger
Au/Ni peak ratio.
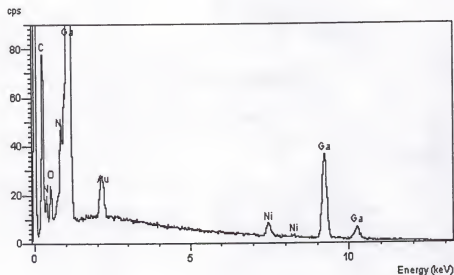
Figure 6.13 EDS analysis of the dark region in Figure 6.16-c showing a larger
Ni/Au ratio.
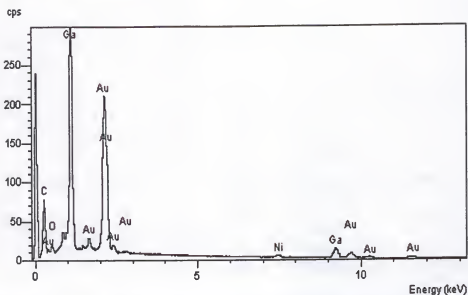
Figure 6.14 EDS analysis of spherical particle in Figure 6.16-d showing a very large Au/Ni ratio.

appear to be some isolated growth of Ni-rich dark pores to larger sizes (~0.5μm). As the annealing time increased from 10 min to 30min, minor changes were observed in the 50/50/50 and 50/100/50 samples, but numerous bright sub-micron spherical particles, surrounded by large dark areas, precipated on the 50/50 samples (Figure 6.8d). Point EDS analysis of these particles showed that they were Au and Ga rich, with no N signal detected (Figure 6.14). The excess Ga must result from dissociation of GaN. This result suggests that the thin Ni/Au contacts are not stable after 600°C, 30min anneal.

For the purpose of understanding the microstructural evolution, single layers of Ni or Au are deposited on GaN or sapphire substrates and annealed in oxygen ambients. The results show that Au without the presence of Ni forms submicron islands on both GaN and sapphire (Figure 6.15), similar to the light precipitates in Figure 6.8-(d). Annealed Ni with no Au cap layer forms a featureless, continuous NiO film (Figure 6.16).
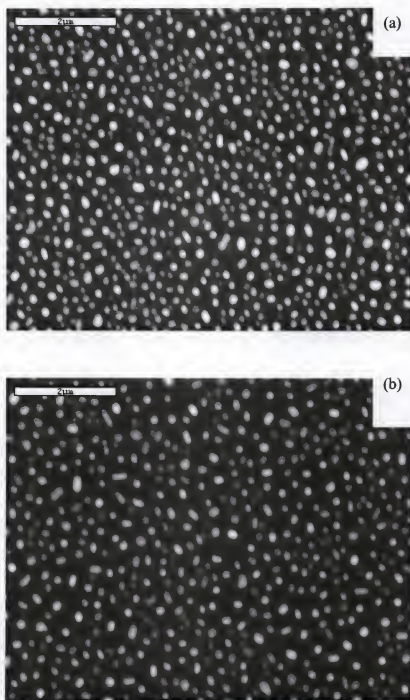
Figure 6.15 Annealed Au film on (a) MOCVD-GaN; (b) sapphire (600°C, 10min).

Figure 6.16 Annealed (600°C, 10min) Ni film on GaN showing no
formation of islands in contrast to Fig.6.15. The white particle is
contamination used for focusing of the SEM.

6.4.2 AES Survey and Depth Profiling

Figure 6.17 shows AES surveys from the 50/50 contact for different processing
conditions, and Figures 6.18 and 6.19 shows similar surveys for 50/50/50 and 50/100/50
contacts. The Au signal was only found at the surface of as-deposited state, but was not
found at the surface after annealing at 500°C or 600°C for 10min or 600°C for 30min. For
the 50/50/50 contact scheme, higher signal of oxygen was found on the as-deposited
surface than for 50/50 scheme due to the presence of original Ni, and the oxygen signal
increased further as the annealing temperature and time increased. The 50/100/50 scheme
showed similar trends to the 50/50/50 contacts.

The AES depth profile for the 50/50 scheme is shown in Figure 6.20, while those
from 50/50/50 and 50/100/50 contacts are shown in Figures 6.21 and 6.22, respectively.
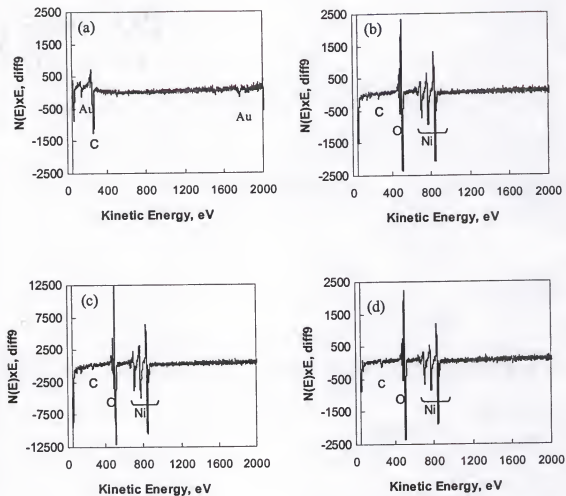
Figure 6.17 AES surface spectra from 50/50 contacts. (a) As-deposited; (b) 500°C for 10min; (c) 600°C for 10min; (d) 600°C for 30min.

For as deposited 50/50 contacts, the interface region between Ni and GaN was relatively sharp and the oxygen level was very low. Annealing at 600°C for 10min changes the surface to be only NiO with no Au detected. Compared to the as-deposited state, the interface between NiO/Au/GaN became very diffuse, either from diffusion or the microstructure shown in Figure 6.8. This is consistent with published reports [Ho99] that Au stayed in the NiO/GaN interfacial region. The oxygen level increased and followed
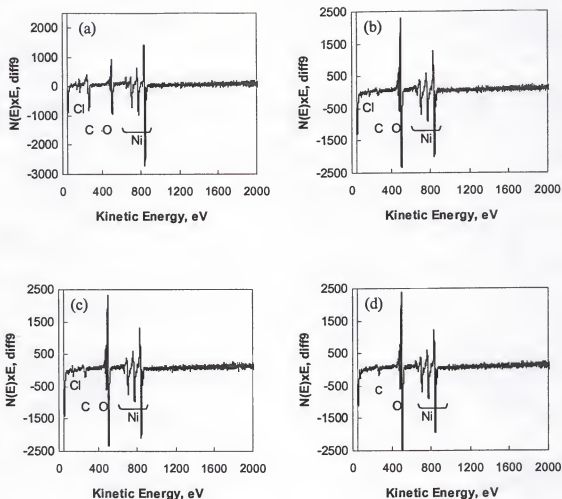
Figure 6.18 AES surface spectra from 50/50/50 contacts. (a) As deposited; (b) 500°C for 10min; (c) 600°C for 10min; (d) 600°C for 30min.

the Ni signal except for lower oxygen concentrations in the interfacial region. Increased annealing temperatures (up to 600°C) increased the O/Ni ratio in the top layer. Increased annealing time to 30 min resulted in no change in the distribution of these elements. There may have been more Ga was also found in the contact interfacial region with higher annealing temperatures and times. A Ga plateau in the contact interface at all temperature and time suggests formation of a Ni-Au-Ga compound (Figure 6.20-(b), (c)
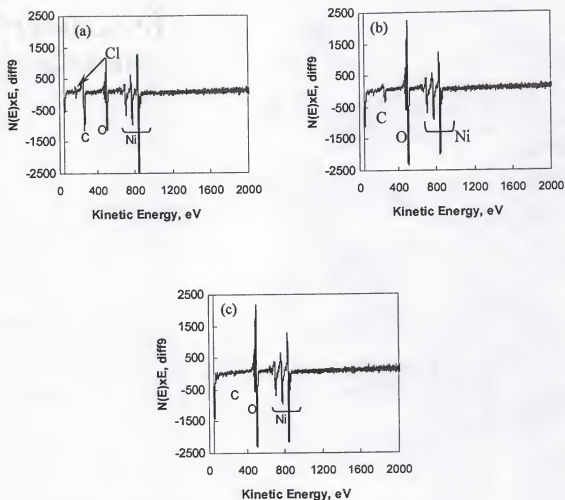
Figure 6.19 AES surface spectra from 50/100/50 contacts. (a) As-deposited; (b) 600°C for 10min; (c) 600°C for 30min.

and (d)). In the 50/50/50 and 50/100/50 schemes, Figure 6.21 and 6.22, the Ni and Au signals showed the two Ni layers and the sandwiched Au layer in the as-deposited states. Annealing at 600°C for 10min leveled the Ni humps and made the Au move into the interfacial region. A large oxygen to nickel ratio was found as the annealing temperature or time increased. The increase in the annealing time to 30min at 600°C did not result in significant changes in the depth profiles.
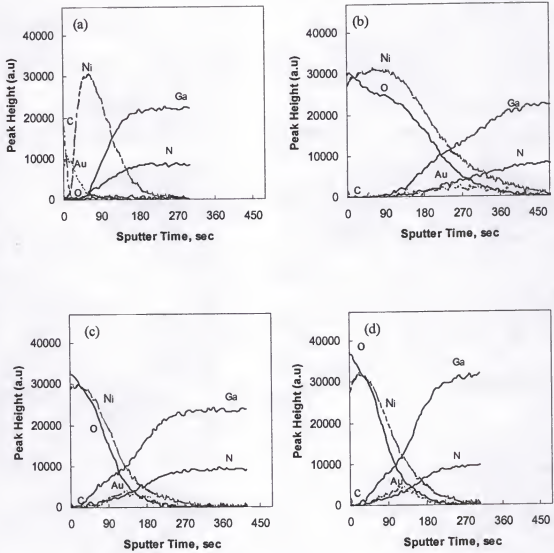
Figure 6.20 AES depth profile of 50/50 contacts. (a) As-deposited; (b) 500°C for 10min; (c) 600°C for 10min anneal; (d) 600°C for 30min.
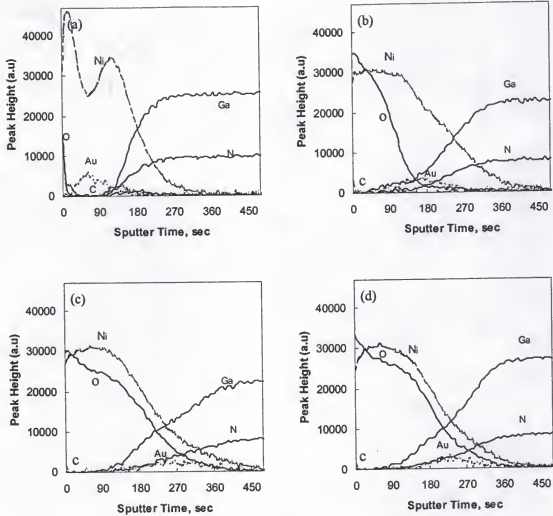
Figure 6.21 AES depth profile of 50/50/50 contact. (a) As deposited; (b) 500°C for 10min; (c) 600°C for 10min anneal; (d) 600°C for 30min.

6.4.3 XPS Analysis

To show the evolution of chemical states associated with the contact Ni metal and interfacial reaction products, XPS surveys were taken from the 50/50 and 50/50/50 contacts after annealing at 600°C for 10min. The bonding data were collected from the fresh surface after sputtering for a short time with an Ar ion beam (see Chapter 3).
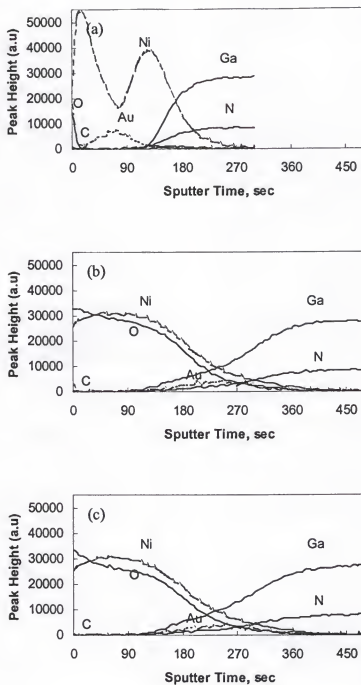
Figure 6.22 AES depth profile from 50/100/50 contacts. (a) As deposited; (b) 600°C for 10min; (c) 600°C for 30min.

Figures 6.23 and 6.24 shows the Ni2p peaks at different sputtering times in 50/50 and 50/50/50 contacts. For 50/50 contacts, the as received surface showed the Ni2p binding energy of 855eV. After 5min sputtering, this energy decreased to 853.5 eV. After 15min sputtering, this energy decreased further to 852.5eV, and only a small amount of Ni was detected after 15min sputtering. The presence of NiO is supported with the presence of shake up structures and chemical shift in Figure 6.23-(a) and (b) [Mou95], The lack of shake up peaks and energy shift indicates that the XPS spectrum in Figure 6.23-(c) is from metallic Ni. For 50/50/50 contact surfaces, the binding energy of Ni2p was again high and the shake-up stucture showed the compound to be NiO. The binding energy decreased after sputtering for 5min, and corresponds to the binding energy of NiO, and then decreased further to 853eV representing a mixture of oxide and metallic bond at the contact/p-GaN interface.

Changes in binding energy was also observed for the O1s signal (Figure 6.25 and 6.26) and Ga2p (Figure 6.27 and 6.28) peaks. The high energy shoulder on the O1s peak from both 50/50 and 50/50/50 contacts suggest the presence of hydroxides, consistent with higher binding energies on as-annealed surfaces from the Ga2p and 3d spectra. Sputtering for 5min, removed the high binding energy O1s shoulder and reduced the Ga2p and 3d binding energies, consistent with removal of a surface layer of $Ni(OH)_2$. The lower binding energies for Ni 2p and 3d after sputtering to near the contact/GaN interface and the loss of shake-up structure in the Ni 2p spectra showed the presence of a Ni-Au-Ga metallic layer at the interface, consistent with the AES depth profile plateaus obvious in Figures 6-20, 6-21 and 6-22.

Figure 6.23 XPS spectra of Ni2p from 50/50 contact after annealing at 600°C for 10min. (a) As-annealed surface; (b) 5 min sputtering; (c) 15min sputtering.
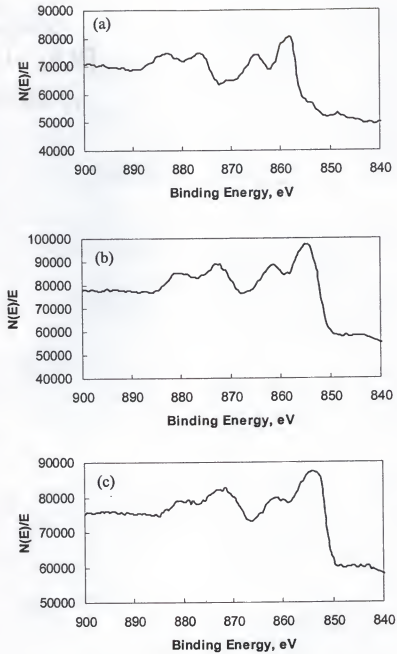
Figure 6.24 XPS spectra of Ni2p from 50/50/50 contact after annealing at 600°C

for 10min. (a) As annealed surface; (b) 5 min sputtering; (c) 15min
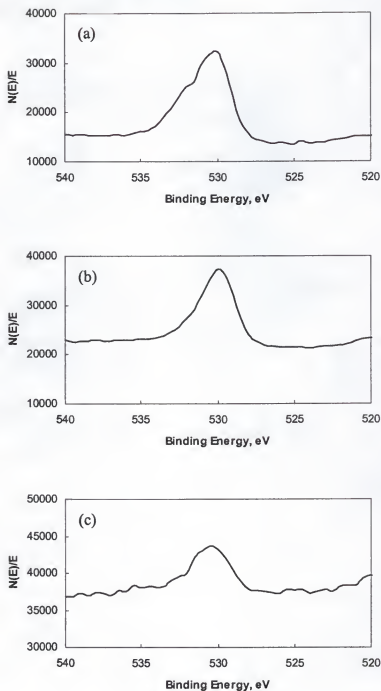
sputtering.

Figure 6.25 XPS spectra of O1s from 50/50 contact after annealing at 600°C for 10min. (a) As-received Contact; (b)5 min sputtering; (c) 15min sputtering
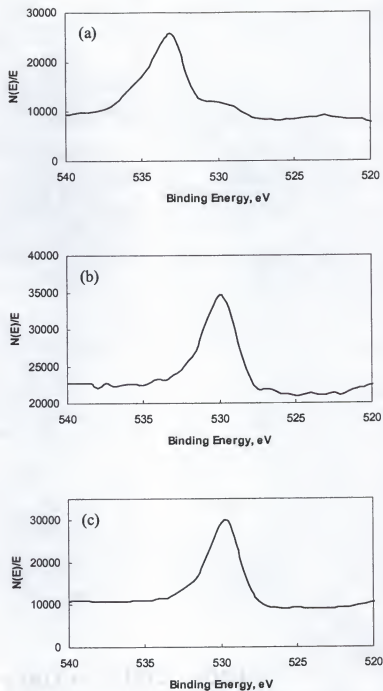
Figure 6.26 XPS spectra of O1s from 50/50/50 contact after annealing at 600°C for 10min. (a) As-received contact; (b)5 min sputtering; (c) 15min sputtering
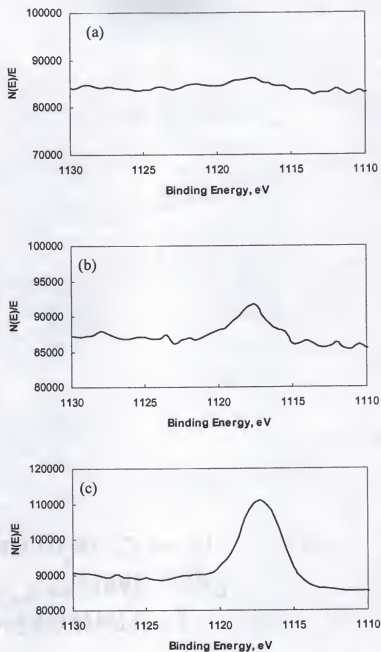
Figure 6.27 XPS spectra of Ga2p from 50/50 contact after annealing at 600°C for 10min. (a) As received contact; (b) 5 min sputtering; (c) 15min sputtering
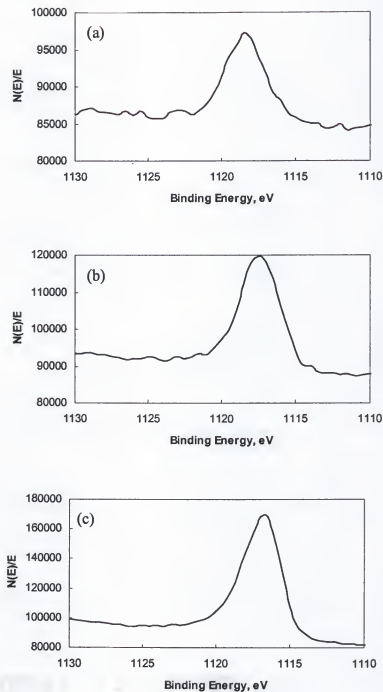
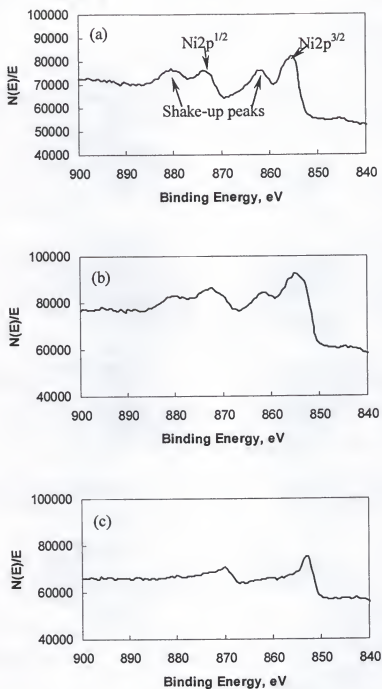Figure 6.28 XPS spectra of Ga2p from 50/50/50 contact after annealing at 600°C for 10min. (a) As-received Contact; (b) 5 min sputtering; (c) 15min sputtering

6.5 Discussion

The mechanism by which oxidized thin Ni/Au films lead to ohmic contact to p-GaN has been discussed [Ho99b]. The effects of thick versus thin p-NiO were considered. With a thick NiO layer, a large portion of the applied voltage is dropped across the p-NiO. The impedance increases with increasing reverse bias voltage because of the barrier and the resistive NiO layer. With a thin NiO layer, the existence of a hole notch close to p-GaN makes the carrier transport easily in the contact region due to a field emission mechanism, thus formation of an ohmic contact is possible. However, the microstructure development and the effects of a Au-Ni-Ga interfacial layer has not been included in the model.

In Ho's model [Ho99b], the distribution of barrier between GaN and p-NiO was calculated. With a carrier concentration of 2×10^{17} cm^{-3}, the Fermi level in p-GaN was calculated to be 0.13 eV above the top of the valence band at 300 K. For undoped p-NiO, the carrier concentration was estimated to be 1×10^{16} cm^{-3}, and the Fermi level was calculted to be 0.5 eV above the top of the valence band. From these parameters, and by equaling the built-in potential across the p-NiO/p-GaN isotype heterojunction to the work function difference between p-GaN and p-NiO (before the formation of a junction), a barrier value of 2.47 eV was obtained. The distribution of this barrier was further calculated to be 2.415 eV in p-NiO and 0.055 eV in p-GaN. The structure of this contact to p-GaN was regarded as Au/p-NiO/p-GaN as shown in Figure 6-29. An ideal ohmic contact would be formed between Au and p-NiO because the work function of Au ($\phi_{Au} = 5.10$ eV) is larger than that of p-NiO ($\phi_{p-NiO} = 4.9$ eV). A hole notch is formed at the NiO/p-GaN hetereojunction because of the large band offset between p-NiO and p-GaN.
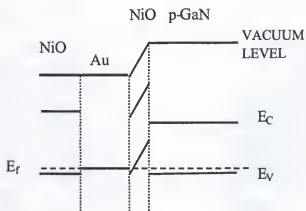
Figure 6.29 Energy diagram of oxidized thin Ni/Au contact to p-GaN

Because the Au network dispersed in the matrix of NiO is covered with NiO, the energy diagram presented in [Ho99b] for thin p-NiO contacts to p-GaN is modified as in Figure 6.29 by the addition of the NiO levels to the left of Au. The above discussion successfully explains the mechanism of ohmic contact between thin oxidized Ni/Au and p-GaN, however, no explanation was given for ignoring Fermi level pinning in NiO or GaN. Fermi level pinning of GaN was described in Chapter 2 [Ren98].

The validity of ignoring the pinning of the Fermi level in these contacts might be justified by the reaction between Ni and GaN. These reactions to form Ni-Ga compounds (e.g. Ga_4Ni_3 and Ga_3Ni_2 [Che99]) can lead to intimate interface bonding between Ni and GaN. This would reduce the density of surface states from dangling bonds, which is believed to be the major source of Fermi level pinning [Bar47].

Besides the reaction between Ni and GaN, the match of lattice constants is also important to reduced contact resistivity by reducing the defects in the contact region. The lattice constants of GaN, Ni, NiO and Au are listed in Table 6.1 [Edg98, Liu89]. The lattice constants of NiO and Au differ by only ~2.5%, and a reaction between Ni and

Table 6.1 Lattice constants (Å) of components in oxidized Ni/Au contacts to p-GaN

GaN	Ni	NiO	Au
a = 3.189	3.499	4.177	4.065
c = 5.185			

GaN to form a compound might also improve the ~12% mismatch of the lattice constants between GaN and Ni. The large mismatch in lattice constants between Ni and NiO can be modified continuously by change of the oxygen composition. In this way, a lattice matched contact system of NiO-Au-NiO-Ni-GaN could be formed. Which would be expected to reduce the interfacial defect. In fact, orientation relationships are found among NiO, Au and GaN [Che99], which is:

$$NiO(111)//Au (11\underline{1})//GaN(0002) \text{ and}$$

$$NiO[1\underline{1}0]//Au [1\underline{1}0]//GaN[11\underline{2}0].$$

Lack of development of strong texture or even epitaxy at the contact interface could explain why sputter deposited thick NiO/Au resulted in poor contact properties [Mae00].

The AES data (Figures 6.17 to 6.22) showed the as-deposited surface were metals (either Au or Ni) with a NiO layer formed at all the contact surfaces after annealing. The Au rearranged to the contact interfacial region, and most of the Ni diffused out to form NiO. This is consistent with published work [Che99]. After addition of the Ni cap layer, the inner Ni layer still diffused out to the surface region to react with oxygen, but the contact properties changed, and the mechanism need to be discussed.

The Ni cap-layer was converted to NiO after annealing in O_2. As discussed above, NiO is a wide-bandgap semiconductor which is semi-insulating, so the conductivity of the contact pad (contact sheet resistance) would decrease, as observed in this study. However, the specific contact resistances of annealed 50/50/50 contacts were close to

those of the 50/50 scheme for the optimum annealing condition (Figure 6.2). From

calculation of the depletion width, W, in the tunneling current regime [Sze81]

$$W = \sqrt{\frac{2\varepsilon_s V_{bi}}{qN_B}},\tag{6.2}$$

we have the relation of

$$V_{bi} = \frac{W^2 \cdot q \cdot N_B}{2 \cdot \varepsilon_s}\tag{6.3}$$

where W is the total depletion distance, ε_s is semiconductor permittivity, V_{bi} is built-in

potential, q is magnitude of electronic charge, and N_B is either acceptor or donor impurity

density. This shows that an increased NiO thickness (equal to an increase of the depletion

distance W) should form a larger barrier. For light Transmittance, the Au layer thickness
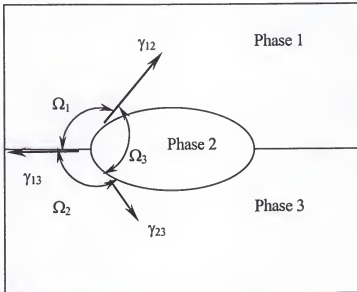
Figure 6.30. Schematic diagram of interface equilibrium between

three phases

was the same for both contact schemes, but the increased NiO thickness should normally be expected to decrease the amount of transmitted light

The Ni/Au ratio of unity [Ho99b] was reported to yield the lowest contact resistivity. With the sandwich Ni/Au/Ni contacts, the critical parameter appears to be the Au thickness rather than the ratio of Au/Ni thickness.

The microstructure evolution of the Ni/Au and Ni/Au/Ni contacts may be explained using the concept of surface tension. Advanced modeling of thin film morphologies is based on work by Srolovitz and Safran [Sro86] which shows the Ni cap-layer is effective in improving the thermal stability of the contacts. Last, reaction kinetics are considered to show that the microstructural morphology differences are possible reasons for different light transmittance in these samples.

The surface tension in thin films is shown in Figure 6.30. A three phase equilibrium situation is considered. The simple Dupre equation [Mur75] governing the balance of interfacial free energies for three phases of 1, 2 and 3 in equilibrium in the absence of interfacial torques is:

$$\frac{\gamma_{23}}{\sin\Omega_1} = \frac{\gamma_{13}}{\sin\Omega_2} = \frac{\gamma_{12}}{\sin\Omega_3} \qquad (6.4)$$

where γ_{12}, γ_{13} and γ_{23} represent the phase boundary free energies between phases _1_ and _2_, _1_ and _3_, and _2_ and _3_, respectively. The Ω_1, Ω_2 and Ω_3 are the dihedral contact angles measured in phases _1, 2_ and _3_, respectively. Phase _1, 2_ and _3_ may be solid, liquid or vapor, or any variation thereof.

To show the effects of Ni cap-layer on the microstructure evolution, the surface tensions values involved are listed in Table 6.2. No surface tension data were found for Ni/GaN, Ni/sapphire, Au/GaN and Au/sapphire interfaces. These values were calculated

Table 6.2 Values of surface tension of Ni and Au [Mur75b, Cha87]

System	Surface Tension (J/m^2)
Au/Vac	1.658
Au/Ni	0.114
Au/NiO	~2.0
Au/Au (grain boundary)	0.438
Ni/Vac	2.533
Ni/NiO	0.392
Ni/Ni (grain boundary)	0.958
Ni/Ni (twin boundary)	0.052
NiO/NiO	1.00

at 400°C, which is similar to the temperature used in this work. The surface tension decreased after replacing the gold/vacuum interface, Au/Vac, with a gold/nickel, Au/Ni, interface.

In Ni/Au contacts with no Ni cap-layer, the three phases of Au, air and Ni exist in the contact. With the Ni cap layer, these three phases become Ni, Au and Ni. The contact angle of Au on Ni in these two situations was calculated using the values listed in Table 6.2. Before annealing, the equilibrium contact angles of the Au on Ni (γ_3 in Figure 6.30 where Ni is phase 3 and Au is phase 2) were calculated to be 0°, for the contact with and without a Ni cap layer. This explains the results shown in Figure 6.16-19 which showed that Au and Ni spread on the whole contact surface and the as-deposited surfaces were featureless. After annealing in O$_2$, the surface layer became NiO for both situations and the Au moved to the interfacial region. Because a value of surface tension for GaN is unknown, the Au was assumed to be sandwiched between two NiO layers as reported by [Ho99b]. Using the above equation, this contact angle (Ω_3) was calculated to be 150°,

which means the Au would not remain flat, but islands or porous networks should form as shown schematically in Figure 6.30.

This is consistent with the formation of islands of Au in the annealed single Au film on GaN and sapphire, as seen in Figure 6.15. However, this argument does not explain the formation of cavities (holes), rather than "islands" in the annealed Ni/Au or Ni/Au/Ni contacts.

Hole formation in thin films have been widely reported. Chao *et al* [Cho87] observed porosities in thin Ni/Au metallization layers annealed in oxidizing environments from 250 to 400°C. Kane *et al* [Kan66] observed hole formation in gold films deposited onto or between cadmium sulphide (CdS) layers upon heating to 450°C in the atomosphere of helium. Gimpl *et al* [Gim64] reported agglomeration in gold and nickel, and formation of holes was also reported by Jaeger *et al* [Jae69] in silver films prepared under ultrahigh vacuum conditions followed by exposure to air.

Numerous mechanisms have also been suggested for the formation of porosity in metallization, such as grain boundary and bulk interdiffusion [Bac80, Nak80], generation of stresses [Hum71], and grain boundary grooving [Hum81]. Grain boundary grooving driven by capillarity (surface tension) was shown to be detrimental to the stability of thin gold films. The effects of grain boundary grooving on the film continuity was modeled by considering the surface and grain boundary energies and conserving the total volume of metal [Sro86].

The stability of the pores in thin film contacts was evaluated using the Srolovitz and Safran model [Sro86]. For pores with a radius r_p existing in a film of thickness a and
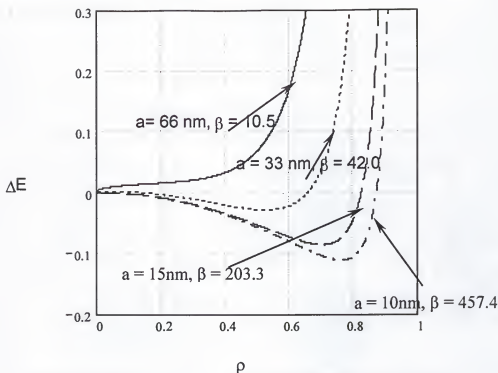
Figure 6.31 ΔE versus ρ (= r_p/R) calculated for 50/50 and 50/50/50

contacts, respectively. See text for assumption.

an average distance between pores of $2R$, the energy change between a porous and a

continuous thin film, ΔE, can be written as:

$$\frac{\Delta E}{\pi \cdot a^2 \cdot \gamma_v} = \frac{-4}{3 + 4 \cdot \ln \rho - 4 \cdot \rho^2 + \rho^4} - \beta \cdot \rho^2 \qquad (6.5),$$

where $\qquad \beta = (1 + \frac{\gamma_s}{\gamma_v}) \cdot \frac{R^2}{a^2},$

$$\rho = \frac{r_p}{R},$$

and γ_v is the surface energy of gold in ambient, $\gamma_s = \gamma_{sv} - \gamma_{fs}$, γ_{sv} is the substrate-ambient

surface energy, and γ_{fs} is the film-substrate interfacial energy.

Because all the samples are heat treated in oxidizing ambients, a NiO overlayer exists on the Au film as shown with AES data. The samples were actually Au films sandwiched between Ni at the substrate and NiO at the surface, just as was true in the work of Chao *et al* [Cha87]. The Srolovitz and Safran model can be extended to the present thin film contacts by replacing the Au/ambient surface energy by the Au/NiO solid surface energy, i.e., by replacing the ambient vapor by a solid NiO layer, i.e. the substrate/vapor energy γ_{sv} is the interfacial energy of Ni and NiO. To calculate β, the values of $\gamma_{Au/NiO}$, $\gamma_{Au/Ni}$, and $\gamma_{Ni/NiO}$ in Table 6.2 are used. The results in [Ho99b] showed that for 50Å Ni/50Å Au metallization, the contact thickness is around 330Å after oxidation, with no explanation given for the expansion. However it seems reasonable to assume this results from conversion of Ni to NiO, reactions between Ni-GaN-Au, and changed microstructure. Assuming the same ratio for the 50Å Ni/50Å Au contacts also applies to Ni/Au/Ni contacts, the thickness is calculated to be 660Å. For comparison, the initial thickness of 150 Å and 100 Å are also included for calculation. Substituting these surface energies into the expression for β and taking $2R = 0.2$ μm (as measured in Figure 6.8), $a = 330$Å and 100 Å for the 50Å Ni/50Å Au and $a = 660$ Å and 150 Å for the 50Å Ni/50Å Au/50Å Ni, the value of β is calculated to be 42, 457.4, 10.5 and 203.3, respectively.

The plots of ΔE vs r_p/R (ρ) are shown in Figure 6.30. For $\beta \sim 10.5$, the energy of the system increases as the pore radius increases, so spontaneous growth of pores is not expected in contacts with Ni cap layers. For $\beta \sim 42$, 203.3 and 457.4, the energy of the system is reduced as pores grow, and it reaches a minimum at $r_p/R = 0.55$. Spontaneous growth of pores is expected since growth will lower the system free energy. For

Ni/Au/Ni, smaller pore size is expected as compared to Ni/Au contacts with no Ni cap layer.

Contrary to the data in Figure 6.31 for $\beta = 10.5$, pores do grow in contacts with Ni cap layers, as shown in Figure 6.9 and 6.10. This inaccurate prediction probably results from oversimplification of the actual situations. The Srolovitz and Safran model assumes a single value for grain size and idealized geometry. While these facts do not invalidate the model, they do cause inaccuracies. Stress in the thin films may also influence the growth of pores, but the model does not consider strain energy which would certainly modify the curves in Figure 6.31.

It should also be recognized that the Srolovitz and Safran model assumes that no defects exist in the gold film prior to heat treatments. Gold is well known to contain pinholes and pores in the as-deposited films which might grow to bigger sizes as observed in this study. However, the porosity in this work is not believed to come from inherent defects in the deposited Au film because the pore density is extremely high and uniform over the sample. Random, large inherent defects were observed, but they did not lead to such uniform microstructures as shown in Figure 6.8 to 6.11.

To explain the increased light transmittance in 50/50/50 contacts, the microstructural morphology must be considered. With the thin Au film, the out-diffusion of Ni from the inside layer still allows the Ni-Au-Ni structure to exist for at least a short time. This results in a contact angle (Ω_3 in Figure 6.29) of 153.64°(using the twin boundary energy in Table 6.2) is equilibrium is approached. Because of limited transport distances, the density of nucleation sites required to approach this equilibrium structure would be large and would result in the very uniform microstructure as observed. Once

(a)

(b)

(c)
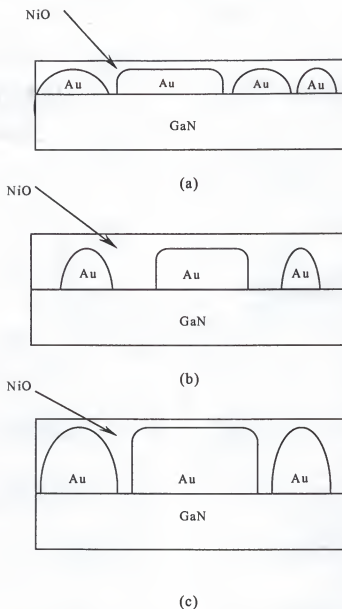
Figure 6.32 Schematic diagram of contact microstructure showing (a) 50ÅNi/ 50Å Au,
(b) 50Å Ni/50Å Au/50Å Ni and (c) 50Å Ni/100Å Au/50Å Ni contacts. In
50Å Ni/50Å Au contacts, the Au network pore area is less, causing more
light absorption in the thin Au regions. In 50Å Ni/50Å Au/50Å Ni contacts,
the area of pores is larger with a subsequent thicker Au network, resulting in
less absorption, more transmittance of light. Finally in 50Å Ni/100Å
Au/50Å Ni contacts, a thicker Au network and lower pore area
microstructure leads to less transmitted light.

this microstructure had developed after an anneal of 600°C for10min, it did not

significantly change with longer time annealing (to 30min). The lack of large Au islands

as shown in Figure 6.8-(d) shows much better thermal stability for 50/50/50 contacts

versus 50/50 contacts.

In the SEM pictures (Figure 6.8 to 6.11), the light color region corresponds to Au

and the dark region is NiO. In the 50/50 contact, the Au film stayed as a continuous layer

with dark "pores" (the term used in [Cha87]). The Au-rich regions occupied a larger

fraction (~70%) of surface area as compared to the pores (~30%, Figure 6.8-(c)). In the

50/50/50 contact, however, it was hard to tell which component was dominant between

the Au network and "pores" (~50% for each component, Figure 6.9-(c)). The Au and NiO

interlace with each other and form a very uniform mixture, but the Au was still

continuous. The Au network covered a smaller fractional area of the surface as compared

to the 50/50 contact. Since the original Au thickness was the same in both contact

schemes before annealing, the Au areas in the 50/50/50 should be thicker than those in

the 50/50 contacts after annealing.

The schematic diagram of the microstructure is shown in Figure 6.32 for the three

contact schemes. Although the NiO would be thicker in the 50/50/50 scheme, the

increased Au thickness would still allow significant current through the contact because

of its continuous network. As a result, similar contact specific resistance was obtained for

50/50/50 contacts as in 50/50 contacts. On the other hand, the Au film in the 50/100/50

contact was thick and occupied a large area again (Figure 6.11-(c)), and the

microstructure was similar to that of the 50/50 contact (Figure 6.8-(c)).

The schematic diagram of microstructures in Figure 6.32 explains the higher light transmittance in the 50/50/50 contacts. If light transmittance through the Au film is ignored (the characteristic penetration depth is 150Å in Au film at a wavelength of 589.3 nm [Hum92]), then the light only goes through the "dark" pores (as seen in the SEM pictures). The annealed 50/50/50 contacts cause a larger area percent of surface to be pores and would allow more transmittance of light. In practice, some light still goes through the thin Au film although it experiences attenuation (to 37% of the initial intensity if the Au film is equal to the characteristic thickness of 150Å). In the 50/100/50 contact, the increased Au feature size was due to the thicker Au film resulting in lower transmittance.

In this argument, light scattering from the microstructure has been ignored. Since the features are typically less than half the wavelength of light, this seems reasonable. However, diffraction effects can still change the intensity and direction of light scattering from such small patterns. This needs to be explored in future research.

6.6 Summary

Formation of low resistance "transparent" ohmic contacts using oxidized thin Ni/Au films on p-GaN was a major achievement. Using this scheme, the specific contact resistance was reported in the literature to be as low as 4×10^{-6} $\Omega \cdot cm^2$, although the best results in this study was 10^{-4} $\Omega \cdot cm^2$. While thinner ohmic contact would be more transparent allowing better light output from high brightness LEDs or LDs, thin contacts may exhibit thermal instability, coverage problems, and higher contact sheet resistances. To increase the contact thickness while retaining good electrical properties and high light

transmittance, a thin Ni capping layer was placed on top of Au/Ni/GaN contacts. The Ni cap-layer was shown to transform into transparent NiO upon annealing and result in higher light transmittance (~93% versus 85% for 50/50 contacts) while retaining the same low contact resistance (~10^{-4} Ω-cm^2). Thicker Au with the same 50ÅNi cap-layer resulted in higher contact resistance (~10^{-3} Ω-cm^2) and lower light transmittance (60%). Based on SEM backscattering images, the microstructures consist of a continuous Au network with Ni-rich pores reaching the GaN surface. The area fraction of pores was larger for 50/50/50 contacts versus 50/50 contacts, which explains the higher light transmittance. Using AES and XPS depth profiling, the Ni layer was found mainly to diffuse out and form NiO on the surface, but a fraction of the Ni metal reacted with GaN.

The development of the microstructure consisting of a Au network with Ni-rich pores was modeled based on the concept of surface tension and grain boundary grooving. The Srolovitz and Safran model predicted that without a Ni cap-layer, pores would lower the system free energy and grow automatically to a limiting critical radius. With the addition of a Ni cap-layer, the pores increased the system free energy and should not grow. However, it was speculated that strain energy still allowed them to grow, but to a smaller, more uniform size. This is consistent with the observed improved thermal stability of Ni capped contacts.

CHAPTER 7
CONCLUSIONS

Formation and improvement of ohmic contacts to p-GaN has been studied using I-V data from patterned TLM contacts. H_2O_2 was used in passivating the surface of p-type MBE GaN, resulting in higher conductivities. A "NOG" scheme was proposed to help understand formation of ohmic contacts to p-GaN, and addition of a Ni cap-layer to thin transparent Ni/Au contact was shown to increase the light but still maintain a low contact resistance.

Using the H_2O_2 treatment, an increase in the carrier concentration up to 100% for MBE grown p-GaN doped 2×10^{17} cm^{-3} with Mg. Peroxide: water solutions ranging from 1:5 to pure (37%) H_2O_2 were tested for times ranging from 30sec to 60min. For treatment time, 30sec < t < 30min, increased carrier concentrations were demonstrated for 1:1 solutions. For t = 60min, reduced carrier concentrations were found. H_2O_2 treatment did not affect n-GaN or p-GaN grown by MOCVD. Possible explanations for the effects of H_2O_2 were discussed, with the best model being reduction of acceptor compensation by either hydrogen removal or reduction of nitrogen vacancies. Nanopipe transport of H2O2 species are thought to help the kinetics.

The "NOG" contact scheme was developed based on the knowledge of metallurgical reactions between transition metals and GaN. The approach of using a nitride-forming metal over a gallide-forming metal can modify the thermodynamic activity of N and Ga near the interface. This in turn can change the near-surface point

defect concentrations, particularly the N vacancies and excess Ga. The principles of this contact scheme were shown to qualitatively agree with literature data from Ni/Au, Ni/Zn-Au, Ta/Ti, and Ni/Mg/Ni/Si contact schemes. In the current experimental study, the "NOG" scheme was used to design metallizations of Ni/Ti/Au, Ni/Al/Au, Pt/Si/Pt/Au and Pt/Mg/Pt/Au. The addition of Ti, Al and Si as nitride-forming metals to the Ni or Pt gallide-forming metal led to improved current transport across the interfacial barrier. Ti was shown to be better than Al as the nitride-forming metal in as-deposited contacts. Compared to Ni/Au, four times more current was measured in Ni/Ti/Au contacts to p-GaN after annealing at $300^{\circ}C$ for 5 min. However, selection of metallization schemes based on the "NOG" model was not able to decrease the contact resistivity to a level low enough for device applications. This was ascribed to interfacial diffusion which consumes the extra N atoms in the interface region. Besides, addition of Ti metal led to lower thermal stability of the Ni/Au contact. Addition of Mg to Pt/Au contacts also led to serious thermal stability problems.

Addition of a Ni cap-layers to thin transparent Ni/Au ohmic contacts to p-GaN was aimed at improving the contact microstructure. This Ni cap layer was oxidized to a transparent NiO layer and resulted in a higher light transmission (~93%), same low contact resistivity (~10^{-4} Ω-cm^2) and better thermal stability.

The changes in the electrical and optical properties as well as the microstructure evolution after adding the Ni cap-layer were explained using surface tensions and the total system energy of thin film structures. With a capping layer of Ni, the increased contact angles from interface tension led to a finer structure and allowed more light

transmittance through the contact. Because of the increased thickness, high anneal times and temperatures were needed to reach the optimized properties.

CHAPTER 8
FUTURE WORK

GaN and related materials have presented exciting opportunities in materials research and device engineering. This has become an example of the beneficial interplay between science and technology. The continued advancement of new devices made from GaN requires better understanding of the mechanisms controlling the formation of ohmic contacts to p-GaN, and this understanding needs to result in lower ohmic contact resistance.

For the H_2O_2 solution treatment of p-GaN, the most important thing should be to find a good procedure to clean the newly formed oxides after the H_2O_2 treatment, with the purpose of removing the excess Ga atoms but not increasing the oxides at the contact interfacial region. More work in finding better parameters will be definitely helpful in improving of the contact properties.

For the "NOG" scheme, work must be continued to find a contact scheme that provides both low resistance and good thermal stability to p-GaN. Titanium has been shown to form contacts with higher currents than the Ni/Au scheme, but the resistance is still too high to be used in practical devices, although it can be used in Hall measurement at room temperature in place of In. Ta is probably a good candidate to form better contact than Ti. A diffusion barrier to prevent the formation of stable nitrides should also result in an improvement in device performance. Nb might be a good candidate for the diffusion barrier due to its slow diffusion rates in Ni.

In the oxidized thin Ni/Au and Ni/Au/Ni schemes, more experimental work on sample cleaning, effects of annealing temperature and time, and O_2 flowing rates is needed to find better processing parameters to decrease the contact resistance. On the other hand, while a low resistance of 4×10^{-6} Ω-cm^2 was reported, the work performed in this dissertation only showed specific contact resistance of $10^{-4} \sim 10^{-3}$ Ω-cm^2, which means the reported low value is not a typical result for this contact scheme.

Also, this work showed that the contact pads have high resistances. Thick NiO layer on the contact would not allow much current to flow through the contacts, so those contacts with a thick NiO layer would be difficult to meet the specifications for applications requiring a thicker contact. More work is needed to decrease the resistivity of the NiO film. If the NiO can be made more conductive, the thickness of the cap-layer in the Ni/Au/Ni scheme can be increased further, while still keep the good electrical and optical properties. Doping with lithium is an option for this purpose.

While this dissertation provides simple models for the high light transmittance and low specific contact resistance of the 50/50/50 scheme, they are only the beginning to address this complex problem. The effects of light absorption and scattering in the Au films need to be considered, as well as the effects of Ni cap-layer on reaction kinetics. Computer simulation on the microstructure evolution in the annealed state should be helpful in obtaining a more in-depth and detailed understanding of the positive roles of Ni cap-layer in the thin Ni/Au contact scheme. Finally the role of the metallic Ni-rich layer in contact formation should be further investigated.

LIST OF REFERENCES

Abe96 C. R. Abernathy, S. J. Pearton, J. D. MacKenzie, J. W. Lee, C. B. Vartuli, R. G. Wilson, R. J. Shul, J. C. Zolper, J. M. Zavada, *Gallium nitride and related materials*, Pittsburgh, Penn. :*Mater. Res. Soc. Symp. Proc.* **395**, 685(1996)

Abe97 C. R. Abenathy, *GaN and related materials*, edited by S. J. Pearton, Gordon and Breach, New York, 1997

Ade93 I. Adesida, A. Mahajan, E. Andideh, M. A. Khan, D. T. Olsen and J. N. Kuznia, *Appl. Phys. Lett.* **63**, 2777(1993)

Adl70 D. Adler and J. Feinleib, *Phys. Rev.* **B2**, 3112(1970)

Aka89 I. Akasaki, H. Amano, Y. Koide, H. Matsa and N. Sawaki, *J. Cryst. Growth*, **98**, 209(1989)

Ama86 H. Amano, N. Sawaki, I. Akasaki and Y. Toyada, *Appl. Phys. Lett.*, **48**, 353(1986)

Amb98 O. Ambacher, *J. Phys.* **D31**, 2653(1998)

Bar47 J. Bardeen, *Phys. Rev.*, **71**: 71(1947)

Ber72 H. H. Berger, *Solid state electron*, **15**(2), 145(1972)

Ber93 V. M. Bermudez, R. Kaplan, M. A. Khan, J. N. Kuznia, *Physical Review*, **B48**, 2436(1993)

Ber96a V. M. Bermudez,. *J. Appl. Phys.*, **80**(2), 1190(1996)

Ber96b V. M. Bermudez, T. M. Jung, K. Doverspike, A. E. Wichenden, *J. Appl. Phys.*, **79**(1), 110(1996)

Ber97 F. Bernardini and V. Fiorentini, *Appl. Phys. Lett.*, **70**(22) 2990(1997)

Bin97 S. C. Binari and H. B. Dietrich, *GaN and related materials*, edited by S. J. Pearton (Gordon and Breach Science Publishers, NY, 1997), 509

Boe88 F. R. Boer, D. R. Boom, W. C. M. Mattern and A. R. Miedema, *Cohesion in metals : transition metal alloys* Amsterdam ; New York : North-Holland ; New

York, N.Y., U.S.A. : Sole distributors for the U.S.A. and Canada, Elsevier Scientific Pub. Co., 1988

Bou00   D. P. Bour, N. M. Nickel, C. G. Van de Walle, M. S. Kneissl, B. S. Krusor, Ping Mei, and N. M. Johnson, *Appl. Phys. Lett.* **76**, 2182(2000)

Bri93   L. J. Brillson (ed.) *Contacts to Semiconductors*. Park Ridge, N.J. : Noyes, c1993

Bru92   C. R. Brundle, C. A. Evans, Jr., S. Wilson, *Encyclopedia of materials characterization : surfaces, interfaces, thin films*, managing editor, L. E. Fitzpatrick, Boston : Butterworth-Heinemann ; Greenwich, CT : Manning, c1992

Cao00   X. A. Cao, *Advanced Processing of GaN for Novel Electronic Devices*, Ph.D dissertation, University of Florida, 2000

Cha87   Y.-K. Chao, S. K. Kurinec, I. Toor, H. Shillingford and P. H. Holloway, *J. Vac. Sci. Technol.* **A5(3)**, 337(1987)

Che97   W. M. Chen, I. A. Buyanova, W. X. Ni, G. V. Hanson and B. Monemar, *Appl. Phys. Lett.* **70**, 369(1997)

Che99   L. C. Chen, F. R. Chen, J. J. Kai, L. Chang, J. K. Ho, C. S. Jong, C. C. Chiu, C. N. Huang, C. Y. Chen and K. K. Shih, *J. Appl. Phys.* **86**, 3826(1999)

Cho94   T. P. Chow and R. Tyagi, *IEEE Trans. Electron. Dev.*, **41**, 1481(1994)

Chu92   B.-C. Chung and M. Gershenzon, *J. Appl. Phys.* **72**, 651(1992)

Cor97   H. Cordes and Y.A. Chang, *Mat. Res. Soc. Inter. J. Nitride Semi. Res.* **2**, 2(1997)

Dav88   R. F. Davis, Z. Sitar, B. E. Williams, H. S. Kong, H. J. Kim, J. W. Palmour, J. A. Edmond, J. Ryu, J. T. Glass and C. H. Carter, Jr., *Mater. Sci. Engr.* **B1**, 77(1988)

Dav97   R. F. Davis, M. J. Paisley, Z. Sitar, D. J. Kester, K. S. Ailey, K. Linthicum, L. B. Rowland, S. Tanaka and R. S. Kern, *J. Cryst. Growth*, **178**, 87(1997)

Dav99   A. V. Davydov and T. J. Anderson, *III-V Nitride Materials and Processess III, Electrochemical Society Proceedings* **98-18**, 38(1999)

Deh93   R. T. DeHoff, *Thermodynamics in Materials Science*, McGrain-Hill, inc. 1993

Den97   S. P. Benbaars, *Proceedings of the IEEE*, **85**(11): 1740(1997)

Dux97   K. J. Duxstad, E. E. Haller, K. M. Yu, M. T. Hirsch, W. R. Imler, D. A. Steigerwald, F. A. Ponce and L. T. Romano, *III-V Nitrides*, *Mater. Res. Soc. Symp. Proc.* **449**, 1049(1997)

Edg98   J. H. Edgar, S. Strite and I. Akasaki, H. Amano and C. Wetzel, *Properties, processing and applications of gallium nitride and related semiconductors*, London, U.K. : IEE, INSPEC, c1999

Fan96   Z. Fan. S. N. Mohammad, W. Kim, O. Aktas, A. E. Botchkarev and H. Morkoc, *Appl. Phys. Lett.* **68**, 1672(1996)

Fre81   J. L. Freeouf and J.M. Woodall, *Appl. Phys. Lett.*, **39**, 727(1981)

Fuk93   Y. Fukai, *Metal-Hydrogen System : basic bulk properties*, Berlin ; New York : Springer-Verlag, c1993

Fun99   A. K. Fung, J. A. Borton, M. I. Nathan, J. M. Von Hove and R. Hickman, *J. Electrical Materials*, **28**, 572(1999)

Gas98   R. Gaska, J. W. Yang, A. Osinsky, Q. Chen, M. A. Khan, A. O. Orlov, G. L.Snider and M. S. Shur, *Appl. Phys. Lett.* **72**, 707(1998)

Geo96   T. George, E. Jacobsohn, W. T. Pike, P. Chang-Chien, M. A. Khan, J. W. Yang and S. Mahajan, *Appl. Phys. Lett.*, **68**, 337(1996)

Got81   H. Gotoh, T. Suga, H. Suzuki and M. Kimata, *Jpn. J. Appl. Phys.*, 20, L545(1981)

Got95   W. Gotz, N. M. Hohnson, J. Walker, D. P. Bour, H. Amano and I. Akasaki, *Appl. Phys. Lett.* **67**, 2606(1995)

Gri97   I. S. Grigoriew and E. Z. meilikhov, eds. *Handbook of Physical Quantities*, CRC Press, Inc, 1997

Guo95   J. D. Guo, M. S. Feng and R. J. Guo, F. M. Pan and C. Y. Chang., *Appl. Phys. Lett.*, **67**, 2657(1995)

Guo96   J. D. Guo, F. M. Pan, M. S. Feng, R. J. Guo, P. F. Chou and C. Y. Chang, *J. Appl. Phys.*, **80**, 1623(1996)

Ham98   F. Hamdani, M. Yeadon, D. J. Smith, H. Tang, W. Kim, A. Salvador, A. E. Botchkarev, J. M. Gibson, A. Y. Polyakov, M. Showronski and H. Morkoc, *J. Appl. Phys.*, **83**, 983(1998)

Her97   S. D. Hersee, J. C. Ramer and K. J. Malloy, *MRS Bull.* July, **22**, 45(1997)

Ho99a   J. K. Ho, C. S. Jong, C. C. Chiu, C. N. Huang, C. Y. Chen and K. K. Shih, *Appl. Phys. Lett.* **74**, 1275(1999)

Ho99b   J. K. Ho, C. S. Jong, C. C. Chiu, C. N. Huang, K. K. Shih, L. C. Chen, F. R. Chen and J. J. Kai, *J. Appl. Phys.* **86**, 4491(1999)

Hol97   P. H. Holloway, T. J. Kim, J. T. Trexler, S. Miller and J. J. Fijol, *Applied Surface Science*, **117-118**, 362(1997)

Hsu00   D. Hsu, *http://tech-two.mit.edu/Chemicool/*, as to December, 2000

Hüf92   S. Hüfner, P. Steiner, I. Sander, F. Reinert, and H. Schmitt, *Zeitschrift fur Physik. B, Condensed matter*, **86**, 207(1992)

Hum92   R. E. Hummel, *Electronic Properties of Materials*, 2nd edition, Springer International Student Edition, 1994

Hum98   R. E. Hummel, *Understanding Materials Science: History, Properties, Applications*, New York : Springer, c1998

Hun93   R. M. Hunt, L. Vanzetti, T. Castro, K. M. Chen, L. Sorba., *Physica*,, **B185**, 415(1993)

Ish97   H. Ishikawa, S. Kobayashi, Y. Koide, S. Yamasaki, S. Nagai, J. Umezaki, M. Koike and M. Murakami, *J. Appl. Phys.* **81**, 1315(1997)

Iwa97   K. Iwata, H. Asahi, K. Asahi, R. Kuroiwa and S. Gonda, *Jpn. J. Appl. Phys.*, Part 2, **36**, L661(1997)

Jai98   S. C. Jain, K. Pinardi, H. E. Maes, R. Van Overstraeten, M. Willander and A. Atkinson, *Mater. Res. Soc. Symp, Proc.* **482**, 875(1998)

Jai00   S. C. Jain, M. Willander, J. Narayan, R. Van Overstraeten, *Appl. Phys. Rev.* **87**, 965(2000)

Jan99   J. S. Jang, I.-S. Chang, H.-K. Kim, T.-Y. Seong, S. Lee and S.-J. Park, *Appl. Phys. Lett.*, **74**, 70(1999)

Kan99   J. Kang, T. Ogawa, *J. Mater. Res.* **14**, 1(1999)

Kan00   T. W. Kang, C. S. Chi, S. H. Park, T. W. Kim, *Japan. J. Appl. Phys.*, **39A**, 1062(2000)

Kat94   Y. Kato, S. Kitamura, K. Hiramatsu and N. Sawaki, *J. Cryst. Growth*, **144**, 133(1994)

Kel96   S. keller, P. B. Keller, Y. F. Wu, B. Heying, d. Kapolnek, J. S. Speck, U. K. Mishra and S. P. DenBaars, *Appl. Phys. Lett.*, **68**, 1525(1996)

Kha93   M. A. Khan, J. N. Kuznia, D. T. Loson and R. Kaplan, *J. Appl. Phys.*, **73**, 3108(1993)

Kha94   M. A. Khan, J. N. Kuznia, D. T. Loson, W. Schatt, J. Burm and M. S. Shur, *Appl. Phys. Lett.* **65**, 1121(1994)

Kim91   E. K. Kim, H. Y. Cho, Y. Kim, H. S. Kim, M. S. Kim and S. K. Min, *Appl. Phys. Lett.* **58**, 2405(1991)

Kim97a   T. Kim, M. C. Yoo and T. Kim, *III-V nitrides, Mater. Res. Soc. Proc.*, **449**, 1061(1997)

Kim97b   T. Kim, J. Kim, S. Chae and T. Kim, *III-V nitrides, Mater. Res. Soc. Symp. Proc.*, **468**, 427(1997)

Kim98   J. K. Kim, J.-L. Lee, J. W. Lee, H. E. Shin, Y. J. Park and T. Kim, *Appl. Phys. Lett.*, **73**, 2953(1998)

Kin96   S. W. King, L. L. Smith, J. P. Barnak, J.-H. Ku, J. A. Christman, M. C. Benjamin, M. D. Bremser, R. J. Nemanich and R. F. Davis, *Mat. Res. Soc. Symp. Proc.*, **395**, 739(1996)

Kin97   D. J. King, L. Zhang, J. C. Ramer, S. D. Hersee and L. F. Lester, *III-V nitrides, Mat. Res. Soc. Symp. Proc.*, **468**, 421(1997)

Kum93   A. Kumar, W. Christian, A. Wilisch and N. S. Lewis, *Critical Reviews in Solid State and Materials Sciences*, **18**, 327(1993)

Kun96   P. Kung, A. Saxler, X. Zhang, D. Walker, R. Lavado and M. Razeghi, *Appl. Phys. Lett.*, **69**, 2116(1996)

Kur88   S. K. Kurinec, I. Toor, Y.-K. Chao, H. Shillingford, P. Holloway, S. Ray and K. Beckham, *Thin Solid Films*, **162**, 247(1988)

Kur95   A. Kuramata, K. Horino, K. Domen, K. Shinohara and T. Tanahashi, *Appl. Phys. Lett.*, **67**, 2521(1995)

Lee93   R. E. Lee, *Scanning electron microscopy and x-ray microanalysis*, Englewood Cliffs, N.J. : PTR Prentice Hall, c1993

Lee99   J. L. Lee, J. K. Kim, J. W. Lee, Y. J. Park and T. I. Kim, *Solid State Electron.* **43**, 435(1999)

Les96   L. F. Lester, J. M. Brown, J. C. Ramar, L. Ahang, S. D. Hersee and J. C. Zolper, *Appl. Phys. Lett.*, **69**, 2737(1996)

Li96   W. Li and W-X Ni, *Appl. Phys. Lett.*, **68**, 2705(1996)

Li00   Y.-L. Li, E. F. Schubert, J. W. Graff, A. Osinsky and W. F. Schaff, *Appl. Phys. Lett.* **76**, 2728(2000)

Lin94   M. E. Lin, Z. Ma, F. Y. Huang, Z. F. Fan, L. H. Allen and H. Morkoc, *Appl. Phys. Lett.* **64**, 1003(1994)

Liu89   W. X. Liu, X. Y. Huang and Y. R. Chen, *Materials Structure Analysis by Electron Microscopy*, Tianjin University press, Tianjin, China, 1989

Liu98   Q. Z. Liu and S. S. Lau, *Solid-State Electron.* **42**, 677(1998)

Kob97   N. P. Kobayashi, J. T. Kobayashi, P. d. Daphus, W.-J. Choi, A. E. Bond, X. Zhang and D. H. Rich, *Appl. Phys. Lett.*, **71**, 3569(1997)

Mae99   T. Maeda, Y. Koide and M. Murakami, *Appl. Phys. Lett.* **75**, 4145(1999)

Mar69   H. P. maruska and J. J. Tietjen, *Appl. Phys. Lett.*, **15**, 327(1969)

Mar82   G. S. Marlow and M.B. Das, *Solid state electronics*, **25**, 91(1982)

May90   J. W. Mayer and S. S. Lau, *Electronic Materials Science for Integrated Circuits in Si and GaAs*, New York : Macmillan ; London : Collier Macmillan, c1990

Min96   M. S. Minsky, M. White and E. L. Hu, *Appl. Phys. Lett.*, **68**, 513(1996)

Moc98   N. Mochida, T. Honda, T. Shirasawa, A. Inoue, T. Sakaguch, F. Koyama, K. Iga., *J. Cryst. Growth*, **189/190**, 716(1998)

Moh96   S. E. Mohney and X. Lin, *J. Elec. Mater.*, **25**, 811(1996)

Moh97   S. E. Mohney, B.P. Luther, and T.N. Jackson, *III-V nitrides, SiC and Diamond Materials for Electronic Devices, Mat. Res. Soc. Symp. Proc.*, **449**, 843(1997)

Mol93   R. J. Molnar and T. D. Moustakas, *Bull. Am. Phys. Soc.* **38**, 445(1993)

Mor81   M. Morita, S. Isogai, N. Shimizu, K. Tsubouchi and N. Mikohiba, *Jpn. J. Appl. Phys.* **19**, L173(1981)

Mor96a   T. Mori, T. Kozawa, T. Ohwaki, Y. Taga, S. Nagai, S. yamasaki, S. Asami, N. Shibta and M. Koike, *Appl. Phys. Lett.*, **69**, 3537(1996)

Mor96b   H. Morkoc, S. Strite, G. B. Gao, M. E. Lin, B. Sverdlov and M. Burns, *J. Appl. Phys.* **76**, 1363(1994)

Mor97   H. Morkoc, *Mater. Sci. Engr.*, **B43**, 137(1997)

Mou93   T. D. Moustakas, T. Lei and R. J. Molnar, *Physica* **B185**, 39(1993)

Mou95   J. F. Moulder, W. F. Stickle, P. E. Sobol and K. D. Bomben, *Handbook of X-ray Photoelectron Spectroscopy*, eds. J. Chastain and R. C. King, Jr., Physical Electronics, Inc, 1995

Mur90   M. Murakami, *Mater. Sci. Rep.*, **5**, 273(1990)

Mur99   M. Murakami, private communication, 1999

Mur75   L. E. Murr, *Interfacial Phenomena in Metals and Alloys*, Reading, Mass. : Addison-Wesley Pub. Co., Advanced Book Program, 1975

Nak94   S. Nakamura, T. Mukai and M. Senoh, *Appl. Phys. Lett.* **64**, 1687(1994)

Nak96   S. Nakamura, M. Senoh, S. Nagahama, N. Iwasa, T. Yamada, T. Matsushita, H. Kiyoku and Y. Sugimoto, *Jpn. J. Appl. Phys.* **35**, L74(1996)

Nak97   S. Nakamura, M. Senah, S. Nagahama, N. Isawa, T. Yamada, T. Matsushita, Y. Sugimoto and H. Kiyoku, *Jpn. J. Appl. Phys.* **36**, L1059(1997)

Neu94   J. Neugebauer and C. G. van der Walle, *Physical review* **B50**, 8067(1994)

Neu95   J. Neugebauer and C. G. van der Valle, *Proc. ICPS*, **22**, 2327 (1995)

Neu96   J. Neugebauer and C. G. Van.der Walle, *Appl. Phys. Lett.*, **68**, 1929(1996)

Oka90   Hiroaki Okamoto, P.R. Subramanian, Linda Kacprzak(ed.), *Binary alloy phase diagrams*, 2nd edtion, editor-in-chief, Thaddeus B. Massalski; publisher, William W. Scott, Jr, Materials Park, Ohio : ASM International, 1990

Pal00   S. Pal, T. Sugino, *Appl. Surf. Sci.* **161**, 263(2000)

Pan71   J. I. Pankove, E. A. Miller, D. Richman and J. E. Berkeyheiser, *J. Lumin.*, **4**, 63(1971)

Pan76   J. I. Pankove, and J. A. Hutchby, *J. Appl. Phys.*, **47**, 5387(1976)

Pan97   J. I. Pankove, *GaN and Related Materials*, ed. S. J. Pearton, Gordon and Breach Science Publishers, Amsterdam, Netherlands, 1997, 1

Pea93   S. J. Pearton, C. R. Abernathy, F. Ren, J. R. Lothian, P. W. Wisk and A. Katz, *J. Vac. Sci. Technol.* **A11**, 1772(1993)

Pea94   S. J. Pearton, C. R. Abernathy and F. Ren, *Appl. Phys. Lett.* **64**, 2294(1994)

Pea96   S. J. Pearton, R. J. Shul, R. G. Wilson, F. Ren, J. M. Zavada, C. R. Abernathy, C. B. Vartuli, J. W. Lee, J. R. Mileham, J. D. Mackenzie., *J. Elec. Mater.*, **25**, 845(1996)

Pea97a   S. J. Pearton, F. Ren, R. J. Shur, J. C. Zolper and A. Katz, *Gallium nitride and related materials II*, ed. C.R.Abernathy, H.Amano, J.C.Zol-per, *Mat. Res. Soc. Symp. Proc.* **468**, 331(1997)

Pea97b   S. J. Pearton (ed.), *GaN and related materials*, Amsterdam : Gordon and Breach, c1997

Pea98   S. J. Pearton, R. G. Wilson, J. M. Zavada, J. Han and R. J. Shul, *Appl. Phys. Lett.*, **73**, 1877(1998)

Pea99   S. J. Pearton, F. Ren, C. R. Abernathy, R. K. Singh, P. H. Holloway, T. J. Anderson, A. Sher, M. Berding, S. Krishnamurthy, D. Palmer and G. E. McGuire, *5th Quarterly report EPRI agreement W08069-07*, July 1- September 30, 33(1999)

Pen98a   L.-H. Peng, C.-W. Chuang, J.-K. Ho, C.-N. Huang, and C.-Y. Chen, *Appl. Phys. Lett.*, **72**, 939(1998)

Pen98b   L.-H. Peng, C.-W. Chuang, Y.-C. Hsu, J.-K. Hu, C.-N. Huang and C.-Y. Chen, *IEEE J. Select. Topics Quantum Electron.*, 4, 564(1998)

Per00   US Peroxide, *http://www.h2o2.com/intro/properties/thermodynamic.html#12*, as to December, 2000

Piq98   E. C. Piquette, Z. Z. Bandic, and T. C. McGill, *Mat. Res. Soc. Symp. Proc.* **482**, 1089(1998)

Pon97   F. A. Ponce, *MRS Bull.* **22**, 51(1997)

Pop97   G. Popovici, W. Kim, A. Botchkarev, H. Tang, H. Morkoc and J. Solomon, *Appl. Phys. Lett.*, **71**, 3385(1997)

Pop98   G. Popovici, H. Morkoc, and S. Noor Mohammad, *Group III Nitride Semiconductor Compounds*, edited by B. Gil, Clarendon, Oxford, 1998, p19

Rea68   D. W. Ready and R. E. Jech, *J. Am. Ceram. Soc.* **51**, 201(1968)

Ren97   F. Ren, *GaN and related materials*, edited by S. J. Pearton (Gordon and Breach Science Publishers, New York, 1997)

Ren98   J. Rennie, M. Onomura, S.-Y. Nunoue, G.-I. Hatakoshi, H. Sugawara, M. Ishikawa, *J. Cryst. Growth*, **189/190**, 711(1998)

Ren99   F. Ren, M. Hong, S. N. G. Chu, M. A. Marcus, M. J. Schurman, A. G. Baca, S. J. Pearton and C. R. Abernathy, *Appl. Phys. Lett.* **73**, 3893(1999)

Rho88   E. H. Rhoderick, *Metal-semiconductor contacts*, New York: Oxford University Press, 1988

Rid75   V. L. Rideout, *Solid State Electronics*, **18**, 541(1975)

Roy52   R. Roy, V. G. Hill and E. F. Osborn, *Am. Chem. Soc.* **74**, 719(1952)

Ruv96a   S. Ruvimov, Z. Liliental-Weber, J. Washburn, K. J. Duxstad, E. E. Haller, Z. F. Fan, S. N. Mohammad, W. Kim, A. E. Botchkarev, H. Morkoc, *III-V nitrides, SiC and Diamond Materials for Electronic Devices, Mat. Res. Soc. Symp. Proc.*, **423**, 201(1996)

Ruv96b   S. Ruvimov, Z. Liliental-Weber, J. Washburn, K. J. Duxstad, E. E. Haller, Z. F. Fan, S. N. Mohammad, W. Kim, A. E. Botchkanev and H. Mokoc, *Appl. Phys. Lett.* **69**, 1556(1996)

Saa98   K. Saarinen, P. Seppala, J. Oila, P. Hautojarvi, and C. Corbel, O. Briot and R. L. Aulombard., *Appl. Phys. Lett.*, **73**, 3253(1998)

Sam73   G. V. Samsonov, *The Oxide Handbook*, Translated from Russian by C. N. Turton and T. I. Turton, (IFI/Plenum, New York, 1973)

Sam75   G. V. Samsonov and I. M. Vinitskii, *Handbook of refractory compounds*: translated from Russian by Kenneth Shaw, New York : Plenum Press, 1979

Sei83   W. Seifert, R. Franzheld, E. Butter, H. Sobotta, V. Riede, *Crystal Res. & Technol.*, **18**, 383(1983)

She92   T. C. Shen, G. B. Gao, and H. Morkoc, *J. Vac. Sci. Tech.*, **B10**, 2113(1992)

She99a   S. T. Sheppard, K. Doverspike, W. L. Pribble, S. T. Allen, J. W. Palmour, L. T. Kehias and T. J. Jenkins, *IEEE Electron. Dev. Lett.* **20**, 161(1999)

She99b   J. K. Sheu, Y. K. Su, G. C. Chi, P. L. Koh, M. J. Jou, C. M. Chang, C. C. Liu and W. C. Hung, *Appl. Phys. Lett.* **74**, 2340(1999)

Shu99   M. S. Shur, R. Gaska and A. Bykhovski, *Solid State Electron*, **43**, 1451(1999)

Sib96   J. P. Sibilia (ed), *A guide to materials characterization and chemical analysis*, 2nd ed., New York : Wiley-VCH, c1996

Smi96   L. L. Smith, S. W. King, R. J. Nemanich and R. F. Davis, *J. Electron. Mater.* **25**, 805(1996)

Smi96b L. L. Smith, M. D. Bremser, E. P. Carlson and T. W. Weeks, *Mat. Res. Soc. Symp. Proc.*, **395**, 861(1996)

Spi86   W. E. Spicer, T. J. Kendelevica, N. Newman, K. K. Chin and J. Lindau, *Surf. Sci.*, **168**, 240(1986)

Sto98   D. A. Stocker, E. F. Schubert, and J. M. Redwing, *Appl. Phys. Lett.* **73**, 2654(1998)

Str91   S. Strite, J. Ruan, Z. Li, N. Manning, A. Salavador, H. chen, D. J. Smith, W. J. Choyke and H. Morkoc, *J. Vac. Sci. Tech.*, **B9**, 1924(1991)

Sug98   L. M. Sugiura, M. Suzuki, and J. Nishio, *Appl. Phys. Lett.*, **72**, 1748(1998)

Sun96   C. J. Sun, J. W. Yang, Q. Chen, M. A. Khan, T. George, P. Chang-Chien, and S. Mahajan, *Appl. Phys. Lett.*, **68**, 1129(1996)

Sun97   C. J. Sun, J. W. Yang, B. W. Lim, Q. Chen, M. Z. Anwar, and M. A. Khan, *Appl. Phys. Lett.*, **70**, 1444(1997)

Suz99   M. Suzuki, T. Kawakami, T. Arai, S. Kobayashi, Y. Koide, T. Uemura, N. Shibata and M. Murakami , *Appl. Phys. Lett.* **74**, 275(1999)

Sze81   S. M. Sze, *Physics of semiconductor devices*, 2nd edition, New York: Wiley, c1981

Tre96   J. T. Trexler, S. J. Miller, P. H. Holloway and M. A. Khan, *Mater. Res. Soc. Symp. Proc.* **395**, 819(1996)

Tre97   J. T. Trexler, S. J. Pearton, P. H. Holloway, M. G. Mier, K. R. Evans and R. F. Karlicek, *III-V nitrides*, *Mater. Res. Soc. Symp. Proc.*, **449**, 1091(1997)

Uza95   Y. Uzawa. Z. Wang, A. Kawakami and B. Komiyama, *Appl. Phys. Lett.* **66**, 1992(1995)

Van58   L. J. van der Pauw, *Philips Res. Repts.* **13**, 1(1958)

Var96a C. B. Vartuli, S. J. Pearton, C. R. Abernathy, J. D. MacKenzie, R. J. shul, J. C. Zolper, M. L. Lovejoy, A. G. Baca, M. Hagerott-Crawford, *J. Vac. Sci. Tech.*, **B14**, 3520(1996)

Var96b C. B. Vartuli, S. J. Pearton, J. w. Lee, C. R. abernathy, J. D. Mackenzie, J. C. Zolper, R. J. Shul and F. Ren, *J. Electrochem. Soc.*, **143**, 3681(1996)

Var97a C. B. Vartuli, S. J. Pearton, C. R. Abernathy, J. D. Mackenzie, M. L. Lovejoy, R. J. Shul, J. C. Zolper, A. G. Baca M. Hagerott-Crawford, A. Jones and F. Ren, *Solid-state electronics*, . **41**, 531(1997)

Var97b C. B. Vartuli, S. J. Pearton, C. R. Abernathy, J. D. MacKenzie, M. L. Lovejoy, R. J. Shul, J. C. Zolper, A. G. Baca, M. Hagerott-Crawford, K. A. Jones, F. Ren, *III-V nitrides, Mat. Res. Soc. Symp. Proc.* **449**, 257(1997)

Ven97 H. S. Venugopalan, S. E. Mohney, B. P. Luther, J. M. Delucca, S. D. Wolter, J. M. Redwing and G. E. Bulman, *Gallium nitride and related materials II*, ed. C.R. Abernathy, H. Amano, J. C. Zolper, *Mater. Res. Soc. Symp. Proc.*, **449**, 431(1997)

Ven99 P. Vennegues and B. Beaumont, *JEOL News*, **32E**, No. 1, 22(1996)

Vik91 P. Viktorovitch, M. Gendry, S. K. Krawczk, F. Krafft, P. Abraham, A. Bekkaoui and Y. Monteil, *Appl. Phys. Lett.* **58**, 2387(1991)

Vis95 R. D. Vispute, J. Nrayan, H. Wu and K. Jagannadham, *J. Appl. Phys.* **77**, 4724(1995)

Wal97 D. Walker, X. Zhang, A. Saxler, P. Kung and M. Raxeghi, *Appl. Phys. Lett.*, **70**, 949(1997)

Wil84 R. E. Williams, *Gallium arsenide processing techniques*. Dedham, MA : Artech House, c1984

Wet97 C. Wetzel, T. Suski, J. W. Ager III, E. R. Weber, E. E. Haller, S. Fischer, B. K. Meyer, R. J. Molnar and P. Perlin, *Phys. Rev. Lett.* **78**, 3923(1997)

Wey97 J. L. Weyher, S. Muller, I. Grzegory and S. Porowski, *J. Cryst. Growth*, **182**, 17(1997)

Wol97 S. D. Wolter, S. E. Mohney, H. Venugopalan and D. L. Waltemyer., *Gallium nitride and related materials II*, Ed. C.R. Abernathy, H. Amano, and J.C. Zolper, *Mat. Res. Soc. Symp. Proc.*, **468**, 495(1997)

Yan71 C. Y. Yang, Y.K. Fang, and S.M. Sze, *Solid state electron*, **14**, 541(1971)

Yoo96 M. C. Yoo, J. W. Lee, J. W. Myoung, K. H. Shim and K. Kim, *Mater. Res. Soc. Symp. Proc.*, **423**, 131(1996)

You97 C. Youtsey, I. Adesida and G. Bulman, *Appl. Phys. Lett.*, **71**, 2151(1997)

You98 D.-H. Youn, M. Hao, H. Sato, T. Sugahara, Y. Nao and S. Sakai, *Jpn. J. Appl. Phys.*, **37**, 1768(1998)
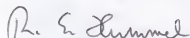
BIOGRAPHICAL SKETCH

Bo Liu was born in Linshu, Shangdong province, in the People's Republic of China, on February 7, 1969. After completing 11 years of primary and secondary education in his home town, he moved to Harbin in the northeast region and enrolled in the Department of Metal Materials and Technology (now the College of Materials Science and Engineering) at the Harbin Institute of Technology (HIT) in 1987. In 1991, he was admitted to the graduate program at HIT with the highest grade. Under Professor Yang's guidance, he finished his research thesis on formability of intermetallic compound alloys in the spring of 1994 and worked continuously on the same research topic in Professor Yang's group. With a strong interest in the progress of semiconductor materials, Bo came to Gainesville to attend the University of Florida in 1997, majoring in electronic materials in the Department of Materials Science and Engineering. Under the supervision of Dr. Paul H. Holloway, Bo worked on ohmic contact technology for gallium nitride and received his Ph.D in May 2001.

I certify that I have read this study and that in my opinion it conforms to acceptable standards of scholarly presentation and is fully adequate, in scope and quality, as a dissertation for the degree of Doctor of Philosophy.
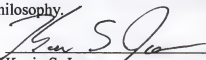
Paul H. Holloway, Chairman
Professor of Materials Science and
Engineering

I certify that I have read this study and that in my opinion it conforms to acceptable standards of scholarly presentation and is fully adequate, in scope and quality, as a dissertation for the degree of Doctor of Philosophy.

Rolf E. Hummel
Professor of Materials Science and
Engineering

I certify that I have read this study and that in my opinion it conforms to acceptable standards of scholarly presentation and is fully adequate, in scope and quality, as a dissertation for the degree of Doctor of Philosophy.

Kevin S. Jones
Professor of Materials Science and
Engineering

I certify that I have read this study and that in my opinion it conforms to acceptable standards of scholarly presentation and is fully adequate, in scope and quality, as a dissertation for the degree of Doctor of Philosophy.

Wolfgang M. Sigmund
Assistant Professor of Materials Science
and Engineering

I certify that I have read this study and that in my opinion it conforms to acceptable standards of scholarly presentation and is fully adequate, in scope and quality, as a dissertation for the degree of Doctor of Philosophy.

Fan Ren
Professor of Chemical Engineering

This dissertation was submitted to the Graduate Faculty of the College of Engineering and to the Graduate School and was accepted as partial fulfillment of the requirements for the degree of Doctor of Philosophy.

May 2001

M. Jack Ohanian
Dean, College of Engineering

Winfred M. Phillips
Dean, Graduate School